8

Probing strongly coupled plasma

As discussed in Sections 2.3 and 2.4, two of the most informative probes of strongly coupled plasma that are available in heavy ion collisions are the rare highly energetic partons and quarkonium mesons produced in these collisions. In this chapter and in Chapter 9, we review results obtained by employing the AdS/CFT correspondence that are shedding light on these classes of phenomena. In Sections 8.1 and 8.2, we describe how a test quark of mass M moving through the strongly coupled $\mathcal{N} = 4$ SYM plasma loses energy and picks up transverse momentum. In Section 8.3 we consider how the strongly coupled plasma responds to the hard parton plowing through it; that is, we describe the excitations of the medium which result. In Section 8.4, we discuss calculations of the stopping distance of a light quark moving through the strongly coupled plasma. Throughout Sections 8.1, 8.2, 8.3 and 8.4 we assume that all aspects of the phenomena associated with an energetic parton moving through the plasma are strongly coupled. In Section 8.5, we present an alternative approach in which we assume that QCD is weakly coupled at the energy and momentum scales that characterize gluons radiated from the energetic parton, while the medium through which the energetic parton and the radiated gluons propagate is strongly coupled. In this case, one uses the AdS/CFT correspondence only in the calculation of those properties of the strongly coupled plasma that arise in the calculation of radiative parton energy loss and transverse momentum broadening. In Section 8.6, we describe a calculation of synchrotron radiation in strongly coupled $\mathcal{N} = 4$ SYM theory that allows the construction of a narrowly collimated beam of gluons (and adjoint scalars) which we can then watch as it is quenched by the strongly coupled plasma. This opens a new path toward analyzing jet quenching.

In Section 8.7, we review those insights into the physics of quarkonium mesons in heavy ion collisions that have been obtained via AdS/CFT calculations of the temperature-dependent screening of the potential between a heavy quark and antiquark. To go farther, we need to introduce a holographic description of

261

quarkonium-like mesons themselves. In Chapter 9, we first present this construction and then describe the insights that it has yielded. In addition to shedding light upon the physics of quarkonia in hot matter that we have introduced in Section 2.4, as we describe in Section 9.6.2 these calculations have also resulted in the discovery of a new process by which a hard parton propagating through a strongly coupled plasma can lose energy: Cherenkov radiation of quarkonium mesons.

8.1 Parton energy loss via a drag on heavy quarks

When a heavy quark moves through the strongly coupled plasma of a conformal theory, it feels a drag force and consequently loses energy [452, 394]. We shall review the original calculation of this drag force in $\mathcal{N} = 4$ SYM theory [452, 394]; it has subsequently been done in many other gauge theories with dual gravitational descriptions [453, 224, 225, 610, 645, 772, 395, 418, 468, 144, 161]. In calculations of the drag on heavy quarks, one determines the energy per unit time needed to maintain the forced motion of the quark in the plasma. In these calculations one regards the quark as an external source moving at fixed velocity, v, and one performs thermal averages over the medium. This picture can be justified if the mass of the quark is assumed to be much larger than the typical momentum scale of the medium (temperature), and if the motion of the quark is studied in a time window that is large compared with the relaxation scale of the medium but short compared to the time it takes the quark to change its trajectory. In this limit the heavy quark is described by a Wilson line along the worldline of the quark.

The dual description of the Wilson line is given by a classical string hanging down from the quark on the boundary of AdS. Since we are considering a single quark, the other end of the string hangs down into the bulk of the AdS space. We consider the stationary situation, in which the quark has been moving at a fixed velocity for a long time, meaning that the shape of the string trailing down and behind it is no longer changing with time. For concreteness, we will assume that the quark moves in the x_1 direction, and we choose to parametrize the string world sheet by $\tau = t$ and $\sigma = z$. By symmetry, we can set two of the perpendicular coordinates, x_2 and x_3 to a constant. The problem of finding the string profile reduces, then, to finding a function

$$x_1(\tau, \sigma), \tag{8.1}$$

that fulfills the string equations of motion. The string solution must also satisfy the boundary condition

$$x_1(t, z \to 0) = vt. \tag{8.2}$$

Since we are interested in the stationary situation, the string solution takes the form

$$x_1(t, z) = vt + \zeta(z), \tag{8.3}$$

with $\zeta(z \to 0) = 0$. We work in an $\mathcal{N} = 4$ plasma, whose dual gravitational description is the AdS black hole with the metric $G_{\mu\nu}$ given in (5.34). The induced metric on the string worldsheet $g_{\alpha\beta} = G_{\mu\nu}\partial_\alpha x^\mu \partial_\beta x^\nu$ is then given by

$$ds_{ws}^2 = \frac{R^2}{z^2}\left(-\left(f(z) - v^2\right)d\tau^2 + \left(\frac{1}{f(z)} + \zeta'^2(z)\right)d\sigma^2 \right.$$
$$\left. + v\,\zeta'(z)v\,(d\tau d\sigma + d\sigma d\tau)\right), \tag{8.4}$$

where, as before, $f(z) = 1 - z^4/z_0^4$ and $\zeta'(z)$ denotes differentiation with respect to z.

The Nambu–Goto action for this string reads

$$S = -\frac{R^2}{2\pi\alpha'}\mathcal{T}\int \frac{dz}{z^2}\sqrt{\frac{f(z) - v^2 + f(z)^2\zeta'^2(z)}{f(z)}} = \mathcal{T}\int dz\mathcal{L}, \tag{8.5}$$

with $\mathcal{T}$ the total time traveled by the quark. Extremizing this action yields the equations of motion that must be satisfied by $\zeta(z)$. The action (8.5) has a constant of motion given by the canonical momentum

$$\Pi_z^1 = \frac{\partial\mathcal{L}}{\partial x_1'} = -\frac{R^2}{2\pi\alpha'}\frac{1}{z^2}\frac{f(z)^{3/2}\zeta'(z)}{\sqrt{f(z) - v^2 + f(z)^2\zeta'^2(z)}}, \tag{8.6}$$

which coincides with the longitudinal momentum flux in the z direction. In terms of Π_z^1, the equation of motion for ζ obtained from (8.5) takes the form

$$\zeta'^2(z) = \left(\frac{2\pi\alpha'}{R^2}\Pi_z^1\right)^2 \frac{z^4}{f(z)^2}\frac{f(z) - v^2}{f(z) - \left(\frac{2\pi\alpha'}{R^2}\Pi_z^1\right)^2 z^4}. \tag{8.7}$$

The value of Π_z^1 can be fixed by inspection of this equation, as follows: both the numerator and the denominator of (8.7) are positive at the boundary $z = 0$ and negative at the horizon $z = z_0$; since $\zeta'(z)$ is real, both the numerator and the denominator must change sign at the same z; this is only the case if

$$\Pi_z^1 = \pm\frac{R^2}{2\pi\alpha' z_0^2}\gamma v, \tag{8.8}$$

with $\gamma = 1/\sqrt{1 - v^2}$ the Lorentz γ factor. Thus, stationary solutions can only be found for these values of the momentum flux. (Or, for $\Pi_z^1 = 0$, for which $\xi =$ constant. This solution has real action only for $v = 0$.)
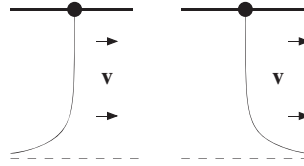
Figure 8.1 String solutions of Eq. (8.8). The physical (unphysical) solution in which momentum flows into (out of) the horizon and the string trails behind (curves ahead) of the quark at the boundary is plotted in the left (right) panel. Figure from Ref. [452].

The two solutions (8.8) correspond to different choices of boundary conditions at the horizon. Following Refs. [452, 394], we choose the solution for which the momentum flux along the string world sheet flows from the boundary into the horizon, corresponding to the physical case in which the energy provided by the external agent that is pulling the quark through the plasma at constant speed is dissipated into the medium. This solution to (8.7) is given by

$$\zeta(z) = -\frac{v z_0}{2} \left(\text{arctanh}\left(\frac{z}{z_0}\right) - \arctan\left(\frac{z}{z_0}\right) \right) . \tag{8.9}$$

As illustrated in Fig. 8.1, this solution describes a string that trails behind the moving quark as it hangs down from it into the bulk spacetime.

The momentum flux flowing down from the boundary, along the string world sheet (8.9), and towards the horizon determines the amount of momentum lost by the quark in its propagation through the plasma. In terms of the field theory variables,

$$\frac{dp}{dt} = -\Pi_z^1 = -\frac{\pi T^2 \sqrt{\lambda}}{2} \gamma v . \tag{8.10}$$

Note, however, that in the stationary situation we have described, there is by construction no change in the actual momentum of the quark at the boundary; instead, in order to keep the quark moving with constant speed v against the force (8.10) there must be some external agent pushing the quark through the strongly coupled plasma. This force can be viewed as due to a constant electric field acting on the string endpoint, with the magnitude of the field given by

$$\mathcal{E} = \frac{\pi T^2 \sqrt{\lambda}}{2} \gamma v . \tag{8.11}$$

The physical set-up described by the string (8.9) is thus that of forced motion of the quark through the plasma at constant speed in the presence of a constant electric field. The external force on the quark balances the backward *drag force* (8.10) on

the quark exerted by the medium through which it is moving. To make it explicit that the medium exerts a drag force, we can rewrite (8.10) as

$$\frac{dp}{dt} = -\eta_D p\,, \tag{8.12}$$

with $p = M\gamma v$ the relativistic expression of the momentum of the quark and M the mass of the heavy particle. The drag coefficient is then

$$\eta_D = \frac{\pi\sqrt{\lambda}T^2}{2M}\,. \tag{8.13}$$

For test quarks with $M \to \infty$, as in the derivation above, this result is valid for motion with arbitrarily relativistic speeds v. It is remarkable that the energy loss of a heavy quark moving through the quark–gluon plasma with constant speed is described so simply, as due to a drag force. In contrast, in either a weakly coupled plasma [628] or a strongly coupled plasma that is not conformal [585], dp/dt is not proportional to p even at low velocities.

We shall see in Section 8.2 that a heavy quark moving through the strongly coupled plasma of $\mathcal{N} = 4$ SYM theory experiences transverse and longitudinal momentum broadening, in addition to losing energy via the drag that we have analyzed above. We shall review the implications of the understanding of how the presence of the strongly coupled plasma affects the motion of heavy quarks for heavy ion collision phenomenology at the end of Section 8.2.

8.1.1 Regime of validity of the drag calculation

In the derivation of the drag force above, we considered a test quark with $M \to \infty$. The result is, however, valid for quarks with finite mass M, as long as M is not too small. As we now show, the criterion that must be satisfied by M depends on the velocity of the quark v. The closer v is to 1, the larger M must be in order for the energy loss of the quark to be correctly described via the drag force calculated above. In deriving the regime of validity of the drag calculation, we shall assume for simplicity that we are interested in large enough $\gamma = 1/\sqrt{1 - v^2}$ that the M above which the calculation is valid satisfies $M \gg \sqrt{\lambda}T$. We will understand the need for this condition in Chapter 9.

The introduction of quarks with finite mass M in the fundamental representation of the gauge group corresponds in the dual gravitational description to the introduction of D7-branes [513], as we have reviewed in Section 5.5 and as we will further pursue in Chapter 9. The D7-brane extends from the boundary at $z = 0$ down to some z_q, related to the mass of the quarks it describes by

$$M = \frac{\sqrt{\lambda}}{2\pi z_q} , \tag{8.14}$$

a result that we shall explain in Section 9.1. The physical reason that the calculation of the drag force breaks down if M is too small or v is too large is that if the electric field $\mathcal{E}$ required to keep the quark moving at constant speed v gets too large, one gets copious production of pairs of quarks and antiquarks with mass M, and the picture of dragging a single heavy quark through the medium breaks down completely [253]. The parametric dependence of the critical field $\mathcal{E}_c$ at which pair production becomes copious can be estimated by inspection of how the Dirac–Born–Infeld action for the D7-brane depends on $\mathcal{E}$, namely

$$S_{DBI} \sim \sqrt{1 - \left(\frac{2\pi\alpha'}{R^2}\mathcal{E} z_q^2\right)^2} . \tag{8.15}$$

The critical maximum field strength that the D7-brane can support is the $\mathcal{E}_c$ at which this action vanishes. This yields a criterion for the validity of the drag calculation, namely that $\mathcal{E}$ must be less than of order

$$\mathcal{E}_c = \frac{2\pi M^2}{\sqrt{\lambda}} . \tag{8.16}$$

This maximum value of the electric field implies a maximum value of γ up to which the drag calculation can be applied for quarks with some finite mass M. From Eq. (8.11) and Eq. (8.16), this criterion is

$$\gamma v < \left(\frac{2M}{\sqrt{\lambda}T}\right)^2 . \tag{8.17}$$

We shall assume that $M \gg \sqrt{\lambda}T$, meaning that in (8.17) we can take $\gamma v \simeq \gamma$. And, the estimate is only parametric, so the factor of two is not to be taken seriously. Thus, the result to take away is that the drag calculation is valid as long as

$$\gamma \lesssim \left(\frac{M}{\sqrt{\lambda}T}\right)^2 . \tag{8.18}$$

The argument in terms of pair production for the limit (8.18) on the quark velocity gives a nice physical understanding for its origin, but this limit arises in a variety of other ways. For example, at (8.18) the velocity of the quark v becomes equal to the local speed of light in the bulk at $z = z_q$, where the trailing string joins onto the quark on the D7-brane. For example, at (8.18) the screening length L_s (described below in Section 8.7) at which the potential between a quark and antiquark is screened becomes as short as the Compton wavelength of a quark of mass M, meaning that the calculation of Section 8.7 is also valid only in the regime (8.18) [584].

Yet further understanding of the meaning of the limit (8.18) can be gained by asking the question of what happens if the electric field is turned off, and the quark moving with speed v begins to decelerate due to the drag force on it. We would like to be able, at least initially, to calculate the energy loss of this now decelerating quark by assuming that this energy loss is due to the drag force, which from (8.10) means

$$\left.\frac{dE}{dt}\right|_{\text{drag}} = -\frac{\pi}{2}\sqrt{\lambda}T^2\gamma v^2 = -\frac{\pi}{2}\sqrt{\lambda}T^2\frac{pv}{M} \,. \tag{8.19}$$

However, once the quark is decelerating it is natural to expect that, due to its deceleration, it radiates and loses energy via this radiation also. The energy lost by a quark in strongly coupled $\mathcal{N}=4$ SYM theory moving in vacuum along a trajectory with arbitrary acceleration has been calculated by Mikhailov [618].[1] For the case of a linear trajectory with deceleration a, his result takes the form

$$\left.\frac{dE}{dt}\right|_{\text{vacuum radiation}} = -\frac{\sqrt{\lambda}}{2\pi}a^2\gamma^6 = -\frac{\sqrt{\lambda}}{2\pi}\frac{1}{M^2}\left(\frac{dp}{dt}\right)^2 \,. \tag{8.20}$$

At least initially, dp/dt will be that due to the drag force, namely (8.10). We now see that the condition that dE/dt due to the vacuum radiation (8.20) caused by the drag-induced deceleration (8.10) be less than dE/dt due to the drag itself (8.19) simplifies considerably and becomes

$$\gamma < \left(\frac{2M}{\sqrt{\lambda}T}\right)^2 \,, \tag{8.21}$$

the same criterion that we have seen before. This gives further physical intuition into the criterion for the validity of the drag calculation and at the same time demonstrates that this calculation cannot be used in the regime in which energy loss due to deceleration-induced radiation becomes dominant.

Motivated by the above considerations, the authors of Ref. [346] considered the (academic) case of a test quark moving in a circle of radius L with constant angular frequency ω. They showed that in this circumstance, dE/dt is given by (8.19), as if due to drag with no radiation, as long as $\omega^2 \ll (\pi T)^2\gamma^3$, with γ the Lorentz factor for velocity $v = L\omega$. But, for $\omega^2 \gg (\pi T)^2\gamma^3$, the energy loss of the quark moving in a circle through the plasma is precisely what it would be in vacuum according to Mikhailov's result, which becomes

$$\left.\frac{dE}{dt}\right|_{\text{vacuum radiation}} = \frac{\sqrt{\lambda}}{2\pi}v^2\omega^2\gamma^4 = \frac{\sqrt{\lambda}}{2\pi}a^2\gamma^4 \tag{8.22}$$

---

[1] Mikhailov's general result for an accelerating quark in $\mathcal{N}=4$ SYM theory at $T=0$ is equivalent to Liénard's classical result for electromagnetic radiation from an accelerating charge upon replacing the QED coupling constant $2e^2/3$ by $\sqrt{\lambda}/(2\pi)$. Finite mass corrections to Mikhailov's result have been explored in Ref. [280].

for circular motion. Note that the radiative energy loss (8.22) is greater than that due to drag, (8.19), for

$$\omega^2 \gg (\pi T)^2 \gamma^3 , \tag{8.23}$$

so the result of the calculation is that energy loss is dominated by that due to acceleration-induced radiation or that due to drag wherever each is larger. (Where they are comparable in magnitude, the actual energy loss is somewhat less than their sum [346].) This calculation shows that the *calculational method* that yields the result that a quark moving in a straight line with constant speed v in the regime (8.21) loses energy via drag can yield other results in other circumstances (see [280, 283, 282] for further examples). In the case of circular motion, the criterion for the validity of the calculational method is again (8.21), but there is a wide range of parameters for which this criterion and (8.23) are both satisfied [346]. This means that, for a quark in circular motion, the calculation is reliable in a regime where energy loss is as if due to radiation in vacuum. As we shall see in Section 8.6, this opens the possibility to using this calculation as a device with which to make a beam of strongly coupled gluons and adjoint scalars, whose quenching in the strongly coupled plasma can then be analyzed.

8.2 Momentum broadening of a heavy quark

In the same regime in which a heavy quark moving through the strongly coupled plasma of $\mathcal{N} = 4$ SYM theory loses energy via drag, as described in Section 8.1, it is also possible to use gauge/gravity duality to calculate the transverse (and, in fact, longitudinal) momentum broadening induced by motion through the plasma [252, 396, 253, 254]. We shall review these calculations in this section. They have been further analyzed [328, 311, 378], and extended to study the effects of nonconformality [585, 675, 419] and acceleration [808, 227].

For non-relativistic heavy quarks, the result (8.12) is not surprising. The dynamics of this particle is that of Brownian motion which can be described by the effective equation of motion

$$\frac{dp}{dt} = -\eta_D p + \xi(t) , \tag{8.24}$$

where $\xi(t)$ is a random force that encodes the interaction of the medium with the heavy probe and that causes the momentum broadening that we describe in this section. For heavy quarks, we have seen in (8.13) that η_D is suppressed by mass. This reflects the obvious fact that the larger the mass of the quark the harder it is to change the momentum of the particle. Thus, for a heavy quark the typical time for such a change, $1/\eta_D$, is long compared to any microscopic time scale of

the medium τ_{med}. This fact allows us to characterize the force distribution by the two-point correlators

$$\begin{aligned}
\langle \xi_T(t)\xi_T(t') \rangle &= \kappa_T \delta(t - t'), \\
\langle \xi_L(t)\xi_L(t') \rangle &= \kappa_L \delta(t - t'),
\end{aligned} \tag{8.25}$$

where the subscripts L and T refer to the forces longitudinal and transverse to the direction of the particle's motion. Here, we are also assuming an isotropic plasma which leads to $\langle \xi_L(t) \rangle = \langle \xi_T(t) \rangle = 0$. In general, the force correlator would have a nontrivial dependence on the time difference (different from $\delta(t - t')$). However, since the dynamics of the heavy quark happens on time scales that are much larger than τ_{med}, we can approximate all medium correlations as happening instantaneously. It is then easy to see that the coefficient κ_T (κ_L) corresponds to the mean squared transverse (longitudinal) momentum transferred to the heavy quark per unit time. For example, the transverse momentum broadening is given by

$$\langle \mathbf{p}_\perp^2 \rangle = 2 \int dt\, dt' \, \langle \xi_T(t)_T \xi_T(t') \rangle = 2\kappa_T \mathcal{T}, \tag{8.26}$$

where $\mathcal{T}$ is the total time duration (which should be smaller than $1/\eta_D$) and where the 2 is the number of transverse dimensions. It is clear from the correlator that κ_T is a property of the medium, independent of any details of the heavy quark probe. Our goal in this section is to calculate κ_T and κ_L. We shall do so first at low velocity, and then throughout the velocity regime in which the calculation of the drag force is valid.

Before we begin, we must show that in the limit we are considering the noise distribution is well characterized by its second moment. Odd number correlators vanish because of symmetry, so the first higher moment to consider is the fourth moment of the distribution of the transverse momentum picked up by the heavy quark moving through the plasma

$$\langle \mathbf{p}_\perp^4 \rangle = \int dt_1 dt_2 dt_3 dt_4 \, \langle \xi_T(t_1)\xi_T(t_2)\xi_T(t_3)\xi_T(t_4) \rangle. \tag{8.27}$$

The four-point correlator may be decomposed as

$$\begin{aligned}
\langle \xi_T(t_1)\xi_T(t_2)\xi_T(t_3)\xi_T(t_4) \rangle = {}& \langle \xi_T(t_1)\xi_T(t_2)\xi_T(t_3)\xi_T(t_4) \rangle_c & (8.28) \\
& + \langle \xi_T(t_1)\xi_T(t_2) \rangle \langle \xi_T(t_3)\xi_T(t_4) \rangle \\
& + \langle \xi_T(t_1)\xi_T(t_3) \rangle \langle \xi_T(t_2)\xi_T(t_4) \rangle \\
& + \langle \xi_T(t_1)\xi_T(t_4) \rangle \langle \xi_T(t_2)\xi_T(t_3) \rangle,
\end{aligned}$$

$$\tag{8.29}$$

which is the definition of the connected correlator. Owing to time translational invariance, the connected correlator is a function

$$\langle \xi_T(t_1)\xi_T(t_2)\xi_T(t_3)\xi_T(t_4)\rangle_c = f(t_4 - t_1, t_3 - t_1, t_2 - t_1). \tag{8.30}$$

As before, the correlator has a characteristic scale of the order of the medium scale. As a consequence, since the expectation value due to the connected part has only one free integral, we find

$$\langle \mathbf{p}_\perp^4 \rangle = \left(3\,(2\kappa_T)^2 + \mathcal{O}(\frac{\tau_{\text{med}}}{\mathcal{T}})\right)\mathcal{T}^2, \tag{8.31}$$

where the dominant term comes from the disconnected parts in Eq. (8.28). Since we are interested in times parametrically long compared to τ_{med}, we can neglect the connected part of the correlator.

8.2.1 κ_T and κ_L in the $p \to 0$ limit

The dynamical equations (8.24) together with (8.25) constitute the Langevin description of heavy quarks in a medium. In the $p \to 0$ limit, there is no distinction between transverse and longitudinal, meaning that both the fluctuations in (8.25) must be described by the same correlator with $\kappa_L = \kappa_T \equiv \kappa$. The Langevin equations (8.24) and (8.25) describe the time evolution of the probability distribution for the momentum of an ensemble of heavy quarks in a medium. A standard analysis shows that, independent of the initial probability distribution, after sufficient time any solution to the Langevin equation yields the probability distribution

$$\mathcal{P}(\mathbf{p}, t \to \infty) = \left(\frac{1}{\pi}\frac{\eta_D}{\kappa}\right)^{3/2}\exp\left\{-\mathbf{p}^2\frac{\eta_D}{\kappa}\right\}, \tag{8.32}$$

which coincides with the equilibrium (i.e. Boltzmann) momentum distribution for the heavy quark provided that

$$\eta_D = \frac{\kappa}{2MT}. \tag{8.33}$$

This expression is known as the Einstein relation. Thus, the Langevin dynamics of non-relativistic heavy quarks is completely determined by the momentum broadening κ, and the heavy quarks equilibrate at asymptotic times.

The Einstein relation (8.33) together with the computation of η_D in (8.13) for strongly coupled $\mathcal{N} = 4$ SYM theory allow us to infer the value of κ for this strongly coupled conformal plasma, namely

$$\kappa = \pi\sqrt{\lambda}T^3. \tag{8.34}$$

The dynamical equation (8.12) that we used in the previous section does not include the noise term simply because in that section we were describing the change in the mean heavy quark momentum only.

8.2.2 Direct calculation of the noise term

We would like to have a direct computation of the noise term in the description of a heavy quark in a strongly coupled gauge theory plasma. There are two motivations for this: (1) to explicitly check that the Einstein relation (8.33) is fulfilled and (2) to compute the momentum broadening for moving heavy quarks, which are not in equilibrium with the plasma and to which the Einstein relation therefore does not apply. This computation is somewhat technical; the reader interested only in the results for κ_T and κ_L for a moving heavy quark may skip to Section 8.2.3.

We need to express the momentum broadening in terms which are easily computed within the gauge/gravity correspondence. To do so, we prepare a state of the quark at an initial time t_0 which is moving at given velocity v in the plasma. In quantum mechanics, the state is characterized by a density matrix, which is a certain distribution of pure states

$$\rho(t_0) = \sum_n w(n) \, |n\rangle \, \langle n| \, , \qquad (8.35)$$

where the sum is performed over a complete set of states and the weight $w(n)$ is the ensemble. For a thermal distribution, the states are eigenstates of the Hamiltonian and $w(n) = \exp\{-E_n/T\}$.

In the problem we are interested in, the density matrix includes not only the quark degrees of freedom but also the gauge degrees of freedom. However, we start our discussion using a one-particle system. In this case, the distribution function of the particle is defined from the density matrix as

$$\hat{f}(x, x'; t_0) = \sum_n w(n) \, \langle x| \, n\rangle \, \langle n| \, x'\rangle \, , \qquad (8.36)$$

where, as usual, $\langle x| \, n\rangle$ is the wave function of the particle in the state $|n\rangle$. It is also common to call $f(x, x')$ the density matrix. It is conventional to introduce the mean and relative coordinates and express the density matrix as

$$f(X, r; t_0) = \hat{f}\left(X + \frac{r}{2}, X - \frac{r}{2}; t_0\right) , \qquad (8.37)$$

where $X = (x + x')/2$ and $r = x - x'$. It is then easy to see that the mean position and mean momentum of the single particle with a given density matrix are given by

$$\langle x \rangle = \operatorname{tr}\{\rho(t_0)\, x\} = \int dx\, x\, \hat{f}(x, x; t_0) = \int dX\, X f(X, 0; t_0),$$

$$\langle p \rangle = \operatorname{tr}\{\rho(t_0)\, p\} = \int dx\, \frac{-i}{2}\, (\partial_x - \partial_{x'})\, \hat{f}(x, x'; t_0)\Big|_{x'=x}$$

$$= -i \int dX\, \partial_r f(X, r; t_0)|_{r=0}, \tag{8.38}$$

meaning that r is the conjugate variable to the momentum and the mean squared momentum of the distribution is

$$\langle p^2 \rangle = -\int dX\, \partial_r^2\, f(X, r; t_0)|_{r=0}, \tag{8.39}$$

the result from this analysis of the one-particle system that we shall need below.

Returning now to the problem of interest to us, we must consider an ensemble containing the heavy quark and also the gauge field degrees of freedom. Since we assume the mass of the quark to be much larger than the temperature, we can describe the pure states of the system as

$$\left| A' \right\rangle = Q_a^\dagger(x)\, |A\rangle, \tag{8.40}$$

where $|A\rangle$ is a state of the gauge fields only, $|A'\rangle$ denotes a state of the heavy quark plus the gauge fields, and $Q_a^\dagger(x)$ is the creation operator (in the Schrödinger picture) of a heavy quark with color a at position x. Corrections to this expression are (exponentially) suppressed by T/M. The Heisenberg representation of the operator $Q(x)$ satisfies the equation of motion

$$(iu \cdot D - M)\, Q = 0, \tag{8.41}$$

where u is the four-velocity of the quark and D is the covariant derivative with respect to the gauge fields of the medium. This equation realizes the physical intuition that the heavy quark trajectory is not modified by the interaction with the medium, which leads only to a modification of the quark's phase. (The expression (8.41) can also be derived from the Dirac equation by performing a Foldy–Wouthuysen transformation, which in the heavy quark rest frame is given by $Q = \exp\{\gamma \cdot D/2M\}\, \psi$, where $\gamma = 1/\sqrt{1 - v^2}$.)

The full density matrix of the system, ρ, describes an ensemble of all the degrees of freedom of the system. Since we are only interested in the effects of the medium on the momentum of the heavy quark probe, we can define a one-body density matrix from the full density matrix by integrating over the gauge degrees of freedom

$$f(X, r; t_0) = \left\langle Q_a^\dagger \left(X - \frac{r}{2}; \right) U_{ab} Q_b \left(X + \frac{r}{2} \right) \right\rangle$$

$$= \operatorname{Tr}\left[\rho\, Q_a^\dagger \left(X - \frac{r}{2} \right) U_{ab} Q_b \left(X + \frac{r}{2} \right) \right], \tag{8.42}$$

where the trace is taken over a complete set of states

$$\sum_{A,a} \int dx \, Q_a^\dagger(x) \, |A\rangle \, \langle A| \, Q_a(x) \,. \tag{8.43}$$

Note that the inclusion of the operators in the trace in (8.42) plays the same role as the projectors $|x\rangle$ in (8.36). The gauge link U_{ab} in (8.42) joins the points $X + r/2$ and $X - r/2$ to ensure gauge invariance. In the long time limit, the precise path is not important, and we will assume that U_{ab} is a straight link. To simplify our presentation, we shall explicitly treat only transverse momentum broadening, which means taking the separation r to be in a direction perpendicular to the direction of motion of the heavy quark, $r = |\mathbf{r}_\perp|$.

At a later time t, after the heavy quark has propagated through the plasma for a time $t - t_0$, the one-body density matrix has evolved from (8.42) to

$$\begin{aligned}
f(X, \mathbf{r}_\perp; t) = \mathrm{Tr} \Big[& \rho \, e^{iH(t-t_0)} Q_a^\dagger \left(X - \frac{\mathbf{r}_\perp}{2} \right) e^{-iH(t-t_0)} \\
& e^{iH(t-t_0)} U_{ab} \, e^{-iH(t-t_0)} \\
& e^{iH(t-t_0)} Q_b \left(X + \frac{\mathbf{r}_\perp}{2} \right) e^{-iH(t-t_0)} \Big],
\end{aligned} \tag{8.44}$$

where we have introduced evolution operators to express the result in the Heisenberg picture. We then introduce a complete set of states, obtaining

$$\begin{aligned}
f(X, \mathbf{r}_\perp; t) = \int d\mathbf{x}_1 d\mathbf{x}_2 \sum_{A_1, A_2, A_3, A_4} & \rho_{a_1 a_2}[\mathbf{x}_1, \mathbf{x}_2; A_1, A_2] \\
& \langle A_2| \, Q_{a_2}(\mathbf{x}_2) Q_a^\dagger \left(X - \frac{\mathbf{r}_\perp}{2}; t \right) |A_3\rangle \\
& \langle A_3| \, U_{ab}(t) \, |A_4\rangle \\
& \langle A_4| \, Q_b \left(X + \frac{\mathbf{r}_\perp}{2}; t \right) Q_{a_1}^\dagger(x_1) \, |A_1\rangle \,,
\end{aligned} \tag{8.45}$$

where we have defined

$$\rho_{a_1 a_2}[\mathbf{x}_1, \mathbf{x}_2; A_1, A_2] \equiv \langle A_1| \, Q_{a_1}(\mathbf{x}_1) \, \rho \, Q_{a_2}^\dagger(\mathbf{x}_2) \, |A_2\rangle \,. \tag{8.46}$$

The expression (8.45) can be expressed as a path integral. Note that the expression in the second line of (8.45) is an anti-time-ordered correlator; thus, its path integral representation involves a time reversal of the usual path integral. Instead of introducing two separate path integrals corresponding to the second and fourth lines of (8.45), we introduce the time contour shown in Fig. 8.2 and use this contour to define a single path integral. In this contour the $-i\epsilon$ shift is inherited from the standard $i\epsilon$ prescription in field theory. The fields A_1 and A_2 are the values at the endpoints of the contour. The one-body density matrix then reads

$$X_0 = (t_0, x_0) \qquad t_c \qquad\qquad\qquad X = (t, x_0 + v\,\Delta t)$$

$$X_f = (t_0 - i\epsilon, x_0 - iv\epsilon) \qquad t'_c \qquad X = (t - i\epsilon, x_0 + v\,\Delta t - iv\epsilon)$$
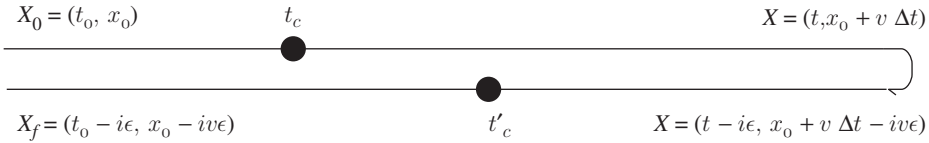
Figure 8.2 Time contour C in the complex time plane for the path integral (8.47). Here, $\Delta t \equiv t - t_0$ and the $i\epsilon$ prescription in time is translated to the longitudinal coordinate x since the quark trajectory is $x = vt$. The two-point functions computed from the partition function (8.47) are evaluated at two arbitrary points t_C and t'_C on the contour. Figure from Ref. [253].

$$f(X, \mathbf{r}_\perp; t) = \sum_{A_1, A_2} \int d\mathbf{x}_1 d\mathbf{x}_2 \int [\mathcal{D}A]\, \mathcal{D}Q\, \mathcal{D}Q^\dagger e^{i \int_C d^4 x \{\mathcal{L}_{YM} + Q^\dagger (iu\cdot D - M)Q\}}$$

$$\rho_{a_1 a_2}[\mathbf{x}_1, \mathbf{x}_2; A_1, A_2]\, U_{ab}(t)$$

$$Q_{a_2}(\mathbf{x}_2, t_0 - i\epsilon)\, Q_a^\dagger\left(X - \frac{\mathbf{r}_\perp}{2}, t - i\epsilon\right)$$

$$Q_b\left(X + \frac{\mathbf{r}_\perp}{2}, t\right) Q_{a_1}^\dagger(\mathbf{x}_1, t_0)\,. \tag{8.47}$$

By generalizing the static heavy quark computations in Ref. [611] to nonzero velocity, standard techniques for fermionic path integrals can be used to do the path integrals over the heavy quark fields in (8.47). To do so, we must compute the Green's function of the quark fields for a fixed configuration of gauge fields, namely

$$i\mathcal{G}(2, 1) = \langle T_C Q_{a_2}(\mathbf{x}_2, t_{2C})\, Q_{a_1}^\dagger(\mathbf{x}_1, t_{1C})\rangle, \tag{8.48}$$

where t_C is the time along the contour and T_C denotes the contour ordered product. Since the quark Lagrangian has only one dynamical spacetime variable, the Green's function satisfies

$$(iu \cdot D - M)\, i\mathcal{G}(2, 1) = i\delta^3(\mathbf{x}_2 - \mathbf{x}_1)\delta_C(t_{2C} - t_{1C})\,, \tag{8.49}$$

which has the solution

$$i\mathcal{G}(2, 1) = e^{+iMu\cdot(X_2 - X_1)} \int_C \frac{dt_C}{\gamma}\, \theta(t_C - t_{1C})\, \delta_C^4(X_2 - X_{x_1}(t_C))$$

$$\times \left[P \exp\left(-i \int_{t_{1C}}^{t_C} \frac{dt'_C}{\gamma}\, u^\mu A_\mu(X_{x_1}(t'_C))\right)\right]_{a_2 a_1}, \tag{8.50}$$

where $X_{x_1}^\mu(t_C) = X_1^\mu + u^\mu(t_C - t_{1C})/\gamma$ is the heavy quark worldline that passes through X_1. Carrying out this integration over the quark field and working to leading order in T/M (which means neglecting the fermionic determinant) yields

$$f(X, \mathbf{r}_\perp; t) = \left\langle \mathrm{tr}\left[\rho\left[X + \frac{\mathbf{r}_\perp}{2}, X - \frac{\mathbf{r}_\perp}{2}; A_1, A_2\right] W_C\left[\frac{\mathbf{r}_\perp}{2}, -\frac{\mathbf{r}_\perp}{2}\right]\right]\right\rangle_A, \tag{8.51}$$
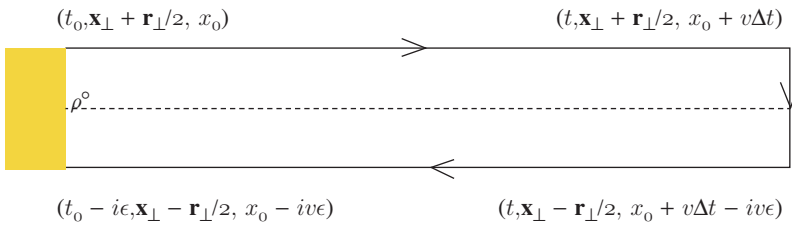
Figure 8.3 Graphical representation of Eq. (8.51). The Wilson line indicated by the black line is denoted $W_{\mathcal{C}}[\mathbf{r}_\perp/2, -\mathbf{r}_\perp/2]$. This Wilson line is traced with the initial density matrix, $\rho^o_{a_1 a_2}$. The horizontal axis is along the time direction and the vertical axis is along one of the transverse coordinates, $x_\perp$. $\Delta t \equiv t - t_0$. Figure from Ref. [253].

where the subscript A indicates averaging with respect to the gauge fields, and where the Wilson line $W_{\mathcal{C}}\left[\mathbf{r}_\perp/2, -\mathbf{r}_\perp/2\right]$ is defined in Fig. 8.3. We have used the fact that the Green's function of Eq. (8.41) is the (contour ordered) Wilson line.

Next, we perform a Taylor expansion of the time-evolved density matrix (8.51) about $\mathbf{r}_\perp = 0$, obtaining

$$
f(X, \mathbf{r}_\perp; t) = f(X, 0; t) +
$$
$$
\frac{\mathbf{r}_\perp^2}{2} \left\langle \mathrm{tr}\left[\frac{\partial^2}{\partial \mathbf{r}_\perp^2} \rho\left[X + \frac{\mathbf{r}_\perp}{2}, X - \frac{\mathbf{r}_\perp}{2}; A_1, A_2 \right] W_{\mathcal{C}}[0] \right] \right\rangle_A +
$$
$$
\frac{\mathbf{r}_\perp^2}{2} \kappa_T \Delta t \, \langle \mathrm{tr}\left[\rho[X, X; A_1, A_2] W_{\mathcal{C}}[0] \right] \rangle_A + \mathcal{O}(\mathbf{r}_\perp^4). \quad (8.52)
$$

The second term in this expression involves only derivatives of the initial density matrix; thus, as in (8.39) it is the mean transverse momentum squared of the initial distribution (which may be supposed to be small). In the last term, which scales with the elapsed time Δt, we have defined

$$
\kappa_T \Delta t = \frac{1}{4} \frac{1}{\langle \mathrm{tr} \rho \, W_{\mathcal{C}}[0]\rangle_A} \int_{\mathcal{C}} dt_{\mathcal{C}} dt'_{\mathcal{C}} \left\langle \mathrm{tr}\, \rho[X, X; A_1, A_2] \frac{\delta^2 W_{\mathcal{C}}[\delta y]}{\delta y(t_{\mathcal{C}})\, \delta y(t'_{\mathcal{C}})} \right\rangle_A, \quad (8.53)
$$

where $t_{\mathcal{C}}$ denotes time along the contour depicted in Fig. 8.2, and $\kappa_T \Delta t$ is the mean transverse momentum squared picked up by the heavy quark during the time Δt. We have expressed the transverse derivatives of the Wilson line as functional derivatives with respect to the path of the Wilson line. The path δy denotes a small transverse fluctuation $\delta y(t)$ away from the path $X_1 = vt$.

The contour δy may be split into two pieces, δy_1 and δy_2, which run along the time-ordered and anti-time-ordered part of the path. Thus, the fluctuation calculation defines four correlation functions

$$iG_{11}(t, t') = \frac{1}{\langle \mathrm{tr}\rho^o W_C[0, 0]\rangle_A} \left\langle \mathrm{tr}\,\rho^o \frac{\delta^2 W_C[\delta y_1, 0]}{\delta y_1(t)\,\delta y_1(t')} \right\rangle_A, \qquad (8.54)$$

$$iG_{22}(t, t') = \frac{1}{\langle \mathrm{tr}\rho^o W_C[0, 0]\rangle_A} \left\langle \mathrm{tr}\,\rho^o \frac{\delta^2 W_C[0, \delta y_2]}{\delta y_1(t)\,\delta y_2(t')} \right\rangle_A, \qquad (8.55)$$

$$iG_{12}(t, t') = \frac{1}{\langle \mathrm{tr}\rho^o W_C[0, 0]\rangle_A} \left\langle \mathrm{tr}\,\rho^o \frac{\delta^2 W_C[\delta y_1, \delta y_2]}{\delta y_1(t)\,\delta y_2(t')} \right\rangle_A, \qquad (8.56)$$

$$iG_{21}(t, t') = \frac{1}{\langle \mathrm{tr}\rho^o W_C[0, 0]\rangle_A} \left\langle \mathrm{tr}\,\rho^o \frac{\delta^2 W_C[\delta y_2, \delta y_2]}{\delta y_1(t')\,\delta y_2(t)} \right\rangle_A. \qquad (8.57)$$

Note that the first two correlators correspond to time-ordered and anti-time-ordered correlators, while the last two are unordered. We can then divide the integration over t_C and $t_{C'}$ in (8.53) into four parts corresponding to the cases where each of t_C and $t_{C'}$ is on the upper or lower half of the contour in Fig. 8.2. In the large Δt limit we can then use time translational invariance to cast (8.53) as

$$\kappa_T = \lim_{\omega \to 0} \frac{1}{4} \int dt\, e^{+i\omega t} \left[iG_{11}(t, 0) + iG_{22}(t, 0) + iG_{12}(t, 0) + iG_{21}(t, 0) \right]. \qquad (8.58)$$

This admittedly rather formal expression for κ_T is as far as we can go in general. In Section 8.2.3 we evaluate κ_T (and κ_L) in the strongly coupled plasma of $\mathcal{N} = 4$ SYM theory.

Although our purpose in deriving the expression (8.58) is to use it to analyze the case $v \neq 0$, it can be further simplified in the case that $v = 0$. On the time scales under consideration, the static quark is in equilibrium with the plasma, and the Kubo–Martin–Schwinger relation which takes the form

$$i\left[G_{11}(\omega) + G_{22}(\omega) + G_{12}(\omega) + G_{21}(\omega)\right] = -4\coth\left(\frac{\omega}{2T}\right)\mathrm{Im}G_R(\omega) \qquad (8.59)$$

once ϵ has been allowed to vanish applies [571]. Here, G_R is the retarded correlator. Thus, we find

$$\kappa_T(v = 0) = \lim_{\omega \to 0}\left(-\frac{2T}{\omega}\right)\mathrm{Im}\,G_R(\omega). \qquad (8.60)$$

If $v \neq 0$, however, we must evaluate the four correlators in the expression (8.58).

8.2.3 κ_T and κ_L for a moving heavy quark

We see from the expression (8.53) that the transverse momentum broadening coefficient κ_T is extracted by analyzing small fluctuations in the path of the Wilson line depicted in Fig. 8.3. In the strongly coupled plasma of $\mathcal{N} = 4$ SYM theory, we can use gauge/gravity duality to evaluate κ_T starting from (8.53). In the dual gravitational description, the small fluctuations in the path of the Wilson line amount

to perturbing the location on the boundary at which the classical string (whose unperturbed shape is given by (8.9)) terminates according to

$$(x_1(t, z), 0, 0) \rightarrow (x_1(t, z), y(t, z), 0) . \tag{8.61}$$

The perturbations of the Wilson line at the boundary yield fluctuations on the string world sheet dragging behind the quark. Because we wish to calculate κ_T, in (8.61) we have only introduced perturbations transverse to the direction of motion of the quark. We shall quote the result for κ_L at the end; calculating it requires extending (8.61) to include perturbations to the function $x_1(t, z)$.

In order to analyze fluctuations of the string worldsheet, we begin by casting the metric induced on the string worldsheet in the absence of any perturbations

$$ds_{\mathrm{ws}}^2 = \frac{R^2}{z^2} \left(- \left(f(z) - v^2 \right) d\tau^2 + \frac{\hat{f}(z)}{f^2(z)} d\sigma^2 - v^2 \frac{z^2/z_0^2}{f(z)} \left(d\tau d\sigma + d\sigma d\tau \right) \right) \tag{8.62}$$

in a simpler form. In (8.62), we have defined $\hat{f}(z) \equiv 1 - z^4/(z_0^4 \gamma^2)$. The induced metric (8.62) is diagonalized by the change of worldsheet coordinates

$$\hat{t} = \frac{t}{\sqrt{\gamma}} + \frac{z_0}{2\sqrt{\gamma}} \left(\arctan \left(\frac{z}{z_0} \right) - \operatorname{arctanh} \left(\frac{z}{z_0} \right) \right.$$
$$\left. - \sqrt{\gamma} \arctan \left(\frac{\sqrt{\gamma} z}{z_0} \right) + \sqrt{\gamma} \operatorname{arctanh} \left(\frac{\sqrt{\gamma} z}{z_0} \right) \right),$$
$$\hat{z} = \sqrt{\gamma} z , \tag{8.63}$$

in terms of which the induced metric takes the simple form

$$ds_{\mathrm{ws}}^2 = \frac{R^2}{\hat{z}^2} \left(- f(\hat{z}) d\hat{t}^2 + \frac{1}{f(\hat{z})} d\hat{z}^2 \right) . \tag{8.64}$$

Note that this has the same form as the induced metric for the worldsheet hanging below a motionless quark, upon making the replacement $(\hat{t}, \hat{z}) \rightarrow (t, z)$. In particular, the metric (8.64) has a horizon at $\hat{z} = z_0$, which means that the metric describing the worldsheet of the string trailing behind the moving quark has a worldsheet horizon at $z = z_{\mathrm{ws}} \equiv z_0/\sqrt{\gamma}$. For $v \rightarrow 0$, the location of the worldsheet horizon drops down toward the spacetime horizon at $z = z_0$. But, for $v \rightarrow 1$, the worldsheet horizon moves closer and closer to the boundary at $z = 0$, i.e. towards the ultraviolet. As at any horizon, the singularity at $z = z_{\mathrm{ws}}$ (i.e. at $\hat{z} = z_0$) in (8.64) is just a coordinate singularity. In the present case, this is manifest since (8.64) was obtained from (8.62) which is regular at $z = z_{\mathrm{ws}}$ by a coordinate transformation (8.63). Nevertheless, the worldsheet horizon has clear physical significance: at $z = z_{\mathrm{ws}}$ the local speed of light at this depth in the bulk matches the speed v with which the quark at the boundary is moving. Furthermore, and of direct relevance

to us here, because of the worldsheet horizon at $z = z_{\text{ws}}$ fluctuations of the string worldsheet at $z > z_{\text{ws}}$, below – to the infrared of – the worldsheet horizon, are causally disconnected from fluctuations at $z < z_{\text{ws}}$ above the worldsheet horizon and in particular are causally disconnected from the boundary at $z = 0$.

The remarkable consequence of the picture that emerges from the above analysis of the unperturbed string worldsheet trailing behind the quark at the boundary moving with speed v is that the momentum fluctuations of this quark can be thought of as due to the Hawking radiation on the string worldsheet, originating from the worldsheet horizon at $z = z_{\text{ws}}$ [396, 253]. It is as if the force fluctuations that the quark in the boundary gauge theory feels are due to the fluctuations of the string worldsheet to which it is attached, with these fluctuations arising due to the Hawking radiation originating from the worldsheet horizon. It will therefore prove useful to calculate the Hawking temperature of the worldsheet horizon, which we denote T_{ws}. As detailed in Appendix B this can be done in the standard fashion, upon using a further coordinate transformation to write the metric (8.64) in the vicinity of the worldsheet horizon in the form $ds_{\text{ws}}^2 = -b^2\rho^2 d\hat{t}^2 + d\rho^2$ for some constant b, where the worldsheet horizon is at $\rho = 0$. Then, it is a standard argument that in order to avoid having a conical singularity at $\rho = 0$ in the Euclidean version of this metric, namely $ds_{\text{ws}}^2 = b^2\rho^2 d\hat{\theta}^2 + d\rho^2$, $b\hat{\theta}$ must be periodic with period 2π. The periodicity of the variable $\hat{\theta}$, namely $2\pi/b$, is $1/T$. Since at the boundary, where $z = 0$, Eq. (8.63) becomes $\hat{t} = t/\sqrt{\gamma}$, this argument yields

$$T_{\text{ws}} = \frac{T}{\sqrt{\gamma}} \,, \tag{8.65}$$

a result that we shall use below.

We have gained significant physical intuition by analyzing the unperturbed string world sheet, but in order to obtain a quantitative result for κ_T we must introduce the transverse fluctuations $y(t, z)$ defined in (8.61) explicitly. We write the Nambu–Goto action for the string worldsheet with $y(t, z) \neq 0$, and expand it to second order in y, obtaining the zeroth order action (8.5) plus a second order contribution

$$S_T^{(2)}[y] = \frac{\gamma R^2}{2\pi\alpha'} \int \frac{d\hat{t}d\hat{z}}{\hat{z}^2} \frac{1}{2} \left(\frac{\dot{y}^2}{f(\hat{z})} - f(\hat{z}) y'^2 \right) \,, \tag{8.66}$$

where $\dot{\ }$ and $'$ represent differentiation with respect to $\hat{t}$ and $\hat{z}$ respectively. This action is conveniently expressed as

$$S_T^{(2)}[y] = -\frac{\gamma R^2}{2\pi\alpha'} \int \frac{d\hat{t}d\hat{z}}{\hat{z}^2} \frac{1}{2} \sqrt{-h} h^{ab} \partial_a y \partial_b y, \tag{8.67}$$

with h_{ab} the induced metric on the unperturbed worldsheet that we have analyzed above. The existence of the worldsheet horizon means that we are only interested

in solutions to the equations of motion for the transverse fluctuations y obtained from (8.67) that satisfy infalling boundary conditions at the worldsheet horizon. This constraint in turn implies a relation among the correlators analogous to those in (8.58) that describe the transverse fluctuations of the worldsheet, and in fact the relation turns out to be analogous to the Kubo–Martin–Schwinger relation (8.59) among the gauge theory correlators [253]. Consequently, for a quark moving with velocity v the transverse momentum broadening coefficient $\kappa_T(v)$ is given by the same expression (8.60) that is valid at $v = 0$ with T replaced by the worldsheet temperature T_{ws} of (8.65) [396, 253]. That is,

$$\kappa_T(v) = \lim_{\omega \to 0} \left(-\frac{2\, T_{\mathrm{ws}}}{\omega} \mathrm{Im} \hat{G}_R(\omega) \right), \qquad (8.68)$$

where $\hat{G}_R$ denotes the retarded correlator at the worldsheet horizon. The fact that in the strongly coupled theory there is a KMS-like relation at $v \neq 0$ after all is a non-trivial consequence of the development of the worldsheet horizon.

The computation of the retarded correlator follows the general procedure of Ref. [747] described in Section 5.3. Since the action (8.66) is a function of $\hat{t}$ which is given by $t/\sqrt{\gamma}$ at the boundary, the retarded correlator is a function of $\hat{\omega} = \sqrt{\gamma}\omega$ (with ω the frequency of oscillations at the boundary). To avoid this complication, and in particular in order to be able to apply the general results for $\mathrm{Im}\, G_R$ that we derived in Section 6.2, it is convenient to define

$$\tilde{t} = \sqrt{\gamma}\, \hat{t}, \qquad (8.69)$$

so that $\tilde{t} = t$ at the boundary. We now wish to apply the general expressions (A.10), (6.17) and (6.18). In order to do so, we identify the world sheet metric h^{ab} and the field y in the action (8.67) with the metric g^{MN} and the field ϕ in the action (6.16), meaning that in our problem the function q in (6.16) takes the specific form

$$\frac{1}{q(z)} = \frac{\gamma R^2}{2\pi\alpha'}\frac{1}{\hat{z}^2} = \frac{\sqrt{\lambda}}{2\pi z^2}. \qquad (8.70)$$

Furthermore, for the two-dimensional worldsheet metric we have $-h = h_{\tilde{t}\tilde{t}}h_{zz}$, meaning that from the general result (6.25) we find

$$-\lim_{\omega \to 0}\frac{\mathrm{Im}\, \hat{G}_R(\omega)}{\omega} = \frac{1}{q(z_{\mathrm{ws}})} = \frac{\gamma\sqrt{\lambda}}{2\pi}(\pi T)^2, \qquad (8.71)$$

and thus

$$\kappa_T = \sqrt{\lambda\gamma}\,\pi T^3, \qquad (8.72)$$

which is our final result for the transverse momentum broadening coefficient.

The analysis of longitudinal fluctuations and the extraction of κ_L proceed analogously to the analysis we have just presented, except that in (8.61) we introduce a

perturbation to the function x_1 instead of a transverse perturbation y. At quadratic order, there is no coupling between the transverse and longitudinal perturbations. Remarkably, the action for longitudinal fluctuations of the string is the same as that for transverse fluctuations, Eq. (8.66) up to a constant:

$$S_L^{(2)}[x] = \gamma^2 S_T^{(2)}[x] \,, \tag{8.73}$$

with γ the Lorentz factor. Following the analogous derivation through, we conclude that

$$\kappa_L = \gamma^2 \kappa_T = \gamma^{5/2} \sqrt{\lambda} \pi T^3 \,. \tag{8.74}$$

This result shows that κ_L depends very strongly on the velocity of the heavy quark. Indeed, κ_L grows faster with increasing velocity than the energy squared of the heavy quark, $\gamma^2 M^2$. Thus, the longitudinal momentum acquired by a quark moving through a region of strongly coupled $\mathcal{N} = 4$ SYM plasma of finite extent does not become a negligible fraction of the energy of the quark in the high energy limit. This is very different from the behavior of a quark moving through a weakly coupled QCD plasma, in which the longitudinal momentum transferred to the quark can be neglected in the high energy limit. However, we should keep in mind that, due to the bound (8.18), for a given value of the mass M and the coupling $\sqrt{\lambda}$ the calculation of κ_L (and of κ_T) is only valid for finite energy quarks, with γ limited by (8.18).

The fact that κ_L grows faster with γ than $\gamma^2 M^2$ would seem to indicate that once the heavy quark has traveled through the medium for a distance L so long that $\kappa_L L > \gamma^2 M^2$, meaning

$$L\pi T > \left(\frac{M}{T}\right)^2 \frac{1}{\sqrt{\gamma \lambda}} \,, \tag{8.75}$$

the calculation in this section must break down since the fluctuations in the longitudinal momentum of the quark have become greater than the momentum itself. In fact, this criterion never comes into play because the calculation always "breaks down", in a trivial sense, earlier. The heavy quark feels a drag force given by (8.12), meaning that after it has traveled a distance $L = 1/\eta_D$, its momentum has been degraded by a factor of order 1. This means that calculating the longitudinal fluctuations as if the γ of the quark is constant, and comparing $\kappa_L L$ to the initial momentum of the quark, only makes sense for $L < 1/\eta_D$, which according to (8.13) means that L must satisfy

$$L\pi T < \frac{2M}{T} \frac{1}{\sqrt{\lambda}} \,. \tag{8.76}$$

We have already seen that the entire calculation is valid only as long as the criterion (8.18) is satisfied, which is to say $(M/T) > \sqrt{\gamma \lambda}$. This means that at the L at

which the criterion (8.76) ends the calculation, $\kappa_L L$ is smaller than $\gamma^2 M^2$ by at least a factor of order $\sqrt{\lambda}$, and the regime (8.75) is never reached.

We see from the expressions (8.72) and (8.74) for κ_T and κ_L derived by explicit analysis of the fluctuations that in the $v \to 0$ limit we have $\kappa_T = \kappa_L = \kappa$ with κ given by (8.34), as we obtained previously from the drag coefficient η_D via the use of the Einstein relation (8.33). This is an example of the fluctuation–dissipation theorem.

In the gauge theory, momentum broadening is due to the fluctuating force exerted on the heavy quark by the fluctuating plasma through which it is moving. In the dual gravitational description, the quark at the boundary feels a fluctuating force due to the fluctuations of the world sheet that describes the profile of the string to which the quark is attached. These fluctuations have their origin in the Hawking radiation of fluctuations of the string worldsheet originating from the worldsheet horizon. The explicit computation of this worldsheet Hawking radiation for a quark at rest was performed in Refs. [311, 751], and these results nicely reproduce those we have obtained within the Langevin formalism. This computation was extended to quarks moving at nonzero velocity in Refs. [378, 254].

8.2.4 Heavy quarks in hot QCD and in heavy ion collisions

So far, we have discussed a general framework for calculating the transverse and longitudinal momentum broadening κ_T and κ_L that enter the Langevin equations (8.24) and (8.25) for non-relativistic heavy quarks. We have then given explicit results for strongly coupled $\mathcal{N} = 4$ SYM theory. We now discuss how these results relate to, and help us to understand, what we know about hot QCD and about the phenomenology of heavy ion collisions. We consider the case in which the relative velocity of the heavy quark and the hot fluid is small, meaning that $\kappa_T = \kappa_L \equiv \kappa$. In this regime, the heavy quark is carried along by the moving fluid, diffusing within it with a diffusion constant that is given by

$$D = \frac{2T^2}{\kappa} \,, \tag{8.77}$$

meaning that the result (8.34) translates into the statement that a heavy quark in the strongly coupled $\mathcal{N} = 4$ SYM theory plasma obeys a Langevin equation with

$$D = D_{\text{SYM}} \equiv \frac{4}{\sqrt{\lambda}} \frac{1}{2\pi T} \approx \frac{1.1}{2\pi T} \sqrt{\frac{1}{\alpha_{\text{SYM}} N_c}} \,. \tag{8.78}$$

The diffusion constant D parametrizes how strongly the heavy quark couples to the medium. At weak coupling, smaller D corresponds to stronger coupling and shorter mean free path. However, D is well defined even if it is so small that it

does not even make sense to define a mean free path for the heavy quark, as is the case in the plasma of strongly coupled $\mathcal{N} = 4$ SYM theory in which D is given by (8.78) with λ large. Recall that in this case we have calculated κ, and hence D, in the earlier parts of this section without ever defining the notion of a mean free path.

In a QCD plasma that is hot enough that it is sufficiently weakly coupled that lowest order perturbation theory can be used as a guide, we also have reliable information about the diffusion constant. In this regime, D is large and the diffusing heavy quark has a long mean free path. Leading order perturbative calculations for a weakly coupled QCD plasma [628] can be summarized by an approximate expression

$$D_{\text{weakly coupled QCD}} \approx \frac{14}{2\pi T} \left(\frac{0.33}{\alpha_s} \right)^2 , \qquad (8.79)$$

in which we have neglected an additional logarithmic dependence on α_s. However, the perturbative expansion converges quite poorly meaning that this result only becomes quantitatively reliable at values of α_s that are much smaller than 0.33 [237, 238]. Nevertheless, we note that if we simply compare (8.78) and (8.79) with $N_c = 3$ and $\alpha_{\text{SYM}} = \alpha_s = 0.33$ (or 0.5) the diffusion constant in a strongly coupled $\mathcal{N} = 4$ SYM plasma is smaller than that in a weakly coupled QCD plasma by a factor of about 12 (or 7). It is reasonable to guess that the diffusion constant for a heavy quark in the strongly coupled QCD plasma produced in heavy ion collisions lies between these two estimates. Indeed, early estimates of nonperturbative contributions to D in the strongly coupled QCD plasma suggested that at a temperature $T = 200$ MeV it should have a D that is smaller than the weakly coupled result by a factor of three or four [784]. Before we turn to a discussion of what can be inferred from experiments to date, we shall discuss in turn two possible paths toward improved theoretical predictions. Neither (8.78) nor (8.79) can be applied quantitatively to the strongly coupled plasma produced in heavy ion collisions even though each is reliable in a certain domain – in one case in the strongly coupled plasma of a non-Abelian gauge theory that is not QCD and in the other case in the weakly coupled QCD plasma at temperatures that are orders of magnitude higher than those accessed in experiment.

We first ask whether it is possible to sharpen inferences concerning the value of D in the strongly coupled plasma of QCD that can be drawn from the result (8.78). Can we do better than just comparing $\mathcal{N} = 4$ SYM theory and QCD at $\alpha_{\text{SYM}} = \alpha_s$? We need to ask how D would change if we could deform $\mathcal{N} = 4$ SYM theory so as to turn it into QCD. This is not a question to which the answer is known, but we can make several observations. First, in a large class of conformal theories, at a given value of T, N_c and λ both the drag coefficient η_D and κ (and therefore

$1/D$) scale with the square root of the entropy density [584]. (The argument is the same as that for the jet quenching parameter $\hat{q}$, and we shall describe it briefly in Section 8.5.) The number of degrees of freedom in QCD is smaller than that in $\mathcal{N} = 4$ SYM theory by a factor of 47.5/120 for $N_c = 3$, suggesting that κ and η_D should be smaller in QCD by a factor of $\sqrt{47.5/120} = 0.63$, making D larger by a factor of $\sqrt{120/47.5} = 1.59$. Note that η_D and $1/D$ scale in the same way even though they are proportional to T^2 and T respectively, meaning that scaling these quantities between two theories with different numbers of degrees of freedom is not equivalent to scaling the temperature. Second, $\mathcal{N} = 4$ SYM theory is of course conformal, while QCD is not. Analysis of one toy model in which nonconformality can be introduced by hand suggests that turning on nonconformality to a degree suggested by lattice calculations of QCD thermodynamics reduces D somewhat, by a few tens of percent or perhaps at most by a factor of two [585]. Turning on nonconformality in $\mathcal{N} = 2^*$ theory also reduces D [468]. In a different model, however, reducing the number of degrees of freedom as in QCD and simultaneously turning on nonconformality (again to a degree benchmarked against lattice calculations of $(\epsilon - 3P)/T^4$) increases D by a factor of two to five [419]. We conclude that, at present, D in a strongly coupled QCD plasma cannot be inferred reliably from these arguments, with the reduction in degrees of freedom increasing D relative to (8.78) while the nonconformality may push in the opposite direction or may increase D further. We can summarize the current uncertainty by estimating that D in the strongly coupled plasma of QCD is larger than that in (8.78) by a factor that lies between one and five.

The other possible route to improved theoretical predictions of D in the strongly coupled plasma of QCD is lattice quantum field theory. This route is not straightforward since diffusion is a real time process meaning that D cannot be written directly in terms of derivatives of the thermodynamic partition function. As we have already seen in our discussion of the lattice determination of spectral functions via the maximum entropy method in Chapter 3, constraining real time correlators using lattice calculations done at finitely many points in imaginary time necessarily involves making additional assumptions. In the particular case of the diffusion constant D, however, it is possible to make progress [240]. In the large quark mass limit, heavy quark effective theory can be used to relate D to a certain Euclidean correlation function involving color–electric fields that can be related by analytic continuation to the random force two-point correlators $\langle \xi(t) \xi(t') \rangle = \kappa \delta(t - t')$ appearing in (8.25). Furthermore, unlike in the case of the transport quantities that we have discussed in Section 6.3, in this case there is no transport peak in the relevant spectral function. Quite unlike the case illustrated in Fig. 6.1, here the relevant spectral function is featureless at small frequency at weak coupling [240]. This indicates that at least in principle it should be possible to constrain D reliably

from Euclidean lattice calculations. A first, exploratory, study based on this method is underway [357], to date only in the $SU(3)$ gluon plasma (QCD without quarks) and to date with the continuum limit and the infinite volume limit not yet taken. Although exploratory, these calculations are already unambiguous in showing that D_{QCD} is significantly smaller than $D_{\text{weakly coupled QCD}}$ in (8.79), as can be anticipated from the general consideration that smaller D corresponds to smaller mean free paths. The calculations suggest that [357]

$$D_{\text{lattice QCD}} \sim \frac{3-5}{2\pi T}, \tag{8.80}$$

for QCD without quarks in a temperature range between $1.5T_c$ and $3T_c$, and taking into account only statistical uncertainties. The systematic uncertainties in this estimate remain to be quantified. It is nevertheless intriguing to see the estimate (8.80) obtained from pioneering lattice calculations landing in the same range as the estimate we came to in the previous paragraph by considering the (also pioneering) attempts to investigate how the estimate (8.78) for D would change if we could deform $\mathcal{N} = 4$ SYM theory so as to turn it into QCD.

In heavy ion collisions, information about the motion of heavy quarks in the plasma is experimentally accessible via measurements of the semi-leptonic or hadronic decay products of heavy-flavored hadrons. In general, two classes of observables can be expected to provide experimental constraints on the Langevin dynamics of heavy quarks. First, heavy quarks lose energy by drag, as discussed in Section 8.1. Therefore, the characterization of heavy quark energy loss via the nuclear modification factor of the observed decay products of heavy-flavored hadrons can constrain the drag coefficient η_D and, via (8.33) and (8.77) in the case where the heavy quark velocity is not large, the diffusion coefficient D. Second, if D is small enough that on the time scales available in a heavy ion collision the motion of the heavy quarks is diffusive (i.e. if the heavy quark mean free path is not so long that the heavy quarks scatter only a few times) then by the time the plasma hadronizes the heavy quarks will have been picked up (or slowed down) and carried along by the collective flow of the strongly coupled liquid in which they find themselves. That is, if D is small enough the heavy quarks diffusing in the moving fluid will end up with the same mean velocity as the fluid itself. This results in a non-vanishing elliptic flow v_2 for heavy quarks with transverse momenta of order their mass or smaller. While there are parton energy loss processes that do not involve Langevin dynamics (see for instance the radiative parton energy loss discussed in Section 2.3), the observation of sizable elliptic flow in the decay products of heavy-flavored hadrons [18] provides strong support for the picture that the dynamics of non-relativistic heavy quarks produced in heavy ion collisions is

described by a Langevin equation with a small enough D that the diffusing heavy quarks end up being carried along by the moving fluid.

The qualitative considerations above indicate that measurements of R_{AA} and v_2 for the decay products of heavy-flavored hadrons can be used to constrain the heavy quark diffusion constant D. Many authors are developing models based upon Langevin dynamics to describe the motion of heavy quarks within the hot expanding fluid produced in heavy ion collisions [628, 785, 464, 784, 32, 138, 410, 706, 656, 658, 41]. Many of these analyses include comparisons to data on isolated electrons, which are most probably produced in the decays of mesons containing either c or b quarks but with which there is no way to separate these two contributions. The more refined measurements needed to separately identify the decay products of hadrons containing c and b quarks are the object of intense experimental effort at the time of writing. There are also significant theoretical uncertainties related to determining the range of validity of a Langevin analysis. For example, to focus on heavy quarks whose relative velocity through the hot strongly coupled fluid was sufficiently small one seeks to study the decay products of heavy-flavored hadrons at sufficiently small transverse momentum, but a quantitative criterion for what "sufficiently small" means is missing. Without discussing these model-dependent uncertainties in more detail, we emphasize here that data from heavy ion collisions show two robust qualitative features: the observed elliptic flow of the decay products of heavy-flavored hadrons and the heavy quark energy loss measured via the nuclear modification factor of the same decay products are comparable to the elliptic flow and nuclear modification factor of light-flavored hadrons. Both these classes of observations provide strong qualitative support to a picture in which heavy quarks lose energy efficiently and end up following the flow field of the strongly coupled plasma. This explains why even given all the uncertainties that make a quantitative determination difficult at present, the comparisons between models of Langevin dynamics and heavy ion collision data all typically favor small values of the diffusion constant D. For example, two studies that compare Langevin dynamics to RHIC data yield [32]

$$D_{\text{QGP@RHIC}} \approx \frac{2-6}{2\pi T} \tag{8.81}$$

and [784]

$$D_{\text{QGP@RHIC}} \approx \frac{3-5}{2\pi T}. \tag{8.82}$$

These phenomenologically determined values of the diffusion constant are remarkably similar to the estimate that the diffusion constant in the quark–gluon plasma of QCD is one to five times greater than the result obtained in (8.78) for the plasma of strongly coupled $\mathcal{N} = 4$ SYM theory and to the estimate (8.80) obtained in lattice

calculations. So, although there is plenty of room for improvement on all fronts, at present this story hangs together rather well indeed.

8.3 Disturbance of the plasma induced by an energetic heavy quark

In Sections 8.1 and 8.2 we have analyzed the effects of the strongly coupled plasma of $\mathcal{N} = 4$ SYM theory on an energetic heavy quark moving through it, focusing on how the heavy quark loses energy in Section 8.1 and on the momentum broadening that it experiences in Section 8.2. In this section, we turn the tables and analyze the effects of the energetic heavy quark on the medium through which it is propagating [713, 763, 245, 719, 727, 708, 244, 246, 709, 363, 811, 399, 810, 288, 403, 408, 400, 289, 655, 652, 401, 648, 657, 649, 423, 147, 148, 650, 410, 651, 149]. From the point of view of QCD calculations and heavy ion collision phenomenology, the problem of understanding the response of the medium to an energetic probe is quite complicated. An energetic particle passing through the medium can excite the medium on many different wavelengths. Furthermore, even if the medium had thermalized prior to its interaction with the probe, the disturbance caused by the probe must drive the medium out of equilibrium, at least close to the probe. And, non-equilibrium processes are difficult to treat, especially at strong coupling.

Furthermore, in general the formulation of how an energetic heavy quark interacts with the medium requires detailed information about the microscropic dynamics that couples the hard probe and the medium, meaning that in almost all analyses quantum field theory and hydrodynamics must be supplemented by model-dependent assumptions. There is but one known example where a field theoretically consistent formulation of heavy quark energy loss in a strongly coupled plasma determines fully and without additional model-dependence how this hard probe excites the medium. This is the holographic formulation of heavy quark energy loss via drag that we have discussed in detail in Section 8.1. That the gauge/gravity correspondence provides such a unique arena for studying plasma excitations induced by hard probes justifies the detailed discussion of these excitations that we shall present in this section.

At various points in the following, we shall compare plasma disturbances calculated via gauge/gravity duality to hydrodynamic excitations. The latter can be formulated in a simple model in which the energetic heavy quark is modeled as a simple line source in the hydrodynamic equations of motion for the fluid. The model-dependence of this fluid dynamic picture of probe–medium interactions resides in the details of the source term entering the hydrodynamic equations and, of course, in the assumption that the hard probe excites only hydrodynamic perturbations. There are, however, several reasons for starting our discussion with this simple model in Section 8.3.1. First, historically, the analysis of jet–medium

interactions started with the discussion of such hydrodynamical models. Moreover, as we have seen throughout this book, the strongly coupled $\mathcal{N} = 4$ SYM plasma is an almost perfect fluid. This makes it natural to discuss within a hydrodynamic picture the perturbations induced by heavy quarks in the strongly coupled $\mathcal{N} = 4$ SYM plasma. In particular, as we shall see in the following, a hydrodynamic model of jet–medium interactions provides a simple setting in which to disentangle different classes of hydrodynamic perturbations in the fluid. For a hard probe that propagates along a straight-line trajectory with a velocity v larger than the sound velocity in the plasma, one expects the excitation of two kinds of hydrodynamic perturbations. First, there should be sound waves that form a Mach cone, namely a sound front moving away from the trajectory of the energetic particle at the Mach angle

$$\cos \Theta_M = \frac{c_s}{v} \, . \tag{8.83}$$

In addition, however, it is reasonable to expect that even a pointlike source in the hydrodynamic equations should perturb the fluid through which the heavy quark has moved, stirring it up and/or setting it into motion following behind the quark that disturbed it. Certainly a macroscopic object moving through a fluid leaves a wake behind, and to some degree so too should a pointlike heavy quark. As we shall discuss, both a Mach cone and a wake can be accommodated in the hydrodynamical modeling of jet–medium interactions, but hydrodynamic considerations alone do not determine their relative importance. And, their relative importance will prove important in assessing the possibility that heavy quark energy loss in heavy ion collisions may result in observable Mach-cone-like patterns in the final state hadrons. We shall see that both a Mach cone and a wake are found in the holographic computation of the response of the $\mathcal{N} = 4$ SYM plasma to a heavy quark probe that we present in Section 8.3.2, and in this context their relative importance is fully determined. Keeping this destination in mind, the detailed discussion in Section 8.3.1 of the hydrodynamic framework within which these phenomena in fluid physics can be pictured easily will be very useful.

8.3.1 Hydrodynamic preliminaries

It is natural to attempt to describe the disturbance of the medium using hydrodynamics, with the energetic particle treated as a source for the hydrodynamic equations. This approach is based on two assumptions. First, one must assume that the medium itself can be described hydrodynamically. Second, one has to assume that the non-equilibrium disturbance in the vicinity of the energetic particle relaxes to some locally equilibrated (but still excited) state after the energetic particle has passed on a timescale that is short compared to the lifetime of the hydrodynamic

medium itself. The first assumption is clearly supported by data from heavy ion collisions at RHIC and the LHC, as discussed in Section 2.2. The second assumption is stronger, and less well justified. Even though, as we saw in Section 2.2, there is evidence from the data that in heavy ion collisions a hydrodynamic medium in local thermal equilibrium forms rapidly, after only a short initial thermalization time, it is not clear *a priori* that the relaxation time for the disturbance caused by an energetic quark plowing through this medium is comparably short, particularly since the density of the medium drops with time. Finally, even if a hydrodynamic approach to the dynamics of these disturbances is valid, the details of the functional form of this hydrodynamic source are unknown, since the relaxation process is not under theoretical control.

Keeping the above difficulties in mind, it is still possible to use the symmetries of the problem and some physical considerations to make some progress toward understanding the source for the hydrodynamic equations corresponding to the disturbance caused by an energetic quark. If the propagating parton is sufficiently energetic, we may assume that it moves at a fixed velocity; this ansatz forces the source to be a function of $x - vt$, with the parton moving in the x-direction. We may also assume that the source has cylindrical symmetry around the parton direction. We may also constrain the source by the amount of energy and momentum that is fed into the plasma, which for the case of the plasma of strongly coupled $\mathcal{N} = 4$ SYM theory we calculated in Section 8.1. In an infinite medium, at late enough times, all the energy lost by the probe must thermalize and be incorporated into heating and/or hydrodynamic motion. (This may not be a good approximation for a very energetic parton propagating through weakly coupled plasma of finite extent since, as we have discussed in Section 2.3, in this setting the parton loses energy by the radiation of gluons whose energy and momentum are large relative to the temperature of the medium, which may escape from the medium without being thermalized.) Although the caveats above caution against attempting to draw quantitative conclusions without further physical inputs, the success of the hydrodynamical description of the medium itself support the conclusion that there must be some hydrodynamic response to the passage of the energetic particle through it.

From the point of view of hydrodynamics, the disturbance of the medium induced by the passage of an energetic probe must be described by adding some source to the conservation equation:

$$\partial_\mu T^{\mu\nu}(x) = J^\nu(x) . \tag{8.84}$$

As we have stressed above, we do not know the functional form of the source, since it not only involves the way in which energy is lost by the energetic particle but also how this energy is thermalized and how it is incorporated into the

medium. The source will in general depend not only on the position of the quark but also on its velocity. In this subsection, we will use general considerations valid in any hydrodynamic medium to constrain the functional form of the source. From Eq. (8.84) it is clear that the amount of energy–momentum deposited in the plasma is given by.

$$\frac{dP^\nu}{dt} = \int d^3x \, J^\nu(x) \,. \tag{8.85}$$

We note as an aside that if the source moves supersonically, one component of its energy loss is due to the emission of sound waves. This is conventionally known as sonic drag, and is a part of the energy loss computed in Section 8.1.

We now attempt to characterize the hydrodynamic modes that can be excited in the plasma due to the deposition of the energy (8.85). We will assume, for simplicity, that the perturbation on the background plasma is small. We will also assume than the background plasma is static. The modification of the stress tensor

$$\delta T^{\mu\nu} \equiv T^{\mu\nu} - T^{\mu\nu}_{\text{background}} \tag{8.86}$$

satisfies a linear equation.

Since in the hydrodynamic limit the stress tensor is characterized by the local energy density, ϵ, and the three components of the fluid spatial velocity, u^i, there are only four independent fields, which can be chosen to be

$$\mathcal{E} \equiv \delta T^{00} \qquad \text{and} \qquad S^i \equiv \delta T^{0i} \,. \tag{8.87}$$

Using the hydrodynamic form of the stress tensor, (2.13), all other stress tensor components can be expressed as a function of these variables. Since we have assumed that these perturbations are small, all the stress tensor components can be expanded to first order in the four independent fields (8.87).

In Fourier space, keeping the shear viscosity correction, the linearized form of Eqs. (8.84) for the mode with a wave vector $\mathbf{q}$ that has the magnitude $q \equiv |\mathbf{q}|$ take the form

$$\partial_t \mathcal{E} + iq S_L = J^0 \,,$$
$$\partial_t S_L + ic_s^2 q \mathcal{E} + \frac{4}{3} \frac{\eta}{\varepsilon_0 + p_0} q^2 S_L = J_L \,,$$
$$\partial_t \mathbf{S}_T + \frac{\eta}{\varepsilon_0 + p_0} q^2 \mathbf{S}_T = \mathbf{J}_T \,, \tag{8.88}$$

where $\mathbf{S} = S_L \mathbf{q}/q + \mathbf{S}_T$, $\mathbf{J} = J_L \mathbf{q}/q + \mathbf{J}_T$, L and T refer to longitudinal and transverse relative to the hydrodynamical wave-vector $\mathbf{q}$ and ε_0, p_0, $c_s = \sqrt{dp/d\epsilon}$ and η are the energy density, pressure, speed of sound and shear viscosity of the unperturbed background plasma. We observe that the longitudinal and transverse modes are independent. This decomposition is possible since the homogeneous equations

have a *SO*(2) symmetry corresponding to rotation around the wave-vector **q**. The spin zero (longitudinal) and spin one (transverse) modes correspond to the sound and diffusion mode respectively. (The spin two mode is a subleading perturbation in the gradient expansion, since its leading contribution is proportional to velocity gradients.) After combining the first two equations of Eqs. (8.88) and doing a Fourier transformation, we find

$$\left(\omega^2 - c_s^2 q^2 + i \frac{4}{3} \frac{\eta}{\epsilon_0 + p_0} q^2 \omega \right) S_L = i c_s^2 q J^0 + i \omega J_L \,,$$

$$\left(i\omega - \frac{\eta}{\epsilon_0 + p_0} q^2 \right) \mathbf{S}_T = -\mathbf{J}_T \,. \tag{8.89}$$

The sound mode (S_L) satisfies a wave equation and propagates with the speed of sound while the diffusion mode ($\mathbf{S}_T$), which does not propagate, describes the diffusion of transverse momentum as opposed to wave propagation. We also note that only the sound mode results in fluctuations of the energy density, while the diffusion mode involves only momentum densities (the S^i of Eq. (8.87)). In the linear approximation that we are using, the excitation of the diffusion mode produces fluid motion but does not affect the energy density. This result can be further illustrated by expressing the energy fluctuations in terms of the velocity fields

$$\delta T^{00} = \delta \varepsilon + \frac{1}{2} (\varepsilon + P) (\delta v)^2 + \cdots . \tag{8.90}$$

The second term in this expression corresponds to the kinetic energy contribution of the fluid motion which takes a non-relativistic form due to the small perturbation approximation. This expression is quadratic in the velocity fluctuation, and thus is not described in the linearized approximation. The sound mode corresponds to both compression/rarefaction of the fluid and motion of the fluid; sound waves result in fluctuations of the energy density as a consequence of the associated compression and rarefaction. But, the diffusion mode corresponds to fluid motion only and, to this order, does not affect the energy density.

Solving the linearized hydrodynamic equations (8.88) yields hydrodynamic fields given by

$$\mathcal{E}(t, \mathbf{x}) = \int \frac{d\omega}{2\pi} \frac{d^3 q}{(2\pi)^3} \frac{iq J_L + i\omega J^0 - \Gamma_s q^2 J^0}{\omega^2 - c_s^2 q^2 + i \Gamma_s q^2 \omega} e^{-i\omega t + i\mathbf{q}\cdot\mathbf{x}}, \tag{8.91}$$

$$\mathbf{S}_L(t, \mathbf{x}) = \int \frac{d\omega}{2\pi} \frac{d^3 q}{(2\pi)^3} \frac{\mathbf{q}}{q} \frac{c_s^2 iq J^0 + i\omega J_L}{\omega^2 - c_s^2 q^2 + i \Gamma_s q^2 \omega} e^{-i\omega t + i\mathbf{q}\cdot\mathbf{x}}, \tag{8.92}$$

$$\mathbf{S}_T(t, \mathbf{x}) = \int \frac{d\omega}{2\pi} \frac{d^3 q}{(2\pi)^3} \frac{-\mathbf{J}_T}{i\omega - Dq^2} e^{-i\omega t + i\mathbf{q}\cdot\mathbf{x}}, \tag{8.93}$$

where the sound attenuation length and the diffusion constant are

$$\Gamma_s \equiv \frac{4}{3}\frac{\eta}{\varepsilon_0 + p_0}, \tag{8.94}$$

$$D \equiv \frac{\eta}{\varepsilon_0 + p_0}. \tag{8.95}$$

We note in passing that the integral of the longitudinal momentum density over all space vanishes.

The hydrodynamic solutions (8.91), (8.92) and (8.93) are only of formal value without any information about the source. And, as we have stressed above, a lot of nonlinear, non-equilibrium physics goes into determining the source as a function of the coordinates. Still, we can make some further progress. If we assume that the energetic quark moves at a constant velocity v for a long time (as would be the case if the quark is either ultra-relativistic or very heavy) then we expect

$$J^\mu(\omega, k) = 2\pi\delta(\omega - \mathbf{v}\cdot\mathbf{q})J_v^\mu(\mathbf{q}), \tag{8.96}$$

where the factor $\delta(\omega - \mathbf{v}\cdot\mathbf{q})$ comes from Fourier transforming $\delta(\mathbf{x} - \mathbf{v}t)$. We also note that far away from the source, and at sufficiently small q that we can neglect any energy scales characteristic of the medium and any internal structure of the particle moving through the medium, the only possible vectors from which to construct the source are $\mathbf{v}$ and $\mathbf{q}$. In this regime, we may decompose the source as

$$J_v^0(\mathbf{q}) = e_0(\mathbf{q}),$$
$$\mathbf{J}_v(\mathbf{q}) = \mathbf{v}\,g_0(\mathbf{q}) + \mathbf{q}\,g_1(\mathbf{q}). \tag{8.97}$$

Then, inspection of the solutions (8.91), (8.92) and (8.93) together with the observation that a particle moving with a velocity close to the speed of light loses similar amounts of energy and momentum, shows that, at least for an ultra-relativistic probe, non-vanishing values of $e_0(\mathbf{q})$ must be linked to non-vanishing values of $g_0(\mathbf{q})$. We call this case Scenario 1. However, if the interaction of the probe with the plasma is such that both g_0 and e_0 are zero (or parametrically small compared to g_1), from Eqs. (8.85) and (8.97) and since $\mathbf{q}\,g_1(\mathbf{q})$ is a total derivative, one may mistakenly conclude that the energetic probe has created a disturbance carrying zero energy and momentum. In this scenario, which we shall call Scenario 2, the energy and momentum loss are actually quadratic in the fluctuations. These two scenarios lead to disturbances with different characteristics. In Scenario 2, only the sound mode is excited while in Scenario 1, both the sound and diffusion mode are excited. The correct answer for a given energetic probe may lie in between these two extreme cases.

The phenomenological implications of this analysis depend critically on the degree to which the diffusion mode is excited. This mode leads to an excess of

momentum density along the direction of the source which does not propagate out of the region of deposition, but only diffuses away. Therefore, the diffusion mode excited by an energetic quark moving through the plasma corresponds to a wake of moving fluid, trailing behind the quark and moving in the same direction as the quark. In a heavy ion collision, therefore, the diffusion wake excited by the away-side energetic quark will become hadrons at $\Delta\phi \sim \pi$, whereas the Mach cone will become a cone of hadrons with moment at some angle away from $\Delta\phi = \pi$. If most of the energy dumped into the medium goes into the diffusion wake, even if a Mach cone were produced it would be overwhelmed in the final state, and invisible in the data. Only in the case in which the diffusion mode is absent (or sufficiently small) is the formation of a Mach cone potentially visible as a non-trivial correlation in the data, i.e. in the momenta of the hadrons in the final state.

8.3.2 AdS computation

In Section 8.1 we have computed the amount of energy lost by a heavy quark as it plows through the strongly coupled $\mathcal{N} = 4$ SYM theory plasma. Here, we compute the fate of this energy. Remarkably, every one of the difficulties associated with answering this question in QCD or attempting to do so in a hydrodynamic calculation without microscopic inputs can be addressed for the case of an energetic heavy quark propagating through the strongly coupled plasma of $\mathcal{N} = 4$ SYM theory. As in Sections 8.1 and 8.2, we shall assume that the relevant physics is strongly coupled at all length scales, treating the problem entirely within strongly coupled $\mathcal{N} = 4$ SYM theory. In this calculation, the AdS/CFT correspondence is used to determine the stress tensor of the medium, excited by the passing energetic quark, at all length scales. This dynamical computation will allow us to quantify to what extent hydrodynamics can be used to describe the response of the strongly coupled plasma of this theory to the disturbance produced by the energetic quark, as well as to study the relaxation of the initially far-from-equilibrium disturbance. This calculation applies to quarks with mass M whose velocity respects the bound (8.18). We note here that the calculation whose results we shall describe in Section 8.6 of the waves of energy produced in the strongly coupled plasma of $\mathcal{N} = 4$ SYM theory by the motion of a quark through it along a circular trajectory is done using similar techniques to those that we shall present in full here, here in the simpler setting of a quark moving through the plasma along a straight line.

In order to address the fate of the energy lost by a heavy quark plowing through the strongly coupled plasma of $\mathcal{N} = 4$ SYM theory, we must determine the stress tensor of the gauge theory fluid at the boundary that corresponds to the string (8.9) trailing behind the quark in the bulk. In the dual gravitational theory, this string modifies the metric of the $(4+1)$-dimensional geometry. That is, it produces

gravitational waves. The stress energy tensor of the gauge theory plasma at the boundary is determined by the asymptotic behavior of the bulk metric perturbations as they approach the boundary [363, 288, 289, 403].

The modifications of the $4 + 1$-dimensional metric due to the presence of the trailing string are obtained by solving the Einstein equations

$$\mathcal{R}_{\mu\nu} - \frac{1}{2}G_{\mu\nu}(\mathcal{R} - 2\Lambda) = \kappa_5^2 t_{\mu\nu} \,, \tag{8.98}$$

where $\kappa_5^2 = 4\pi^2 R^3/N_c^2$ and $\Lambda = -6/R^2$ with R the AdS radius and where $t_{\mu\nu}$ is the five-dimensional string stress tensor, which can be computed from the Nambu–Goto action:

$$t^{\mu\nu} = -\frac{1}{2\pi\alpha'} \int d\tau d\sigma \frac{\sqrt{-h}}{\sqrt{-G}} h^{ab} \partial_a X^\mu(\tau,\sigma) \partial_b X^\nu(\tau,\sigma) \delta^{(5)}(x - X(\tau,\sigma)) \,, \tag{8.99}$$

where h^{ab} is the induced metric on the string and $X(\tau,\sigma)$ is the string profile. For the case of a trailing string (8.9), the stress tensor is given by

$$
\begin{aligned}
t_{00} &= s(f + v^2 z^4/z_0^4) \,, \\
t_{0i} &= -s v_i \,, \\
t_{0z} &= -s v^2 z^2/z_0^2 f \,, \\
t_{zz} &= s(f - v^2)/f^2 \,, \\
t_{ij} &= s v_i v_j \,, \\
t_{iz} &= s v_i z^2/z_0^2 f \,,
\end{aligned}
\tag{8.100}
$$

where

$$s = \frac{z\gamma\sqrt{\lambda}}{2\pi R^3}\delta^3(\mathbf{x} - vt - \zeta(z)) \,, \tag{8.101}$$

with $\zeta(z)$ the string profile (8.9). After solving the Einstein equations (8.98) with the string stress tensor (8.100), the expectation value of the boundary stress tensor is then obtained by following the prescription (5.48), namely by performing functional derivatives of the Einstein–Hilbert action evaluated on the classical solution with respect to the boundary metric.

We need to analyze the small fluctuations on top of the background AdS black hole metric. Denoting these fluctuations by $h_{\mu\nu}$ and the background metric by $g_{\mu\nu}$, the left-hand side of the Einstein equations (8.98) are given to leading order in $h_{\mu\nu}$ by

$$
\begin{aligned}
&- D^2 h_{\mu\nu} + 2D^\sigma D_{(\mu} h_{\nu)\sigma} - D_\mu D_\nu h + \frac{8}{R^2} h_{\mu\nu} \\
&\quad + \left(D^2 h - D^\sigma D^\delta h_{\sigma\delta} - \frac{4}{R^2} h \right) g_{\mu\nu} = 0 \,,
\end{aligned}
\tag{8.102}
$$

with D_μ the covariant derivative with respect to the full metric, namely $g_{\mu\nu} + h_{\mu\nu}$. This equation has a gauge symmetry

$$h_{\mu\nu} \rightarrow h_{\mu\nu} + D_\mu \xi_\nu + D_\nu \xi_\mu , \qquad (8.103)$$

inherited from reparameterization invariance, that, together with five constraints from the linearized Einstein equations (8.102), reduces the number of degrees of freedom from fifteen to five. It is therefore convenient to introduce gauge invariant combinations which describe the independent degrees of freedom. These can be found after Fourier transforming the $(3 + 1)$-dimensional coordinates. The gauge invariants can be classified by how they transform under $SO(2)$ rotations around the wave-vector $\mathbf{q}$. Upon introducing $H_{\mu\nu} = z^2 h_{\mu\nu}/R^2$, one possible choice of gauge invariants is given by [288, 289]

$$\begin{aligned}
Z_{(0)} &= q^2 H_{00} + 2\omega q H_{0q} + \omega^2 H_{qq} + \frac{1}{2} \left[(2 - f)q^2 - \omega^2 \right] H, \\
Z_{(1)\alpha} &= \left(H'_{0\alpha} - i\omega H_{\alpha 5} \right), \\
Z_{(2)\alpha\beta} &= \left(H_{\alpha\beta} - \frac{1}{2} H \delta_{\alpha\beta} \right),
\end{aligned} \qquad (8.104)$$

where $q \equiv |\mathbf{q}|$, $\hat{q} \equiv \mathbf{q}/q$, $H_{0q} \equiv H_{0i}\hat{q}^i$, $H_{qq} \equiv H_{ij}\hat{q}^i\hat{q}^j$, α and β (which are each either 1 or 2) are space coordinates transverse to $\hat{q}$, $'$ means ∂_z, and $H \equiv H_{\alpha\alpha}$. When written in terms of these gauge invariants, the Einstein equations (8.102) become three independent equations for $Z_{(0)}$, $Z_{(1)\alpha}$ and $Z_{(2)\alpha\beta}$, which correspond to the spin zero, one and two fluctuations of the stress tensor. We focus on the spin zero and spin one fluctuations, since these are the relevant modes in the hydrodynamic limit. Their equations of motion are given by

$$Z''_{(1)\alpha} + \frac{zf' - 3f}{zf} Z'_{(1)\alpha} + \frac{3f^2 - z(zq^2 + 3f')f + z^2\omega^2}{z^2 f^2} Z_{(1)\alpha} = S_{(1)\alpha} \quad (8.105)$$

and

$$\begin{aligned}
Z''_{(0)} &+ \frac{1}{u} \left[1 + \frac{uf'}{f} + \frac{24(q^2 f - \omega^2)}{q^2(uf' - 6f) + 6\omega^2} \right] Z'_{(0)} \\
&+ \frac{1}{f} \left[-q^2 + \frac{\omega^2}{f} - \frac{32q^2 z^6/z_0^8}{q^2(uf' - 6f) + 6\omega^2} \right] Z_{(0)} = S_{(0)} , \quad (8.106)
\end{aligned}$$

where the sources are combinations of the string stress tensor and its derivatives. Choosing one of the transverse directions (which we shall denote by $\alpha = 1$) to lie in the $(\mathbf{v}, \mathbf{q})$ plane, the source for the trailing string is given explicitly by

$$S_{(1)1} = \frac{2\kappa_5^2 \gamma \sqrt{\lambda}}{R^3} \frac{v q_\perp}{q f} \delta(\omega - \mathbf{v} \cdot \mathbf{q}) e^{-i\mathbf{q} \cdot \zeta} \,,$$

$$S_{(1)2} = 0 \,, \tag{8.107}$$

$$S_{(0)} = \frac{\kappa_5^2 \gamma \sqrt{\lambda}}{3R^3} \frac{q^2(v^2 + 2) - 3\omega^2}{q^2} \frac{z\left[q^4 z^8 + 48i q^2 z_0^2 z^5 - 9(q^2 - \omega^2)^2 z_0^8\right]}{f(fq^2 + 2q^2 - 3\omega^2) z_0^8}$$

$$\times \delta(\omega - \mathbf{v}\mathbf{q}) e^{-i\mathbf{q} \cdot \zeta} \,, \tag{8.108}$$

where $q_\perp$ is the magnitude of the component of $\mathbf{q}$ perpendicular to $\mathbf{v}$. The boundary action can be expressed in terms of the gauge invariants $Z_{(1)\alpha}$ and $Z_{(0)}$ plus certain counterterms (terms evaluated at the boundary). This procedure, which can be found in Ref. [289], is somewhat cumbersome but straightforward, and we shall not repeat it here. Once this is achieved, the stress tensor components can be obtained from the classical solution to (8.105)–(8.106), following the prescription (5.48).

To find the classical solution to (8.105)–(8.106) we must specify boundary conditions. Since the quark propagates in flat space, the metric fluctuations must vanish at the boundary. Also, since we are interested in the response of the medium, the solution must satisfy retarded boundary condition, meaning that at the horizon it must be composed only of infalling modes. Thus, we may construct the Green's function

$$G_s(z, z') = \frac{1}{W_s(z')} \left(\theta(z' - z) g_s^n(z) g_s^i(z') + \theta(z - z') g_s^i(z) g_s^n(z')\right), \tag{8.109}$$

where the subscript s which can be 0 or 1 denotes the spin component and g_s^n and g_s^i denote the normalizable and infalling solutions to the homogeneous equations obtained by setting the left-hand side of (8.105) equal to zero. W_s is the Wronskian of the two homogeneous solutions. The full solution to (8.105) may be then written as

$$Z_s(z) = \int_0^{z_h} dz' G_s(z, z') S_s(z'). \tag{8.110}$$

Close to the boundary, these solutions behave as

$$Z_{(0)} = z^3 Z_{(0)}^{[3]} + z^4 Z_{(0)}^{[4]} + \cdots$$

$$\vec{Z}_{(1)} = z^2 \vec{Z}_{(1)}^{[2]} + z^3 \vec{Z}_{(1)}^{[3]} + \cdots . \tag{8.111}$$

The components $Z_{(0)}^{[3]}$ and $Z_{(1)}^{[2]}$ can be computed analytically and are temperature independent. They yield a divergent contribution to the boundary stress tensor. However, this contribution is analytic in q and, thus, has δ-function support at the position of the heavy quark. This divergent contribution is the contribution of the heavy quark mass to the boundary theory stress tensor. The response of the boundary theory gauge fields to the disturbance induced by the passing energetic quark is encoded in the components $Z_{(0)}^{[4]}$ and $Z_{(1)}^{[3]}$, which must be computed

numerically. After expressing the boundary actions in terms of gauge invariants, the nondivergent spin zero and one components of the boundary stress tensor are given by

$$\mathcal{T}_0 = \frac{4q^2}{3\kappa_5^2(q^2 - \omega^2)^2} Z_{(0)}^{[4]} + D + \varepsilon_0 , \qquad (8.112)$$

$$\vec{\mathcal{T}}_1 = -\frac{L^3}{2\kappa_5} \vec{Z}_{(1)}^{[3]}, \qquad (8.113)$$

where $\mathcal{T}_0 = T^{00}$ and $\vec{\mathcal{T}}_1 = T^{0a}\hat{\epsilon}_a$, with $\hat{\epsilon}_a$ the spatial unit vectors orthogonal to the spatial momentum **q**, and where the counterterm D is a complicated function of ω and q that depends on the quark velocity and the plasma temperature and that is given in Ref. [289].

Results from Ref. [289] on the numerical computation of the disturbance in the gauge theory plasma created by a supersonic quark moving with speed $v = 0.75$ are shown in Fig. 8.4. The top panel shows the energy density of the disturbance and clearly demonstrates that a Mach cone has been excited by the supersonic quark. The front is moving outwards at the Mach angle Θ_M, where $\cos\Theta_M = c_s/v = 4/(3\sqrt{3})$. Recall from our general discussion above that fluid motion is invisible in the energy density, to the linear order at which we are working; the energy density is nonzero wherever the fluid is compressed. Thus, the Mach cone is made up of sound modes, as expected. In the bottom panel of Fig. 8.4, we see the density of fluid momentum induced by the supersonic quark. This figure reveals the presence of a sizable wake of moving fluid behind the quark, a wake that is invisible in the energy density and is therefore made up of moving fluid without any associated compression, meaning that it is made up of diffusion modes. We conclude that the supersonic quark passing through the strongly coupled plasma excites both the sound mode and the diffusion mode, meaning that the interaction of the quark with the plasma is as in what we called Scenario 1 above. Quantitatively, it turns out that the momentum carried by the sound waves is greater than that carried by the diffusion wake, but only by a factor of $1 + v^2$ [408].

Since hydrodynamics describes the long-wavelength limit of the stress tensor excitation, it is reasonable to find a Mach cone at long distances. And, since the gravitational equations whose solution we have described are linear, the long distance behavior of the gauge theory fluid must be described by linearized hydrodynamics. It is easy to justify the linearization from the point of view of the field theory: the background plasma has an energy density that is proportional to N_c^2 while that of the perturbation is proportional to the number of flavors, which is just $N_f = 1$ in the present case since we are considering only one quark. The strong coupling computation leads to a perturbation of magnitude $N_f\sqrt{\lambda}$. Thus,
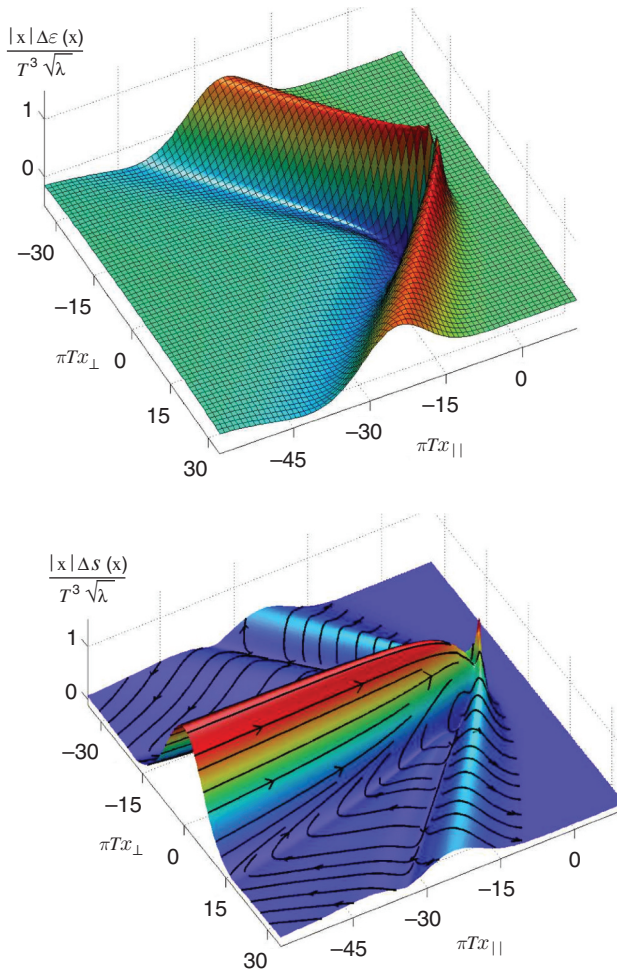
Figure 8.4 Energy density (top) and momentum flux (bottom) induced by the passage of a supersonic heavy quark moving through the strongly coupled $\mathcal{N} = 4$ SYM theory plasma in the $x_\parallel$ direction with speed $v = 0.75$. ($\Delta\varepsilon(\mathbf{x})$ is the difference between $\varepsilon(\mathbf{x})$ and the equilibrium energy density; since $\mathbf{S} = 0$ in equilibrium, $\Delta\mathbf{S}(\mathbf{x})$ is simply $\mathbf{S}(\mathbf{x})$.) The flow lines on the surface are flow lines of $\Delta\mathbf{S}(\mathbf{x})$. These disturbances are small compared to the background energy density and pressure of the plasma (both of which are $\propto N_c^2$). The perturbation is small and it is well described by linearized hydrodynamics everywhere except within a distance $R \approx 1.6/T$ from the quark. Since the perturbation is small, the kinetic energy contribution of the diffusion mode to the energy density is suppressed by N_c^2 and, thus, it does not contribute in the upper panel. Figure taken from Ref. [298].

the energy density of the fluctuations are suppressed by $\sqrt{\lambda}/N_c^2$ with respect to that of the background plasma, justifying the linearized treatment. Remarkably, it turns out that disturbances like those in Fig. 8.4 are well described by hydrodynamics everywhere except within $\approx 1.6/T$ of the position of the quark [289]. So, the calculation that we have reviewed in this Section is important for two reasons. First, it demonstrates that a *pointlike* probe passing through the strongly coupled plasma does indeed excite hydrodynamic modes. And, second, it demonstrates that in the strongly coupled plasma, the resulting disturbance relaxes to a hydrodynamic excitation in local thermal equilibrium surprisingly close to the probe.

The observation that point particles moving through the strongly coupled fluid excite sound waves, which are collective excitations, is at odds with intuition based upon the interaction of, say, electrons with water. In this example, most of the energy lost by the electron is transferred to photons and not to the medium. These photons, in turn, have long mean free paths and dissipate their energy far away from the electron (or escape the medium entirely). Thus, the effective size of the region where energy is dissipated is very large, given by the photon mean free path. Hydrodynamics will only describe the physics on longer length scales than this. The reason that no Mach cone is formed is that the length scale over which the energy is deposited is long compared to the length scale over which the electron slows and stops. The situation is similar in weakly coupled gauge theory plasmas; even though the gauge modes in these theories do interact, they still have long mean free paths proportional to $1/g^4$. In sharp contrast, in the strongly coupled plasma of $\mathcal{N} = 4$ SYM theory there are no long-lived quasiparticle excitations (let alone photons) that could transport the energy deposited by the pointlike particle over long distances. Instead, all the energy lost by the pointlike probe is dumped into collective hydrodynamic modes over a characteristic length scale $\sim 1/T$, which is the only length scale in this conformal plasma.

8.3.3 *Implications for heavy ion collisions*

The calculation that we have reviewed in this section suggests that a high energy quark plowing through the strongly coupled plasma produced in heavy ion collisions at RHIC should excite a Mach cone. As we argued just above, this phenomenon is not expected in a weakly coupled plasma. The Mach cone should have consequences that are observable in the soft particles on the away-side of a high energy trigger hadron. However, for a hydrodynamic solution like that in Fig. 8.4, it turns out that the diffusion wake contains enough momentum flux along the direction of the energetic particle to "fill in" the center of the Mach cone,

meaning that the Mach cone is not sufficiently prominent as to result in peaks in the particle distribution at $\Delta\phi = \pi \pm \Theta_M$ [245, 657]. As we discussed above, the observed peaks at $\Delta\phi = \pi \pm \phi_v$ receive a significant contribution from the event-by-event v_3 due to event-by-event fluctuations that introduce "triangularity". Detecting evidence for Mach cones in heavy ion collisions will require careful subtraction of these effects from the data or the design of new observables based upon multi-particle correlations, as well as careful theoretical analysis of the effects of the rapid expansion of the fluid produced in heavy ion collisions on the putative Mach cones.

8.3.4 Disturbance excited by a moving quarkonium meson

Strong coupling calculations like that of the disturbance excited by an energetic quark moving through the plasma of $\mathcal{N} = 4$ SYM theory can help guide the construction of more phenomenological models of the coupling of energetic particles to hydrodynamic modes. To further that end, we close with an example which shows that not all probes behave in the same way.

As we shall describe in Section 8.7, a simple way of modeling a "quarkonium" meson made from a heavy quark and antiquark embedded in the strongly coupled plasma of $\mathcal{N} = 4$ SYM theory is to consider a string with both ends at the boundary – the ends representing the quark and antiquark. We shall see in Section 8.7 that even when this string is moving through the plasma, it hangs straight downward into the AdS black hole metric, rather than trailing behind as happens for the string hanging downward from a single moving quark. The fact that the "U" of string hangs straight down and does not trail behind the moving quark and antiquark implies that the heavy quarkonium meson moving through the strongly coupled plasma does not lose any energy, at least at leading order. The energy loss of such a meson has been computed and is in fact nonzero but is suppressed by $1/N_c^2$ [334].

Despite the fact that the leading order quarkonium energy loss vanishes, the leading order disturbance of the fluid through which the meson is moving does not vanish [407]. Instead, the meson excites a Mach cone with no diffusion wake, providing an example of what we called Scenario 2 at the end of Section 8.3.1. It is as though the moving meson "dresses itself" with a Mach cone, and then the meson and its Mach cone propagate through the fluid without dissipation, to leading order. To illustrate this point, the metric fluctuation and consequent boundary stress tensor induced by a semiclassical string with both ends on the boundary moving with a velocity **v** has been calculated [407]. For a string with the two endpoints aligned along the direction of motion and separated by a distance l the long distance part (low momentum) part of the associated stress tensor is given by

$$\delta T^{00} = \frac{\Pi}{q^2 - 3\,(q \cdot \mathbf{v})^2} \left(-q^2 \left(1 + 2v^2\sigma\right) - 3v^2 \left(q \cdot \mathbf{v}\right)^2 \left(1 - 2\sigma\right)\right), \quad (8.114)$$

$$\delta T^{0i} = \frac{\Pi}{k^2 - 3\,(q \cdot \mathbf{v})^2}\, 2q \cdot \mathbf{v} \left(1 - (1 - v^2)\sigma\right) q^i + 2\,\Pi\,\sigma\,v^i, \quad (8.115)$$

$$\delta T^{ij} = \frac{\Pi}{k^2 - 3\,(q \cdot \mathbf{v})^2}\, 2\,(q \cdot \mathbf{v})^2 \left(-1 + (1 - v^2)\sigma\right) \delta^{ij} - \quad (8.116)$$

$$- \frac{\Pi}{v^2} \left(1 + 2v^2\sigma\right) \frac{v^i v^j}{v^2},$$

where $\sigma = \sigma(l, T)$ is a dimensionless function of the length of the meson and the temperature and the prefactor takes the form

$$\Pi = \sqrt{\lambda}\frac{F(lT)}{l}, \quad (8.117)$$

with F a dimensional function.

The expression (8.114) clearly shows that all the spin zero, one and two components of the stress tensor are excited. The spin zero components are multiplied by the sound propagator, signaling the emission of sound waves. (Note that in the low-q limit the width of the sound pole vanishes.) The spin one component corresponds to the terms proportional to the velocity of the particle v^i. These terms are analytic in q; in particular it seems that there is no pole contribution from the diffusive mode. More careful analysis shows that the diffusive mode decays faster than that excited by a quark probe.

The magnitude of the disturbance in the strongly coupled plasma that is excited by a passing quarkonium meson is no smaller than that excited by a passing quark. However, the total integral of the energy and momentum deposited is zero, as can be seen by multiplying the momentum densities by $\omega = \mathbf{v} \cdot \mathbf{q}$ and taking the limit $q \to 0$. This is consistent with the fact that, to the order at which this calculation has been done, the meson does not lose any energy. This is an interesting example since it indicates that the loss of energy and the excitation of hydrodynamic modes are distinct phenomena, controlled by different physics. This example also illustrates the value of computations done at strong coupling in opening one's eyes to new possibilities: without these calculations it would have been very hard to guess or justify that such a separation in magnitude between the strength of the hydrodynamic fields excited by a probe and the energy lost by that probe could be possible. It would be interesting to analyze the soft particles in heavy ion collisions in which a high transverse momentum quarkonium meson is detected, to see whether there is any hint of a Mach cone around the meson – in this case without the complication of soft particles from a diffusion wake filling in the cone.

8.4 Stopping light quarks

As we have discussed extensively in Section 2.3, the dominant energy loss process for a parton moving through the QCD plasma with energy E in the limit in which $E \to \infty$ is gluon radiation, and in this limit much (but not all; see Section 8.5) of the calculation can be done at weak coupling. However, since it is not clear at which energy the $E \to \infty$ approximation becomes reliable, it is also worth analyzing the entire problem of parton energy loss and jet quenching at strong coupling to the degree that is possible. For the case of a heavy quark propagating through the strongly coupled plasma of $\mathcal{N} = 4$ SYM theory, this approach has been pursued extensively, yielding the many results that we have reviewed in the previous three sections. Less work has been done on the energy loss of an energetic light quark or gluon in the $\mathcal{N} = 4$ SYM plasma, in particular since they do not fragment into anything like a QCD jet. This was illustrated by Hofman and Maldacena [457], who considered the following thought experiment. Suppose you did electron–positron scattering in a world in which the electron and positron coupled to $\mathcal{N} = 4$ SYM theory through a virtual photon, just as in the real world they couple to QCD. What would happen in high energy scattering? Would there be any "jetty" events? They showed that the answer is no. Instead, the final state produced by a virtual photon in the conformal $\mathcal{N} = 4$ SYM theory is a spherically symmetric outflow of energy. Similar conclusions were also reached in Refs. [433, 293]. The bottom line is that there are no jets in strongly coupled $\mathcal{N} = 4$ SYM theory, which would seem to rule out using this theory to study how jets are modified by propagating through the strongly coupled plasma of this theory. Many authors have nevertheless used the strongly coupled plasma of $\mathcal{N} = 4$ SYM theory to gain relevant insights, for example by studying the energy loss and momentum diffusion of a heavy quark plowing through the plasma as we have described in Sections 8.1 and 8.2, as well as the wake it produces, described in Section 8.3. In the present section, we ask how a light quark or gluon loses energy in the $\mathcal{N} = 4$ SYM plasma in the hope that, even if this is not a good model for jets and their quenching in QCD, some qualitative strong coupling benchmarks against which to compare experimental results may be obtained. This program has been pursued in Refs. [406, 293, 294, 73, 74]. Furthermore, we shall demonstrate in Section 8.6 that even though there are no jets in strongly coupled $\mathcal{N} = 4$ SYM theory it is still possible to construct a collimated beam of radiation in this theory and watch how it is quenched by the plasma.

As we have seen in Section 5.5, and as we will describe extensively in Chapter 9, dynamical quarks can be introduced into $\mathcal{N} = 4$ SYM theory by introducing a D7-brane that fills the $3 + 1$ Minkowski dimensions and fills the fifth dimension from the boundary at $z = 0$ down to $z = z_q$. The mass of the (heavy) quarks

that this procedure introduces in the gauge theory is $\sqrt{\lambda}/(2\pi z_q)$. Light quarks are obtained by taking $z_q \to \infty$, meaning that the D7-brane fills all of the z dimension. At $T \neq 0$, what matters is that the D7-brane fills the z dimension all the way down to, and below, the horizon. While this construction introduces light fundamental degrees of freedom into the theory, it does not alter the fact that there are no true jets. This is the principal origin of the difficulty in using gauge/string duality to study light quark energy loss: depending on which aspects of real jets in QCD we wish to mimic, we can make different choices in the way we set-up a dual gravitational calculation, choices that correspond on the gauge theory side to different ways of preparing an energetic initial state. This range of possible choices necessarily introduces ambiguity in the analysis since there can be no single gravitational calculation that encompasses all the relevant aspects of jet physics in QCD. Nevertheless, there exist common features across all these choices that allow us to draw some conclusions about the dynamics of energetic light quarks and gluons moving through strongly coupled plasma.

8.4.1 Back-to-back jets as the endpoints of a string

We begin by focusing on the fact that a light quark jet is initiated by a single energetic quark, which suggests that a natural approach is to model a light quark-antiquark pair moving away from each other back-to-back with some initial high energy (as would become a back-to-back pair of jets in QCD) by the endpoints of a string located at some depth z in the bulk that are moving apart from each other in, say, the x-direction [293, 294]. The quark and antiquark must be within the D7-brane, but since this D7-brane fills all of z there is nothing stopping them from falling to larger z as they fly apart from each other, and ultimately there is nothing stopping them from falling into the horizon. It should be evident from this description that there is an arbitrariness to the initial condition: at what z should the quark and antiquark be located initially? What should the string profile be initially? What should the initial profile of the velocity of the string be? These choices correspond in the gauge theory to choices about the initial quantum state of the quark–antiquark pair and the gauge fields surrounding them. And, there is no known way to choose these initial conditions so as to obtain a QCD-like jet so the choices made end up being arbitrary. (The analogous set up for a back-to-back pair of high energy gluons [406] involves a doubled loop of string, rather than an open string with a quark and antiquark at its ends.)

Ambiguities about the initial conditions notwithstanding, several robust qualitative insights have been obtained from these calculations. First, the quark and the antiquark always fall into the horizon after traveling some finite distance x_{stopping}. The string between them falls into the horizon also. An example is shown in
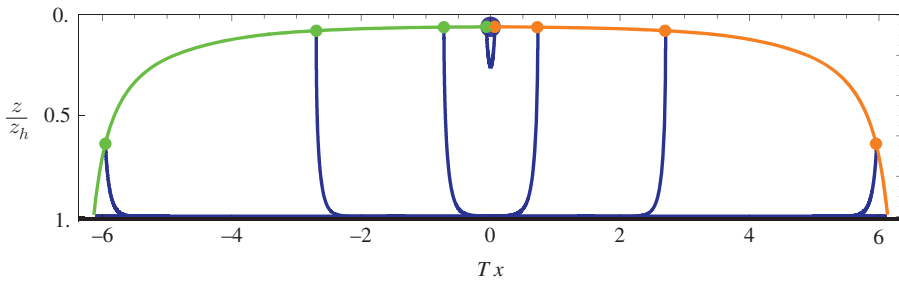
Figure 8.5 A quark–antiquark pair moving away from each other fall into the horizon after a finite stopping distance. The figure shows the quark–antiquark pair (green and orange dots) and the string that connects them (in blue) at four times, starting at an early time when they are close together and the string is near the boundary and ending just before they have traveled their stopping distance and they and the string have reached the horizon. See text for further details. Figure taken from Ref. [294].

Fig. 8.5. In the gauge theory, x_{stopping} corresponds to the stopping distance for the initially energetic quark, namely the distance that it takes this quark to slow down, thermalize, and equilibrate with the bulk plasma – the gauge theory analog of falling into the horizon. This is qualitatively reminiscent of the experimental finding that there are circumstances in which an energetic parton that would have become a jet in vacuum is instead quenched by the plasma to such a degree that it becomes many soft particles with a close-to-thermal momentum distribution.

Second, although x_{stopping} does depend on details of the initial conditions, the dominant dependence is that it scales like $E^{1/3}$, where E is the initial energy of the quark [406, 294]. More precisely, upon analyzing varied initial conditions the maximum possible stopping distance is given by [294]

$$x_{\text{stopping}} = \frac{C}{T}\left(\frac{E}{T\sqrt{\lambda}}\right)^{1/3}, \qquad (8.118)$$

with $C \approx 0.5$. If there is a regime of E and T in which it is reasonable to treat the entire problem of jet quenching at strong coupling, and if in this regime the droplet of plasma produced in a heavy ion collision is large enough and lives long enough that it can stop and thermalize an initial parton with energy E that would in vacuum have become a jet, then the scaling (8.118) has interesting qualitative consequences. For example, if this scaling applies to collisions with two different collision energies $\sqrt{s_1}$ and $\sqrt{s_2}$, yielding plasmas that form at different temperatures T_1 and T_2, then jets in these two experiments whose energies satisfy $E_1/E_2 \sim (T_1/T_2)^4$ should have similar observed phenomenology. Turning this speculation into semi-quantitative expectations for experimental observables

requires careful study of jet stopping in a realistic model of the dynamics in space and time of the expanding droplet of plasma produced in a heavy ion collision.

Third, a light quark with initial energy E that loses this energy over a distance x_{stopping} loses most of its energy near the end of its trajectory, where it thermalizes (falls into the horizon) [294]. This pattern of energy loss is reminiscent of the "Bragg peak" that characterizes the energy loss of a fast charged particle in ordinary matter, where the energy loss has a pronounced peak near the stopping point. It is quite different from the behavior of a heavy quark in strongly coupled plasma which, as we saw in Section 8.1, loses energy at a rate proportional to its momentum, making it reasonable to expect that a heavy quark that slows from a high velocity to a stop loses more energy earlier in its trajectory than later.

8.4.2 A colorless jet sourced by a virtual photon

Although the approach in the previous section is intuitive, it suffers from the inherent ambiguity in defining the initial conditions for the string that joins the quark and antiquark. This arbitrariness originates from the fact that the precise form of the gauge theory source dual to a given initial string configuration selected in the gravity theory is not known. One is specifying initial conditions clearly and explicitly in the gravity theory without knowing in precise terms what those initial conditions correspond to in the gauge theory. There is, however, a complementary approach to the physics of energetic light quarks moving through strongly coupled plasma where one focuses initially on formulating a gauge theory problem which, in QCD, would lead to the formation of energetic jets and then studies the dual description of the set-up one has formulated. An interesting example of this approach is the study of the response of the strongly coupled plasma to an external gauge field wave-packet characterized by a very large time-like four-momentum (energy E and three-momentum $|\vec{k}|$ comparable and both much greater than virtuality q) and a small packet width, L [73, 74]. This is the analog of analyzing the decay of an energetic virtual photon or an electroweak boson. In QCD this excitation decays into a quark–antiquark pair and, since $E \gg q$ by construction, the quark and antiquark are extremely boosted and are therefore almost collinear with each other, forming a single jet. Note that this jet is different from those of interest in heavy ion collisions (or for that matter in elementary particle collisions) since it carries no net color charge. In this way (and perhaps in others) it is not analogous to a QCD jet initiated by a single quark or a gluon. Nevertheless, this construction provides a well-defined way to generate energetic light quarks moving through the plasma in QCD. In the strongly coupled theory, this external source creates a localized excitation of strongly interacting fields which propagate through the strongly coupled

plasma with a large initial boost. We will refer to this excitation loosely as a jet. The advantage of this procedure is that once the gauge theory source has been specified, which is equivalent to specifying the process of creating the jet, there are no remaining ambiguities and one can then analyze the dual problem on the gravitational side. In Section 8.6 we shall describe an (apparently) quite different way of creating a localized high energy excitation of strongly interacting fields which can also be analyzed via gauge/string duality.

It is natural to ask why we do not consider instead an external gauge theory wave-packet with $E \sim q \gg |\mathbf{k}|$, as in QCD this would produce a back-to-back quark–antiquark pair and hence a back-to-back pair of jets. Would making this choice result in a pair of jets that were each more similar to the jets in QCD than the single jet above? Or, at the least, more similar to the back-to-back jets described by the quark–antiquark pair connected by a string in Section 8.4.1? The problem with this line of thought is that in strongly coupled $\mathcal{N} = 4$ SYM theory a source like this produces a spherically symmetric outward flow of energy, rather than a back-to-back pair of jets [457]. The single "jet" that we shall analyze can be obtained by giving this spherically symmetric flow of energy such a large boost that it becomes a tightly focused flow of energy with $E \sim |\mathbf{k}| \gg q$. So, although it sounds artificial from a QCD perspective to consider a color-singlet jet made by boosting a quark–antiquark pair to the point that they are almost collinear, this construction has the virtue that it yields a jet-like object in both QCD and $\mathcal{N} = 4$ SYM theory.

The simplest way to add the external gauge field wave-packet is to modify the Lagrangian for the strongly coupled gauge theory by adding an external $U(1)$ gauge field source:

$$\mathcal{L}_{QFT} \rightarrow \mathcal{L}_{QFT} + j_\mu A_{cl}^\mu , \qquad (8.119)$$

with j_μ the $U(1)$ current in the strongly coupled gauge theory and A_{cl}^μ a classical external field characterized by a narrow envelop function $\Lambda(x)$ of typical size L. The external gauge field can be parametrized as

$$A_{cl}^\mu = \epsilon^\mu \mathcal{N}_A \left[e^{ik^\mu x_\mu} + \text{h.c.} \right] \Lambda(x), \qquad (8.120)$$

with k^μ a four momentum with large energy $k^0 = E$ and three-momentum $|\mathbf{k}| \approx E$ and a small virtuality $k^2 = -q^2$, with $q^2 \ll E^2$. $\mathcal{N}_A$ is a normalization factor that can be arbitrarily small and ϵ^μ is a given polarization vector. This parametrization is chosen to make apparent the large momentum component in the field, k. From the Fourier analysis of this expression it is clear that all Fourier modes will have a typical large momentum k^μ plus a small momentum of order $1/L$ introduced by the spacetime dependence of the envelop function Λ which, in general, has components in all four space-time directions. However, we will see later that the aspects

of the Fourier transform of the function Λ that are most relevant for our discussion are its distribution in energy and in the component of momentum along the **k**-direction. Since we want Λ to contribute only momenta that are small compared to the typical momentum **k**, we must require $E \gg 1/L$.

The presence of this source generates a non-vanishing expectation value for the $U(1)$ current $j^\mu(x)$ in the plasma, which characterizes the jet. At early times after the disappearance of the external field, the current is localized on the same length scale as the external source was and is propagating with the characteristic momentum k^μ. At later times, its interaction with the plasma leads to the attenuation of the current components and its eventual thermalization. As in the previous analysis of a quark–antiquark pair connected by a string, a stopping distance can be defined as the attenuation distance of the expectation value of the current in the presence of the external source

$$\langle j^\mu(t, x) \rangle_{A_{\text{cl}}} \tag{8.121}$$

which, for sufficiently small external sources, can be expressed in terms of three-point correlators in the gauge theory.

As explained in Section 5.1.4, in the gravitational theory the dual of the gauge theory current is a $U(1)$ gauge field living in the D7-brane, with a boundary value given precisely by the external source Eq. (8.120). We now see the advantage of this construction: as soon as we have specified the problem precisely on the gauge theory side, its specification on the gravitational side of the duality is immediately in hand.

For the purpose of this discussion, we can also restrict our attention to excitations confined to five out of the eight dimensions of the D7-brane. The computation of the time evolution of the expectation value of the current demands the determination of three-point functions on the gravity side, as in the gauge theory. This makes the calculation rather demanding and we shall not reproduce it here. We refer the interested reader to Ref. [73], where the calculation is performed in detail. Although at a technical level the calculation is involved, its main features can be understood entirely in terms of simple physical considerations, as we now describe.

The dynamics of the expectation value of the current in the boundary gauge theory, which is what we are after in order to determine the stopping distance for the pulse of energy density propagating through the plasma that is produced by the source we have described, is governed in its dual description by the behavior of excitations in the gravity theory that, at least close to the boundary, have very short wavelengths. This makes it possible to analyze the propagation of these excitations via a geometric optics approximation, as in electromagnetism, which reduces the gravitational problem of interest to the determination of the trajectories of massless particles in the gravitational background. (We shall discuss the range

of applicability of this geometric optics approach momentarily.) These trajectories are given by null geodesics in the AdS_5 black hole metric, the same trajectories as those followed by the end points of the strings in Section 8.4.1, which are characterized by a four-vector that is constant along the trajectory. This four-vector can be interpreted as the initial momentum that the excitation (we shall call it a "particle") in the gravitational background has when it is close to the boundary; in the gauge theory, it coincides with the hard momentum of the gauge field sourced by the external current. Because the infalling particle follows a null geodesic, its position is given by

$$x^{\mu}(z) = \int_{z_q}^{z} dz' \sqrt{g_{zz}} \frac{g^{\mu\nu}k_{\nu}}{\left(-k_{\alpha}k_{\beta}g^{\alpha\beta}\right)^{1/2}} \,, \qquad (8.122)$$

where g_{MN} is the metric (5.34) for the AdS Schwarzschild blackhole, the Greek indices denote the gauge theory directions and where z_q is the initial position of the particle, which we shall relate to the virtuality q of the gauge field it describes in the boundary theory. As in the case of the string endpoints in Section 8.4.1, the gravitational pull of the black branes makes the particle fall into the horizon, which corresponds to the thermalization of the jet. From the expression (8.122) the stopping distance can be estimated by finding the distance travelled by the particle along the gauge theory direction from its production point near the boundary until it falls into the horizon. Choosing the direction of motion of the particle as the x-direction, we find from (8.122) that

$$x_{\text{stopping}} = \int_{z_q}^{z_0} dz \frac{1}{\sqrt{\frac{z^4}{z_0^4} + \frac{q^2}{|\mathbf{k}|^2}}} \,, \qquad (8.123)$$

where $z_0 = \frac{1}{\pi T}$ is the position of the horizon, as in Eq. (5.36). The expression (8.123) is not yet the result that we are after, because the excitation of the gauge theory sourced by (8.120) is described initially by a wave-packet with some spread in virtuality q whereas what we have described so far is the dual description of an excitation with a single value of q. We shall address this momentarily, but must first understand the implications of (8.123).

The integral (8.123) is dominated by values of $z \sim z^*$ with the characteristic value z^* given by

$$z^* \equiv z_0 \, q^{1/2} / |\mathbf{k}|^{1/2} \,. \qquad (8.124)$$

This is the scale at which the trajectory of the dual particle, which at early times moves almost parallel to the brane, with its downward velocity in the z-direction much smaller than its velocity in the x-direction, starts to bend significantly, picking up a significant velocity downward toward the horizon. Recall that we are

analyzing the response to a source with $q \ll |\mathbf{k}|$, meaning that $z^* \ll z_0$. The lower limit of the integration, z_q, must be chosen to correspond to the smallest value of z for which the particle approximation to the wave-packet (i.e. the gravitational analog of the geometric optics approximation) is valid. An explicit analysis [433] which we will not reproduce here shows, perhaps not surprisingly, that $z_q \sim 1/q$. So, the larger the virtuality of the wave is, the closer the initial position of the dual particle is to the boundary. We certainly need $q \gg T$, to ensure that $z_q \ll z_0$. In fact, we shall see that we need q to satisfy the stronger condition $q \gg T^{2/3}|\mathbf{k}|^{1/3}$, which ensures that $z_q \ll z^*$. So, as long as $|\mathbf{k}|$ is very much larger than T, we can proceed with our analysis upon assuming that

$$T \ll T^{2/3}|\mathbf{k}|^{1/3} \ll q \ll |\mathbf{k}|, \quad \text{meaning that} \quad z_0 \gg z^* \gg z_q . \tag{8.125}$$

Since z_q is the smallest of these scales, in our initial analysis of (8.123) we can set $z_q = 0$. Upon so doing, we can immediately check that if we integrate (8.123) from $z = 0$ to $z = z^*$ we find that as the particle falls from its starting point to z_q it travels a distance in the x-direction that is proportional to z_0^2/z^*. This tells us that as we make q smaller and smaller, while still keeping it within the range (8.125), although z^* moves closer and closer to the boundary (see (8.124)) the distance in x that the particle travels before it reaches $z = z^*$ and its trajectory starts to bend significantly downward toward the horizon gets longer and longer. We can think of this delay as reflecting the fact that at smaller and smaller q the initial velocity of the particle in the x-direction is closer and closer to the speed of light, making it harder and harder for the gravitational field of the black hole to turn its trajectory downward.

We now turn our attention to the upper limit of the integral (8.123). As long as $|k| \gg q$, meaning that the virtuality of the jet is much smaller than its energy, the integral is dominated by the region $z \sim z^* \ll z_0$ and is insensitive to the behavior of the integrand in the region $z \sim z_0$ near the horizon, which allows us to take the upper limit of the integrand to infinity. So, upon assuming that (8.125) is satisfied with z_q, z^* and z_0 being well-separated scales, we can safely replace the lower and upper limits of the integral by zero and infinity, do the integral, and find

$$x_{\text{stopping}} = \frac{\Gamma[1/4]^2}{4\pi^{3/2}} \left(\frac{E^2}{q^2}\right)^{1/4} \frac{1}{T} , \tag{8.126}$$

where we have used $|\mathbf{k}| \approx E$. This is the stopping distance of a jet (a jet in the sense of this section) with a particular energy E and virtuality q. The virtuality can be thought of as one of the parameters related to how the jet of energy E is prepared and we see that, as in the description of Section 8.4.1 in which we modeled the jet as a falling string, the stopping distance depends on how the jet is prepared. We should not be concerned about the apparent contradiction between the result here

that the stopping length of a jet with fixed virtuality is proportional to $E^{1/2}$ and the result from Section 8.4.1. What was calculated in Section 8.4.1 was the maximal stopping distance among all possible jets with some energy E. We will evaluate this with more care below, but it is already possible to see how the correct scaling (8.118) will emerge. Clearly, from (8.126) and from our earlier discussion of how reducing q means that the particle can fly farther before gravity manages to bend it downward into the horizon, the maximal stopping distance will be found for the smallest allowed values of q. From (8.125), we see that the smallest allowed values of q are those for which $z_q \sim z^*$ and $q \sim E^{1/3}T^{2/3}$. Substituting this into (8.126), we find

$$x_{\text{maximum stopping}} \sim E^{1/3}T^{-4/3}, \tag{8.127}$$

which is in agreement with the result (8.118) obtained via the analysis of falling strings up to a factor of $\sqrt{\lambda}$. We will discuss this factor only after we first rederive (8.127) in a more careful way.

In our analysis so far we have neglected the fact that the jet-like object that we wish to study has a wave-packet profile parameterized by (8.120). The characteristic size of the envelop function Λ in the parameterization (8.120) introduces an uncertainty in the momentum of the wave of order $1/L$, since the field (8.120) can be understood as an ensemble of excitations with momenta $\tilde{k}$ distributed around $\mathbf{k}$ with spread $1/L$:

$$\tilde{\mathbf{k}} = \mathbf{k} + \left(\mathcal{O}\left(\frac{1}{L}\right), \mathcal{O}\left(\frac{1}{L}\right), \mathcal{O}\left(\frac{1}{L}\right), \mathcal{O}\left(\frac{1}{L}\right) \right). \tag{8.128}$$

These soft components change the virtuality of the different modes, meaning that the wave-packet is a superposition of modes with different virtuality as well as different energy. The largest change in the virtuality is due to the soft components along the direction of $\mathbf{k}$, which yield a typical contribution to the virtuality

$$q_L^2 \sim E/L. \tag{8.129}$$

The contribution to the virtuality from the fluctuations perpendicular to $\mathbf{k}$ is suppressed in comparison and can be neglected. Thus, even if the virtuality $-k^2 = q^2$ is small, the production of jets described via the wave-packet (8.120) results in a jet made from modes whose typical virtuality is q_L as in (8.129) meaning that the stopping distance of a typical mode in the jet is given by

$$T x_{\text{typical stopping}} \sim \frac{(EL)^{1/4}}{T}. \tag{8.130}$$

Since most of the modes have a virtuality of order q_L, the most part of most wave-packets will be attenuated as they travel this typical stopping distance. Nevertheless, by virtue of Eq. (8.126), those components of the wave packet with

$q^2 < q_L^2$ will have a longer propagation length, and it is those components that we must analyze in order to obtain the maximal stopping distance.

We have already seen from the result (8.126) that for a given jet energy the longest stopping distances are achieved for the smallest virtualities q^2. However, Eq. (8.126) is not valid for arbitrarily small values of q^2 since in this limit the geometric optics approximation used to derive the stopping distance (8.126) fails. As in any other context in which a geometric optics approximation is used, its validity requires that the wavelength of the particle in question does not change significantly over a distance given by that wavelength itself. The wavelength of the particle is determined by the particle momentum in the z-direction, which can be obtained from the null geodesic equation, $q_M g^{MN} q_N = 0$, and is

$$q_z(z) = \frac{E}{f(z)} \sqrt{z^4/z_0^4 + z^{*4}/z_0^4} \,, \tag{8.131}$$

with $f(z) = 1 - z^4/z_0^4$ as in (4.33). The wavelength of the particle is then $\lambda = \sqrt{g_{zz}}/q_z$. In the region $z \sim z^*$ that dominates the calculation of the stopping distance, the derivative of λ with respect to the proper length in the z direction, $\ell = \int \sqrt{g_{zz}} dz$, must be small. This yields the condition $1/\sqrt{g_{zz}} \partial_z \lambda \ll 1$. This condition is satisfied, and the result (8.126) is valid, only if

$$\left(\pi^4 T^4 E^2\right)^{1/3} \ll q^2 \,. \tag{8.132}$$

Together with the condition that $q^2 \ll E^2$, required directly from the setup of the calculation, we find that we have now reproduced the range (8.125) within which q must lie. Using (8.132) in (8.126), we reproduce the maximal stopping distance (8.127), which can be phrased as the inequality

$$T x_{\text{stopping}} \ll (E/T)^{1/3} \,. \tag{8.133}$$

For values of q^2 smaller than the lower limit of the range (8.132), the geometric optic calculation stops being valid. Nevertheless, the explicit calculation in terms of three-point functions can be applied to any q^2 and shows that for those small values of q^2 the gauge field excitations are absorbed very quickly by the black hole, as can be inferred from the fact that in this circumstance $z_q > z^*$. So, analysis of this case does not change the conclusion (8.133). We see that the present analysis yields the same $E^{1/3}$ dependence of the maximal stopping distance that was also obtained in Section (8.4.1) via a completely different calculation in which a back-to-back pair of jets was modeled by a string. However, the two results nevertheless do differ parametrically since the stopping distance (8.118) is suppressed relative to (8.133) by a scaling of the energy E by a factor of $\sqrt{\lambda}$. Both calculations find the same stopping distance, but they do so for objects whose energy differs by this factor. At a qualitative level, this factor can be understood as arising from the fact that

the string in Section 8.4.1 describes a hard parton dressed with a cloud (of fields; of softer partons) whose energy is thus greater than that of the object we have analyzed here, it turns out by a factor of $\sqrt{\lambda}$. Loosely speaking, one can think of (8.133) as the stopping distance for an object that is initially a single hard parton with energy E whereas (8.118) is the stopping distance for an object with energy E that is dressed from the beginning.

The parametric difference between the results (8.118) and (8.133) from these two different calculations of the maximal stopping distance are yet further evidence that in this strongly coupled theory the behavior of "jets" depends on the details of how these excitations are prepared. In fact, we could repeat the analysis that in this section we applied to the energetic excitations sourced by an external gauge field for the disturbances sourced by the insertion of other operators with varying scaling dimension Δ. In QCD, operators with large Δ will involve many quark fields, meaning that using them as sources would correspond to injecting multiple partons into the strongly coupled plasma. If done at large enough energy, we would always get a collimated beam resembling a jet. (In Section 8.6 we shall describe a completely different way of creating a collimated beam of many gluons.) In the strongly coupled theory, the treatment of the excitations sourced by operators with dimension Δ would be completely analogous to the calculation of those sourced by the gauge field that we have described except that the mass of the falling particle obtained in the geometric optics approximation would be larger, as it would depend on Δ as in Eq. (5.24). The maximum stopping distance would therefore scale as [74]

$$T x_{\text{stopping}} \ll \left(\frac{ET}{\Delta} \right)^{1/3} , \qquad (8.134)$$

which means that the excitations sourced by higher dimensional operators are easier to stop.

The analysis that leads to Eq. (8.134) was performed only for local operators with Δ parametrically of order one and thus is not applicable to the excitations described by a falling string discussed in Section 8.4.1. Nevertheless, it is tempting to note that for very massive fields the scaling dimension of the dual operator is roughly the mass, as in Eq. (5.24), and to note furthermore that the strings considered in the stopping distance calculations of Section 8.4.1 have a mass of order $M \sim \sqrt{\lambda}/z_c$, with z_c the initial position of the endpoint of the falling string. This suggests that the falling strings of Section 8.4.1 can, loosely, be thought of in the language of this section as the insertion of excitations sourced by an operator with a scaling dimension $\Delta \sim \sqrt{\lambda}$. The result (8.134) would then have the same parametric dependence as the result (8.118) for the falling strings. Or, as we phrased it

loosely above, the result (8.118) for a falling string with energy E can be understood as the stopping distance for a dressed object with energy E containing many partons within it.

We caution, however, that attempting to explain a distinction between results that differ only by a factor of $\sqrt{\lambda}$ is perilous, since this distinction will almost certainly disappear in QCD itself. At high energies in QCD we expect the relevant coupling to become small and the difference between the "jets" created as in Section 8.4.1 and in the present section (8.4.2) should disappear. It is therefore not obvious which of the two calculations describes "jets" that are better caricatures of the jets in QCD. This observation is yet one more way to see the difficulties of interpreting the various holographic calculations of the quenching of "jets" made of energetic light particles, which is to say the difficulties of using calculations done in a strongly coupled theory that has no real jets to gain qualitative insights into jet quenching in QCD. That said, the result that the maximal stopping distance is proportional to $E^{1/3}$ arises in both calculations, and we shall see it arise in a completely different third calculation in Section 8.6, making this result seem rather robust.

In summary, the two different approaches to energetic light particles that we have described have some common features but also some important differences, differences which ultimately arise from the fact that jets in the QCD sense do not exist in strongly coupled theories. Nevertheless, the calculations provide many insights into the physics of energetic light particles propagating through strongly coupled plasma. It will be very interesting to see how these insights fare when compared with results on jet quenching in heavy ion collisions at RHIC and the LHC, and in particular to comparisons between how jets of different energies survive propagation through different lengths of plasma with varying temperatures.

8.5 Calculating the jet quenching parameter

As we have described in Section 2.3, when a parton with large transverse momentum is produced in a hard scattering that occurs within a heavy ion collision, the presence of the medium in which the energetic parton finds itself has two significant effects: it causes the parton to lose energy and it changes the direction of the parton's momentum. The latter effect is referred to as "transverse momentum broadening". In the high parton energy limit, as established first in Refs. [421, 98, 817], the parton loses energy dominantly by inelastic processes that are the QCD analogue of bremsstrahlung: the parton radiates gluons as it interacts with the medium. It is crucial to the calculation of this radiative energy loss process that the incident hard parton, the outgoing parton, and the radiated gluons are all continually being jostled by the medium in which they find themselves: they are *all* subject to transverse momentum broadening. The transverse momentum

broadening of a hard parton is described by $P(k_\perp)$, defined as the probability that after propagating through the medium for a distance L the hard parton has acquired transverse momentum $k_\perp$. For later convenience, we shall choose to normalize $P(k_\perp)$ as follows:

$$\int \frac{d^2k_\perp}{(2\pi)^2} P(k_\perp) = 1 .$$ (8.135)

From the probability density $P(k_\perp)$, it is straightforward to obtain the mean transverse momentum picked up by the hard parton per unit distance travelled (or, equivalently in the high parton energy limit, per unit time):

$$\hat{q} \equiv \frac{\langle k_\perp^2 \rangle}{L} = \frac{1}{L} \int \frac{d^2k_\perp}{(2\pi)^2} k_\perp^2 P(k_\perp) .$$ (8.136)

$P(k_\perp)$, and consequently $\hat{q}$, can be evaluated for a hard quark or a hard gluon. In the calculation of radiative parton energy loss [98, 817, 797, 420, 414, 795, 76] that we have reviewed in Section 2.3 and that is also reviewed in Refs. [101, 551, 422, 490, 251, 13, 799, 591], $\hat{q}$ for the radiated gluon plays a central role, and this quantity is referred to as the "jet quenching parameter". Consequently, $\hat{q}$ should be thought of as a (or even the) property of the strongly coupled medium that is "measured" (perhaps constrained is a better phrase) by radiative parton energy loss and hence jet quenching. But, it is important to note that $\hat{q}$ is *defined* via transverse momentum broadening only. Radiation and energy loss do not arise in its definition, although they are central to its importance.

The BDMPS calculation of parton energy loss in QCD involves a number of scales which must be well separated in order for this calculation to be relevant. The radiated gluons have energy up to $\omega_c \sim \hat{q}L^2$ and transverse momenta of order $\sqrt{\hat{q}L}$. Both these scales must be much less than E and much greater than T. And, α_S evaluated at both these scales must be small enough that physics at these scales is weakly coupled, even if physics at scales of order T is strongly coupled. In heavy ion collisions at RHIC, with the highest energy partons having E only of order many tens of GeV, this separation of scales can be questioned. In heavy ion collisions at the LHC it is possible to study the interaction of partons with energies of order a few hundred GeV, which should improve the reliability of the calculations reviewed in this section. In this section, we shall review the calculation of $\hat{q}$ – the property of the plasma that describes transverse momentum broadening directly and, in the high parton energy limit in which the relevant scales are well separated, controls the transverse momentum and the energy of the gluon radiation that dominates parton energy loss.

It has been shown via several different calculations done via conventional field theoretical methods [251, 576, 317] that the probability for a hard parton in the

representation $\mathcal{R}$ of $SU(N)$ to obtain transverse momentum $k_\perp$ after it travels a distance L through a medium is given by the two-dimensional Fourier transform in $x_\perp$ of the expectation value (8.138) of two light-like Wilson lines separated in the transverse plane by the vector $x_\perp$,

$$P(k_\perp) = \int d^2x_\perp \, e^{-ik_\perp \cdot x_\perp} \, \mathcal{W}_\mathcal{R}(x_\perp) \tag{8.137}$$

with

$$\mathcal{W}_\mathcal{R}(x_\perp) = \frac{1}{d(\mathcal{R})} \left\langle \mathrm{Tr} \left[W_\mathcal{R}^\dagger[0, x_\perp] \, W_\mathcal{R}[0, 0] \right] \right\rangle, \tag{8.138}$$

where

$$W_\mathcal{R}\left[x^+, x_\perp \right] \equiv P \left\{ \exp \left[ig \int_0^{L^-} dx^- A_\mathcal{R}^+(x^+, x^-, x_\perp) \right] \right\} \tag{8.139}$$

is the representation-$\mathcal{R}$ Wilson line along the lightcone, $L^- = \sqrt{2}L$ is the distance along the lightcone corresponding to traveling a distance L through the medium, and where $d(\mathcal{R})$ is the dimension of the representation $\mathcal{R}$. Note that the requirement (8.135) that the probability distribution $P(k_\perp)$ be normalized is equivalent to the requirement that $\mathcal{W}_\mathcal{R}(0) = 1$. The result (8.137) is similar to (8.51) although the physical context in which it arises is different as is the path followed by the Wilson line. One of the derivations [251] of (8.137) is analogous to the derivation of (8.51) that we reviewed in Section 8.2. Another derivation [317] proceeds via the use of the optical theorem to relate $P(k_\perp)$ to an appropriate forward scattering matrix element that can then be calculated explicitly via formulating the calculation of transverse momentum broadening in the language of Soft Collinear Effective Theory [124, 125, 123, 127, 126]. This derivation in particular makes it clear that (8.137) is valid whether the plasma through which the energetic quark is propagating, i.e. the plasma which is causing the transverse momentum broadening, is weakly coupled or strongly coupled.

It is important to notice that the expectation value of the trace of the product of two light-like Wilson lines that arises in $P(k_\perp)$ and hence in $\hat{q}$, namely $\mathcal{W}_\mathcal{R}(x_\perp)$ of (8.138), has a different operator ordering from that in a standard Wilson loop. Upon expanding the exponential, each of the A^+ that arise can be written as the product of an operator and a group matrix: $A^+ = (A^+)^a t^a$. It is clear (for example, either by analogy with our discussion around (8.45) in the analysis of momentum broadening of heavy quarks or from the explicit derivation in Ref. [317]) that in $\mathcal{W}_\mathcal{R}(x_\perp)$ both the operators and the group matrices are path ordered. In contrast, in a conventional Wilson loop the group matrices are path ordered but the operators are time ordered. Because the operators in (8.138) are path ordered, the expectation value in (8.138) should be described by using the Schwinger–Keldysh contour in Fig. 8.6 with one of the light-like Wilson lines on the $\mathrm{Im}\, t = 0$ segment of the contour and the other
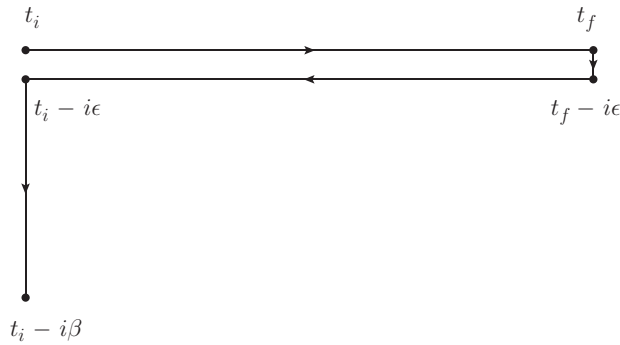
Figure 8.6 The Schwinger–Keldysh contour that must be used in the evaluation of $\mathcal{W}_{\mathcal{R}}(x_\perp)$. It is similar to that in Fig. 8.2. Figure from Ref. [317].

light-like Wilson line on the $\mathrm{Im}\,t = -i\epsilon$ segment of the contour. The infinitesimal displacement of one Wilson line with respect to the other in Fig. 8.6 ensures that the operators from the two lines are ordered such that all operators from one line come before any operators from the other. In contrast, the loop $\mathcal{C}$ for a standard Wilson loop operator lies entirely at $\mathrm{Im}\,t = 0$, and the operators for a standard Wilson loop are time ordered.

The transverse momentum broadening of a hard parton with energy E is due to repeated interactions with gluons from the medium which, if the medium is in equilibrium at temperature T, carry transverse momenta of order T and light-cone momenta of order T^2/E [480, 317]. The relation (8.137) between $P(k_\perp)$ (and hence $\hat{q}$) and the expectation value $\mathcal{W}$ of (8.138) is valid as long as $E \gg \hat{q}L^2$ (which is to say E must be much greater than the characteristic energy of the radiated gluons) even if $\alpha_S(T)$ is in no way small, i.e. it is valid in the large-E limit even if the hard parton is interacting with a strongly coupled plasma and even if the soft interactions that generate transverse momentum broadening are not suppressed by any weak coupling either [317]. However, in this circumstance even though (8.137) is valid it was not particularly useful until recently because there is no known conventional field theoretical *evaluation* of $\mathcal{W}$ for a strongly coupled plasma. (Since lattice quantum field theory is formulated in Euclidean space, it is not well-suited for the evaluation of the expectation value of light-like Wilson lines.) In this section we review the evaluation of $\mathcal{W}$, and hence $\hat{q}$, in the strongly coupled plasma of $\mathcal{N} = 4$ SYM theory with gauge group $SU(N_c)$ in the large N and strong coupling limit using its gravitational dual, namely the AdS Schwarzschild black hole at nonzero temperature [582, 208, 225, 579, 87, 66, 645, 584, 418, 468, 317]. The calculation is not simply an application of results reviewed in Section 5.4 both because the operators are path ordered and because the Wilson lines are light-like.

We begin by sketching how the standard AdS/CFT procedure for computing a Wilson loop in the fundamental representation in the large-N_c and strong coupling

limit, reviewed in Section 5.4, applies to a light-like Wilson loop with standard operator ordering [582, 584], and then below describe how the calculation (but not the result) changes when the operator ordering is as in (8.138). Consider a Wilson loop operator $W(\mathcal{C})$ specified by a closed loop $\mathcal{C}$ in the $(3 + 1)$-dimensional field theory, and thus on the boundary of the $(4 + 1)$-dimensional AdS space. $\langle W(\mathcal{C})\rangle$ is then given by the exponential of the classical action of an extremized string worldsheet Σ in AdS which ends on $\mathcal{C}$. The contour $\mathcal{C}$ lives within the $(3 + 1)$-dimensional Minkowski space boundary, but the string worldsheet Σ attached to it hangs "down" into the bulk of the curved five-dimensional AdS$_5$ spacetime. More explicitly, consider two long parallel light-like Wilson lines separated by a distance $x_\perp$ in a transverse direction.[2] (The string world sheet hanging down into the bulk from these two Wilson lines can be visualized as in Fig. 8.8 below if one keeps everything in that figure at Im $t = 0$, i.e. if one ignores the issue of operator ordering.) Upon parameterizing the two-dimensional worldsheet by the coordinates $\sigma^\alpha = (\tau, \sigma)$, the location of the string worldsheet in the five-dimensional spacetime with coordinates x^μ is

$$x^\mu = x^\mu(\tau, \sigma) \tag{8.140}$$

and the Nambu–Goto action for the string worldsheet is given by

$$S = -\frac{1}{2\pi\alpha'} \int d\sigma d\tau \sqrt{-\det g_{\alpha\beta}} . \tag{8.141}$$

Here,

$$g_{\alpha\beta} = G_{\mu\nu}\partial_\alpha x^\mu \partial_\beta x^\nu \tag{8.142}$$

is the induced metric on the worldsheet and $G_{\mu\nu}$ is the metric of the $(4 + 1)$-dimensional AdS$_5$ spacetime. Denoting by $S(\mathcal{C})$ the classical action which extremizes the Nambu–Goto action (8.141) for the string worldsheet with the boundary condition that it ends on the curve $\mathcal{C}$, the expectation value of the Wilson loop operator is then given by

$$\langle W(\mathcal{C})\rangle = \exp\left[i\left\{S(\mathcal{C}) - S_0\right\}\right] , \tag{8.143}$$

where the subtraction S_0 is the action of two disjoint strings hanging straight down from the two Wilson lines. In order to obtain the thermal expectation value at nonzero temperature, one takes the metric $G_{\mu\nu}$ in (8.142) to be that of an AdS Schwarzschild black hole (5.33) with a horizon at $r = r_0$ and Hawking temperature $T = r_0/(\pi R^2)$. The AdS curvature radius R and the string tension $1/(2\pi\alpha')$ are related to the 't Hooft coupling in the Yang–Mills theory $\lambda \equiv g^2 N_c$ by $\sqrt{\lambda} = R^2/\alpha'$.

---

[2] Note that for a light-like contour $\mathcal{C}$, the Wilson line (5.68) of $\mathcal{N} = 4$ SYM theory reduces to the familiar (8.139).

We shall assume that the length of the two light-like lines $L^- = \sqrt{2}L$ is much greater than their transverse separation $x_\perp$, which can be justified after the fact by using the result for $\mathcal{W}(x_\perp)$ to show that the $x_\perp$-integral in (8.137) is dominated by values of $x_\perp$ that satisfy $x_\perp \ll 1/\sqrt{\hat{q}L} \sim 1/\sqrt{\sqrt{\lambda}LT^3}$. As long as we are interested in $L \gg 1/T$, then $x_\perp \ll 1/(T\lambda^{1/4}) \ll 1/T \ll L$. With $L^- \gg x_\perp$, we can ignore the ends of the light-like Wilson lines and assume that the shape of the surface Σ is translationally invariant along the light-like direction. The action (8.141) now takes the form

$$S = i \frac{\sqrt{2} r_0^2 \sqrt{\lambda} L^-}{2\pi R^4} \int_0^{x_\perp/2} d\sigma \sqrt{1 + \frac{r'^2 R^4}{r^4 - r_0^4}} \,, \tag{8.144}$$

where the shape of the worldsheet Σ is described by the function $r(\sigma)$ that satisfies $r(\pm\frac{x_\perp}{2}) = \infty$, which preserves the symmetry $r(\sigma) = r(-\sigma)$, and where $r' = \partial_\sigma r$. The equation of motion for $r(\sigma)$ is then

$$r'^2 = \frac{\gamma^2}{R^4} \left(r^4 - r_0^4\right) \tag{8.145}$$

with γ an integration constant. Eq. (8.145) has two solutions. One has $\gamma = 0$ and hence $r' = 0$, meaning that $r(\sigma) = \infty$ for all σ: the surface Σ stays at infinity. Generalizations of this solution have also been studied [62, 63]. We shall see below that such solutions are not relevant. The other solution has $\gamma > 0$. It "descends" from $r(\pm\frac{x_\perp}{2}) = \infty$ and has a turning point where $r' = 0$ which, by symmetry, must occur at $\sigma = 0$. From (8.145), the turning point must occur at the horizon $r = r_0$. Integrating (8.145) gives the condition that specifies the value of γ:

$$\frac{x_\perp}{2} = \frac{R^2}{\gamma} \int_{r_0}^\infty \frac{dr}{\sqrt{r^4 - r_0^4}} = \frac{a R^2}{\gamma r_0} \,, \tag{8.146}$$

where we have defined

$$a \equiv \sqrt{\pi}\,\Gamma(\tfrac{5}{4})/\Gamma(\tfrac{3}{4}) \approx 1.311 \,. \tag{8.147}$$

Putting all the pieces together, we find [582, 584]

$$S = \frac{ia\sqrt{\lambda}TL^-}{\sqrt{2}} \sqrt{1 + \frac{\pi^2 T^2 x_\perp^2}{4a^2}} \,. \tag{8.148}$$

We see that S is imaginary, because when the contour $\mathcal{C}$ at the boundary is light-like the surface Σ hanging down from it is space-like. It is worth noting that S had to turn out to be imaginary, in order for $\langle W \rangle$ in (8.143) to be real and the transverse momentum broadening $P(k_\perp)$ to be real, as it must be since it is a probability distribution. The surface Σ that we have used in this calculation descends from

infinity, skims the horizon, and returns to infinity. Note that the surface descends all the way to the horizon regardless of how small $x_\perp$ is. This is reasonable on physical grounds, as we expect $P(k_\perp)$ to depend on the physics of the thermal medium [582, 584]. We shall see below that it is also required on mathematical grounds: when we complete the calculation by taking into account the nonstandard operator ordering in (8.137), we shall see that only a worldsheet that touches the horizon is relevant [317].

We now consider the computation of (8.138), with its nonstandard operator ordering corresponding to putting one of the two light-like Wilson lines on the $\text{Im}\, t = 0$ contour in Fig. 8.6 and the other on the $\text{Im}\, t = -i\epsilon$ contour. The procedure we shall describe is a specific example of the more general discussion of Lorentzian AdS/CFT given in Refs. [743, 744, 786, 120]. In order to compute (8.138) we first need to construct the bulk geometry corresponding to the $\text{Im}\, t = -i\epsilon$ segment of the Schwinger–Keldysh contour in Fig. 8.6. For this purpose it is natural to consider the black hole geometry with complex time. In Fig. 8.7, we show two slices of this complexified geometry. The left plot is the Penrose diagram for the fully extended black hole spacetime with quadrant I and III corresponding to the slice $\text{Im}\, t = 0$ and $\text{Im}\, t = -\frac{\beta}{2}$ respectively, while the right plot is for the Euclidean black hole geometry, i.e. corresponding to the slice $\text{Re}\, t = 0$. Note that because the black hole has a nonzero temperature, the imaginary part of t is periodic with the period given by the inverse temperature β. In the left plot the imaginary time direction can be considered as a circular direction coming out of the paper at quadrant I, going a half circle to reach quadrant III and then going into the paper for a half circle to end back at I. In the right plot the real time direction can be visualized as the direction perpendicular to the paper.

The first segment of the Schwinger–Keldysh contour in Fig. 8.6, with $\text{Im}\, t = 0$, lies at the boundary ($r = \infty$) of quadrant I in Fig. 8.7, where it is shown as a green dot. The second segment of the Schwinger–Keldysh contour, with $\text{Im}\, t = -i\epsilon$, is shown as a red dot at the $r = \infty$ boundary of a copy of I that in the left plot of Fig. 8.7 lies infinitesimally outside the paper and in the right plot of Fig. 8.7 lies at an infinitesimally different angle. We shall denote this copy of I by I′. The geometry and metric in I′ are identical to those of I. Note that I′ and I are joined together at the horizon $r = r_0$, namely at the origin in the right plot of Fig. 8.7. Now, the thermal expectation value (8.138) can be computed by putting the two parallel light-like Wilson lines at the boundaries of I and I′, and finding the extremized string world sheet which ends on both of them. Note that since I and I′ meet only at the horizon, the only way for there to be a non-trivial (i.e. connected) string worldsheet whose boundary is the two Wilson lines in (8.138) is for such a string worldsheet (shown as the red and green lines in Fig. 8.7) to touch the horizon. Happily, this is precisely the feature of the string worldsheet found in the explicit calculation that we reviewed above. So, we can use that string worldsheet in the
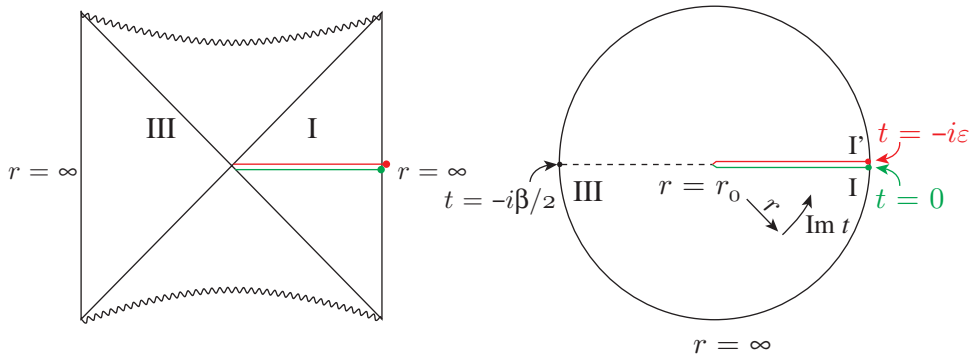
Figure 8.7 Penrose diagrams for Lorentzian ($\mathrm{Im}\,t = 0$ or $-\beta/2$; left panel) and Euclidean ($\mathrm{Re}\,t = 0$; right panel) sections of an AdS black hole. (Penrose diagrams were introduced in Fig. 7.1; a textbook presentation of Penrose diagrams for black hole spacetimes can be found, for example, in Refs. [619, 683].) In the left panel, the black hole horizon is represented by the diagonal lines; the Euclidean section in the right panel touches the horizon only at the point at the origin. The region of the black hole spacetime inside the horizon, which ends at the singularity indicated by wavy lines, is only visible in the left panel. The sections depicted in the left and right panels should be imagined glued together along the horizontal lines across their midpoints, where $\mathrm{Re}\,t = 0$ and the two sections intersect. The Euclidean section, now depicted in the right panel, would then be sticking out of and into the page from the $\mathrm{Re}\,t = 0$ line of the Lorentzian section in the left panel. In the right panel, the two light-like Wilson lines are points at $r = \infty$, indicated by the red and green dots. These dots are the boundaries of a string worldsheet that extends inward to $r = r_0$, which is at the origin of the Euclidean section of the black hole. In the left panel, the string worldsheet and its endpoints at $r = \infty$ are shown at $\mathrm{Re}\,t = 0$; as $\mathrm{Re}\,t$ runs from $-\infty$ to ∞, the string worldsheet sweeps out the whole of quadrant I. Figure redrawn after Ref. [317].

present analysis, with the only difference being that half the string worldsheet now lies on I and half on I′, as illustrated in Fig. 8.8.[3]

We conclude that the result for the expectation value (8.138), with its nonstandard path ordering of operators, is identical to that obtained in Refs. [582, 584] for a light-like Wilson loop with standard time ordering of operators [317]. That

---

[3] The calculation of $\hat{q}$ in $\mathcal{N} = 4$ SYM theory via (8.138) nicely resolves a subtlety. As we saw above, in addition to the extremized string configuration which touches the horizon, the string action also has another trivial solution which lies solely at the boundary, at $r = \infty$. Based on the connection between position in the r dimension in the gravitational theory and energy scale in the quantum field theory, the authors of Ref. [582, 584] argued that physical considerations (namely the fact that $\hat{q}$ should reflect thermal physics at energy scales of order T) require selecting the extremized string configuration that touches the horizon. Although this physical argument remains valid, we now see that it is not necessary. In (8.138), the two Wilson lines are at the boundaries of I and I', with different values of $\mathrm{Im}\,t$. That means that there are no string worldsheets that connect the two Wilson lines without touching the horizon. So, once we have understood how the nonstandard operator ordering in (8.138) modifies the boundary conditions for the string worldsheet, we see that the trivial worldsheet of Refs. [582, 584] and all of its generalizations in Refs. [62, 63] do not satisfy the correct boundary conditions. The non-trivial worldsheet illustrated in Fig. 8.8, which is sensitive to thermal physics [582, 584, 585], is the only extremized worldsheet bounded by the two light-like Wilson lines in (8.138) [317].
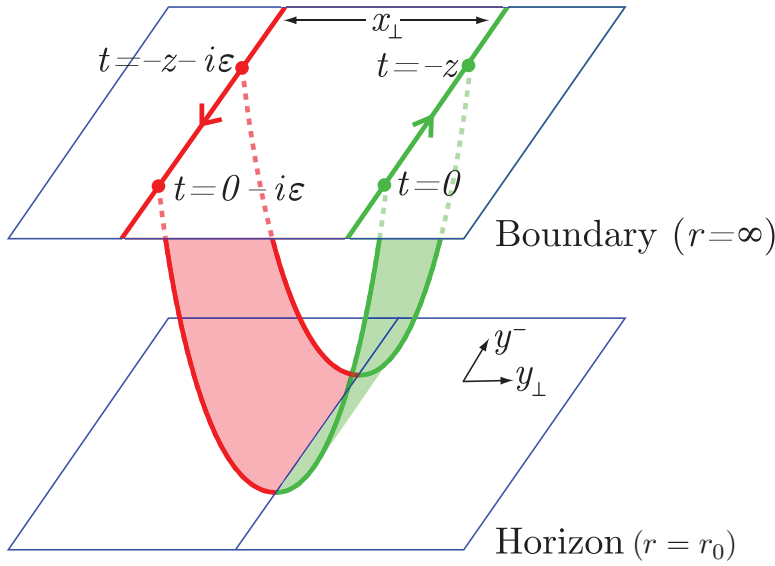
Figure 8.8 String configuration for the thermal expectation value of (8.138). The red and green dots at $t = 0$ and $t = -i\epsilon$ are the red and green dots in Fig. 8.7; the red and green string world sheet "hanging" from them is shown in Fig. 8.7 as the red and green lines. Figure from Ref. [317].

is, in strongly coupled $\mathcal{N} = 4$ SYM theory $\mathcal{W}(x_\perp)$ in the adjoint representation is given by

$$\mathcal{W}_{\mathcal{A}}(x_\perp) = \exp\left[-\sqrt{2}a\sqrt{\lambda}\,L^-T\left(\sqrt{1 + \frac{\pi^2 T^2 x_\perp^2}{4a^2}} - 1\right)\right]. \qquad (8.149)$$

We have quoted the result for $\mathcal{W}_{\mathcal{A}}(x_\perp)$, which is given by $\mathcal{W}_{\mathcal{F}}^2(x_\perp)$ in the large-N_c limit, because that is what arises in the analysis of jet quenching, see Section 2.3.2. (Radiative parton energy loss depends on the medium through the transverse momentum broadening of the radiated gluons, which are of course in the adjoint representation.) The $x_\perp$-independent term in the exponent in (8.149), namely "the -1", is the finite subtraction of S_0, which was identified in Ref. [582] as the action of two disjoint strings hanging straight down from the two Wilson lines to the horizon of the AdS black hole. Our calculation serves as a check of the value of S_0, since only with the correct S_0 do we obtain $\mathcal{W}_{\mathcal{A}}(0) = 1$ and a correctly normalized probability distribution $P(k_\perp)$. Note that our field theory set-up requires $L^-T \gg 1$, and our supergravity calculation requires $\lambda \gg 1$, meaning that our result (8.149) is valid only for

$$\sqrt{\lambda}\,L^-T \gg 1. \qquad (8.150)$$

In this regime, (8.149) is very small unless $\pi x_\perp T/(2a)$ is small. This means that when we take the Fourier transform of (8.149) to obtain the probability distribution $P(k_\perp)$, in the regime (8.150) where the calculation is valid the Fourier transform is dominated by small values of $x_\perp$, for which

$$\mathcal{W}_\mathcal{A}(x_\perp) \simeq \exp\left[-\frac{\pi^2}{4\sqrt{2}a}\sqrt{\lambda}L^- T^3 x_\perp^2\right] , \qquad (8.151)$$

and we therefore obtain

$$P(k_\perp) = \frac{4\sqrt{2}a}{\pi\sqrt{\lambda}T^3 L^-} \exp\left[-\frac{\sqrt{2}a k_\perp^2}{\pi^2\sqrt{\lambda}T^3 L^-}\right] . \qquad (8.152)$$

Thus, the probability distribution $P(k_\perp)$ is a Gaussian with a width, by virtue of (8.150), that is much larger than T and the jet quenching parameter (8.136) can easily be evaluated, yielding [582]

$$\hat{q} = \frac{\pi^{3/2}\Gamma(\frac{3}{4})}{\Gamma(\frac{5}{4})}\sqrt{\lambda}T^3 . \qquad (8.153)$$

The probability distribution (8.152) has a simple physical interpretation: the probability that the quark has gained transverse momentum $k_\perp$ is given by diffusion in transverse momentum space with a diffusion constant given by $\hat{q}L$. This is indeed consistent with the physical expectation that transverse momentum broadening in a strongly coupled plasma is due to the accumulated effect of many soft kicks (by gluons) from the medium: the quark performs Brownian motion in momentum space even though in coordinate space it remains on a light-like trajectory. It is interesting that the result can be interpreted in this way even though, as we have seen in Section 6.3, the strongly coupled plasma of $\mathcal{N}=4$ SYM theory contains no quasiparticles off which the hard quark could scatter. The presence of such quasiparticles at short length scales would give the probability distribution $P(k_\perp)$ a power-law tail at large $k_\perp$; the plasma of $\mathcal{N}=4$ SYM theory is a strongly coupled liquid at all length scales, making (8.152) Gaussian even at large $k_\perp$ [318]. Although there are no pointlike scattering centers present, the hard quark is nevertheless kicked softly many times by the strongly coupled liquid through which it propagates.

If we attempt to plug RHIC-motivated numbers into the result (8.153), taking $T=300$ MeV, $N_c=3$, $\alpha_{SYM}=\frac{1}{2}$ and therefore $\lambda=6\pi$ yields $\hat{q}=4.5$ GeV^2/fm, which turns out to be in the same ballpark as the values of $\hat{q}$ inferred from RHIC data on the suppression of high momentum partons in heavy ion collisions [582, 584].[4] To see this, we can write the result (8.153) as

---

[4] Data from the LHC exhibit somewhat stronger quenching that corresponds to a larger value of $\hat{q}$. This is consistent with the expectation that the plasma produced at the LHC should have a higher initial temperature.

$$\hat{q} \simeq 57\sqrt{\alpha_{\mathrm{SYM}}\frac{N_c}{3}}\,T^3\;, \tag{8.154}$$

which can be compared to the result given in Eqs. (2.43) and (2.44) that was extracted via comparison to RHIC data in Ref. [68]. To make the comparison, we need to relate the QCD energy density ε appearing in (2.43) to T. Lattice calculations of QCD thermodynamics indicate $\varepsilon \sim (9-11)\,T^4$ in the temperature regime that is relevant at RHIC [179]. This then means that if in (8.154) we take α_{SYM} within the range $\alpha_{\mathrm{SYM}} = 0.66^{+.34}_{-.25}$, the result (8.154) for the strongly coupled $\mathcal{N} = 4$ SYM plasma is consistent with the result (2.44) obtained via comparing QCD jet quenching calculations to RHIC data.

We have described the $\mathcal{N} = 4$ SYM calculation, but the jet quenching parameter can be calculated in any conformal theory with a gravity dual [584]. In a large class of such theories in which the spacetime for the gravity dual is $\mathrm{AdS}_5 \times \mathrm{M}_5$ for some internal manifold M_5 other than the five-sphere S_5 which gives $\mathcal{N} = 4$ SYM theory [584],

$$\frac{\hat{q}_{\mathrm{CFT}}}{\hat{q}_{\mathcal{N}=4}} = \sqrt{\frac{s_{\mathrm{CFT}}}{s_{\mathcal{N}=4}}}\;, \tag{8.155}$$

with s the entropy density. This result makes a central qualitative lesson from (8.153) clear: in a strongly coupled plasma, the jet quenching parameter is not proportional to the entropy density or to some number density of distinct scatterers. This qualitative lesson is more robust than any attempt to make a quantitative comparison to QCD. But, we note that if QCD were conformal, (8.155) would suggest

$$\frac{\hat{q}_{\mathrm{QCD}}}{\hat{q}_{\mathcal{N}=4}} \approx 0.63\;. \tag{8.156}$$

And, analysis of how $\hat{q}$ changes in a particular toy model in which nonconformality can be introduced by hand then suggests that introducing the degree of nonconformality seen in QCD thermodynamics may increase $\hat{q}$ by a few tens of percent [585]; $\hat{q}$ also increases with increasing nonconformality in strongly coupled $\mathcal{N} = 2^*$ gauge theory [418, 468]. Putting together these observations that suggest that neither the nonconformality of QCD nor the fact that it has fewer degrees of freedom than $\mathcal{N} = 4$ SYM theory modify $\hat{q}$ dramatically together with the fact that they seem to push $\hat{q}$ in opposite directions, perhaps it is not surprising that the $\hat{q}$ for the strongly coupled plasma of $\mathcal{N} = 4$ SYM theory is in the same ballpark as that extracted by comparison with RHIC data.

8.6 Quenching a beam of strongly coupled gluons

In Section 8.5 we have analyzed jet quenching via the strategy of working as far as possible within weakly coupled QCD and only using a holographic calculation

within $\mathcal{N} = 4$ SYM theory for one small part of the story, namely the calculation of the jet quenching parameter $\hat{q}$ through which the physics of the strongly coupled medium enters the calculation. This approach has been justified in the high jet energy limit, where the dominant energy loss process for an energetic parton plowing through quark–gluon plasma with temperature T is medium-induced gluon bremsstrahlung [421, 98, 817], radiating gluons with energy ω and momentum transverse to the jet direction $k_\perp$ that satisfy $E \gg \omega \gg k_\perp \gg \pi T$ [98, 817, 797, 414, 420]. This set of approximations, i.e. the assumption that all these scales are well separated, is the basis of the approach in Section 8.5, and indeed of all analytic perturbative calculations of radiative energy loss to date. The (perhaps naive) expectation based upon these considerations is that at least some of the energy lost by the high energy parton should emerge as relatively hard particles (since $\omega \ggg \pi T$) near the jet direction (since $\omega \gg k_\perp$), resulting in a jet whose angular distribution has been broadened and whose fragmentation function has been softened. Stimulated by the data from the LHC, several groups have developed more sophisticated implementations of these considerations, formulating an essentially perturbative approach to jet quenching that compares well with the jet quenching measurements published to date for jets with sufficiently high transverse momentum [257, 699, 815, 820, 243, 698, 247, 816, 69, 613, 139, 258, 140, 612, 71, 819]. One still expects that any such perturbative approach must have limitations, even for the hardest processes accessible in heavy ion collisions, since it is based upon the premise that the QCD coupling evaluated at the scale $k_\perp$ (which, recall, is $\lll E$ but $\gg \pi T$) is weak even if the physics at scales $\sim \pi T$ is strongly coupled. This makes it important to analyze models of jet quenching in strongly coupled plasmas in contexts where reliable analyses are possible. Even if such analyses yield only qualitative insight, they can be useful as benchmarks and as guides to how to think about the physics. By pursuing such approaches and the perturbative approach, we expect to bracket the experimentally accessible regime and to gain insight into the extent to which the strongly coupled physics that governs the medium itself is also relevant for hard processes.

With these motivations in mind, in this section we return to assuming that the physics at all relevant scales is strongly coupled, as in Section 8.4. We saw in that section that there is no way to analyze how an actual jet is modified by the strongly coupled plasma of $\mathcal{N} = 4$ SYM theory, relative to how it would have developed in the vacuum of that theory, because hard scattering in strongly coupled $\mathcal{N} = 4$ SYM theory does not produce jets. The results described in Section 8.4, although sensitive to details of the initial conditions, addressed the question of how single partons are stopped and thermalized in the plasma and in particular how far they can travel before they are stopped. However, a reasonable framework for understanding the quenching of jets cannot be based solely on discussing single partons that lose energy in the medium and then are either stopped in the medium or emerge in

isolation and fragment into ordinary-looking jets. The problem with this picture is that what would emerge is a nearly on-shell quark, which would then not fragment into a jet in the usual way. A phenomenologically more meaningful picture is that of a hard parent parton that fragments rapidly into a protojet (a perturbative process that we do not expect to describe by strong coupling methods) with this protojet then propagating through the strongly coupled plasma, interacting strongly with it, and losing energy.

If we are to gain insight into jets in heavy ion collisions from a strongly coupled perspective, it would be useful to have a thought experiment in which we could construct a closely collimated beam of partons that is either propagating through the vacuum or through the strongly coupled plasma. In this section, we shall start by describing a thought experiment [85, 295] by which such a beam of gluons is produced with an angular distribution and a distribution of momenta that is well understood in vacuum. We shall then watch what happens as this beam of gluons shines through the strongly coupled plasma at nonzero temperature and gets rapidly attenuated – with no apparent broadening of its angular distribution or softening of the momenta of the gluons that it is made of – while the lost energy appears as soft collective excitations, sound waves that subsequently dissipate. From a purely theoretical perspective it is instructive to have a thought experiment in which we can see an excitation that is moving at the speed of light and that is made of quanta with momenta $\gg \pi T$ that couple to, and lose energy to, the soft hydrodynamic modes of the strongly coupled plasma. From this perspective, the thought experiment in this section serves as a worked example fitting within the more general discussion of equilibration processes found in Chapter 7. We shall close this section with a phenomenological perspective, however, by noting the ways in which the results of the thought experiment bear qualitative resemblance to results from real experiments on jets in heavy ion collisions.

8.6.1 A beam of strongly coupled synchrotron radiation in vacuum

The trick by which a beam of gluons can be produced in $\mathcal{N} = 4$ SYM theory is to consider a test quark undergoing circular motion with radius R_0 and velocity v (and hence angular velocity $\Omega \equiv v/R_0$) in the vacuum of this theory [85, 471]. At both weak coupling (where the calculation is done conventionally) and strong coupling (where the calculation is done via gauge/gravity duality) the radiation that results is remarkably similar to the synchrotron radiation of classical electrodynamics, produced by an electron in circular motion [85]. In particular, as the limit of ultra-relativistic motion is taken ($\gamma \to \infty$ where $\gamma \equiv 1/\sqrt{1 - v^2}$) the lighthouse-like beam of radiation becomes more and more tightly collimated in angle (it is focused in a cone of angular extent $\sim 1/\gamma$) and is composed of gluons and scalars with shorter and shorter wavelengths (the pulse of gluons in the beam has a
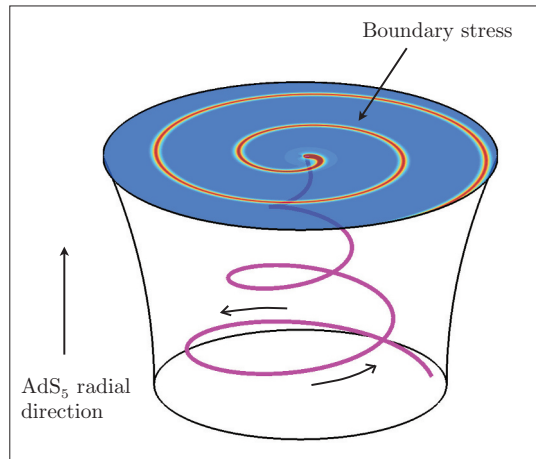
Figure 8.9 Cartoon from Ref. [85] of the gravitational description of synchrotron radiation at strong coupling: the quark rotating at the boundary trails a rotating string behind it which hangs down into the bulk AdS$_5$ space. This string acts as a source of gravitational waves in the bulk, and this gravitational radiation induces a stress tensor on the four-dimensional boundary. By computing the bulk-to-boundary propagator one obtains the boundary theory stress tensor that describes the radiated energy. The entire calculation can be done analytically [85].

width $\sim R_0/\gamma^3$ in the radial direction in which it is moving). The emitted radiation was found to propagate outward at the speed of light forever without broadening either in angle or in pulse width, just as in classical electrodynamics [85, 434, 471, 435, 284, 104, 285]. At weak coupling, the slight differences in the angular distribution of the power radiated to infinity relative to that in classical electrodynamics can be attributed to the fact that scalars are radiated as well as gluons [85]. And, at strong coupling the angular distribution is identical to that at weak coupling [85, 435, 104]. The way the calculation is done at strong coupling is sketched in Fig. 8.9. The logic of the calculation is as we described in Section 8.3, and so we shall not present it in detail. It turns out, however, that in vacuum the shape of the rotating string in the bulk and the corresponding form of the energy density of the outward-propagating radiation on the boundary can both be determined analytically [85]. This beam is not literally a jet, since it is not produced far off shell. But, we know from Hofman and Maldacena that a far off shell "photon" does not result in jets in this theory. And, this beam of non-Abelian radiation yields a different cartoon of a jet than those we have described in Section 8.4 and, as we shall see, allows us to answer questions about its propagation through the medium that have not yet been posed in the formalism of Section 8.4.

Although it has recently been explained from the gravitational point of view in beautifully geometric terms [470], from the point of view of the non-Abelian gauge theory it is surprising that the angular distribution of the radiation at strong coupling seen in Fig. 8.10 is so similar (see Ref. [85] for quantitative comparisons) to
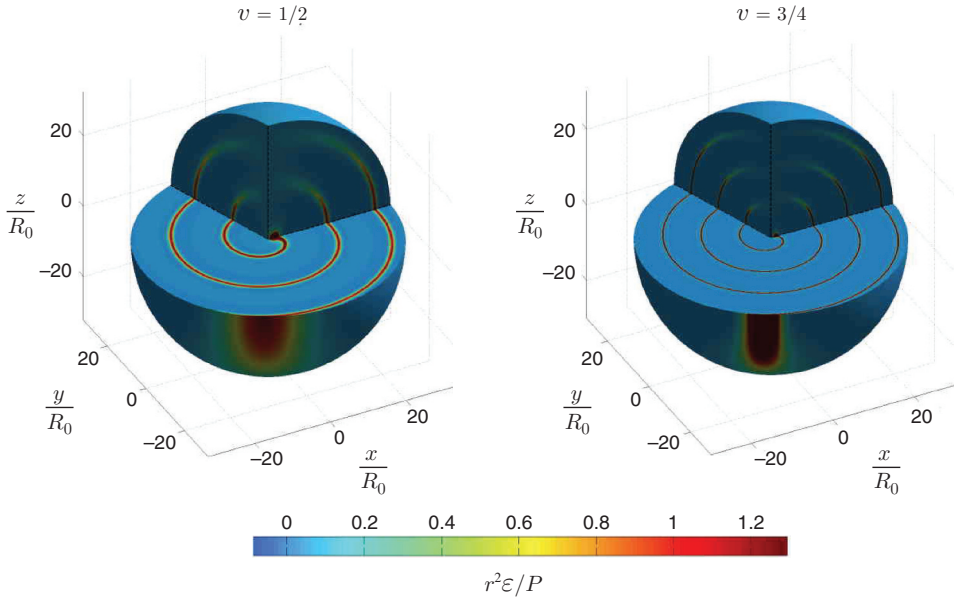
Figure 8.10 Cutaway plots of $r^2 \mathcal{E}/P$ for a test quark in circular motion with $v = 1/2$ and $v = 3/4$. Here, $\mathcal{E}$ is the energy density and P is the total power radiated per unit time. We see a spiral of radiation, propagating radially outwards at the speed of light, without any spreading. The spiral is localized about $\theta = \pi/2$ with a characteristic width $\delta\theta \propto 1/\gamma$. The radial thickness of the spiral is proportional to $1/\gamma^3$. Figure taken from Ref. [85].

that at weak coupling, where what is radiated is a mixture of colored – and therefore interacting – gluons and scalars. The fact that, even when the coupling is arbitrarily strong, as the pulses of radiation propagate outwards they do not spread at all and never isotropize indicates that intuition based upon parton branching [433] (namely that the non-Abelian character of the radiation should result in energy flowing from short to long wavelengths as the pulses propagate outwards and should yield isotropization at large distances) is invalid in this context.[5]

8.6.2 Shining a gluon beam through strongly coupled plasma

For our purposes, the result that the "beam" of radiated gluons (and scalars) produced by a quark in circular motion propagates outward with a fixed angular width that we can select by picking γ is fortuitous. It means that this roundabout method

---

[5] Reference [434] shows that isotropization via some analog of parton branching is also not the correct picture for the radiation studied in Ref. [457] by Hofman and Maldacena: this radiation also propagates outward as a pulse without any spreading, but this pulse is spherically symmetric at all radii. So, in the case studied by Hofman and Maldacena there is no process of isotropization because the radiation is isotropic at all times while in the case illustrated in Fig. 8.10 there is no isotropization because the radiation never becomes isotropic.

yields a state that looks something like a jet. It is not a jet in that it is not produced via the fragmentation of an initially far offshell parton. But, it is a collimated beam of gluons of known, and controllable, angular width. For this reason, results obtained in the formal setting of a test quark moving in a circle open the way to new means of modeling jet quenching in heavy ion collisions [295]. We shall see that when this beam of gluons shines through the strongly coupled plasma it is attenuated over a length scale that can be understood analytically and we shall see that as the beam is attenuated it does not broaden in angle or redden in wavelength.

The first step in the analysis of how the collimated beam of gluons is quenched by the strongly coupled plasma is to determine the shape of the spiraling string (see the cartoon in Fig. 8.9) in the case where the bulk metric is the AdS-black hole (AdS-BH) metric that describes the plasma, rather than the AdS metric that describes only the vacuum [346, 295]. The rotating string in the AdS-BH geometry, spiraling "downward" from the quark in circular motion at the AdS-BH boundary toward its horizon, spiraling around and around infinitely many times just above the horizon, perturbs the AdS-BH geometry via Einstein's equations. The second step in the analysis is to solve Einstein's equations, linearized in the perturbation, and use the perturbations of the bulk metric at the boundary to determine the energy density in the boundary $\mathcal{N} = 4$ SYM plasma, including the beam of gluons that this spiraling string describes. This calculation was performed in Ref. [295] and although it introduces new technical elements its logic is the same as that in the simpler calculation that we have reviewed in Section 8.3, and we shall therefore not describe the calculation here. Below we shall describe the results, as well as analytic arguments that explain all their qualitative features, but first we must establish some further notation and expectations.

To discuss the rate at which a quark undergoing circular motion through the plasma of strongly coupled $\mathcal{N} = 4$ SYM theory loses energy, it is useful to distinguish two regimes [346], depending on whether

$$\Xi \equiv \frac{\Omega^2 \gamma^3}{(\pi T^2)} \tag{8.157}$$

is $\gg 1$ or $\ll 1$. For $\Xi \gg 1$, the energy loss rate is given by the generalized Larmor formula

$$\left. \frac{dE}{dt} \right|_{\text{rad}} = \frac{\sqrt{\lambda}}{2\pi} a^\mu a_\mu, \tag{8.158}$$

where a^μ is the quark's proper acceleration. As we mentioned in Section 8.1, it was shown many years ago by Mikhailov that the energy loss rate of a quark in circular motion in the vacuum of strongly coupled $\mathcal{N} = 4$ SYM theory is given by (8.158) [618] and so in the strongly coupled plasma at $T \neq 0$, in the $\Xi \gg 1$ regime we expect to see the radiation of beam of synchrotron-like radiation as in

vacuum [85], and the subsequent attenuation of this beam. When $\Xi \ll 1$, on the other hand, acceleration becomes unimportant and the energy loss rate is that due to the drag force exerted by the strongly coupled hydrodynamic fluid on a quark moving in a straight line with velocity v [346], namely [394, 452]

$$\left. \frac{dE}{dt} \right|_{\text{drag}} = \frac{\sqrt{\lambda}}{2\pi} (\pi T)^2 v^2 \gamma \ . \tag{8.159}$$

Notice that the parameter Ξ which governs which expression for the energy loss rate is valid is simply the ratio of the rates appearing in Eqs. (8.158) and (8.159). In this respect it is as if both hydrodynamic drag and Larmor radiation are in play with the larger of the two effects dominating the energy loss, but this simplified picture is not quantitatively correct because where $\Xi \sim 1$ the energy loss rate is less than the sum of Eqs. (8.158) and (8.159) [346]. Although our principal interest is in the $\Xi > 1$ regime, where we can study the quenching of a beam of synchrotron gluons, it is also instructive to look at $\Xi < 1$ and $\Xi \sim 1$ as in these regimes the hydrodynamic response of the plasma – i.e. the production of sound waves – is more readily apparent.

Unlike in vacuum, in the plasma at nonzero temperature the energy disturbance created by the rotating quark can excite *two* qualitatively distinct modes in the energy density; a sound mode which at long wavelengths travels at speed $c_s = 1/\sqrt{3}$, and a light-like mode which propagates at the speed of light. The relative amplitude of each mode depends on the trajectory of the quark: when $\Xi < 1$ the dominant modes that are excited are sound waves; when $\Xi > 1$ the dominant modes that are excited propagate at the speed of light. Interestingly, in the $\Xi \sim 1$ regime as the pulse of radiation moving at the speed of light is attenuated in energy, it sheds a sound wave [295].

Figure 8.11 shows three different plots of $r^2 \Delta \mathcal{E}/P$ for quarks in circular motion with each of three different velocities: $v = 0.15$, $v = 0.3$ and $v = 0.5$. Here, $\Delta \mathcal{E}$ is the total energy density minus that of the undisturbed plasma and $P \equiv dE/dt$ is the energy lost by the circulating quark (and hence dumped into the plasma) per unit time. In all plots, the quark's trajectory lies in the equatorial plane $\theta = \pi/2$, the quark is rotating counter-clockwise. And, in all plots the temperature of the plasma is given by $\pi T = 0.15/R_0$ and the units are chosen such that the radius of the quark's trajectory is $R_0 = 1$. This means that Ξ defined in (8.157) is given by 1.0, 4.6 and 17.1 in the left, middle and right columns respectively. At the time shown, the quark is located at $x = R_0$, $y = 0$ and the quark is rotating counter-clockwise in the plane $z = 0$. The three plots in the top row are cutaway plots with the cutaways coinciding with the planes $z = 0$, $\phi = 0$ and $\phi = 7\pi/5$. The three plots in the middle row show the energy density on the plane $z = 0$ and the bottom three plots give the energy density at $z = 0$, $\phi = \pi/2$, namely a slice through the
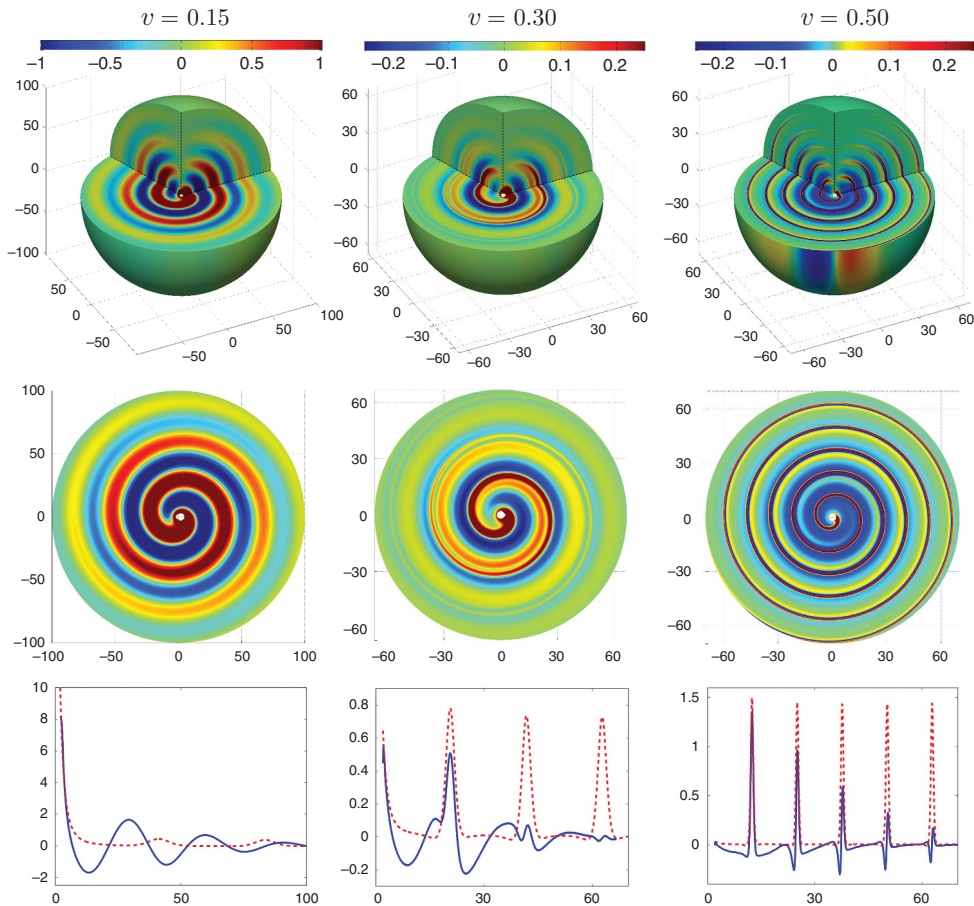
Figure 8.11 Plots from Ref. [295] illustrating the energy density of strongly coupled $\mathcal{N} = 4$ SYM plasma in which a test quark is rotating on a circle with radius R_0 with angular velocity $\Omega = v/R_0$ for $v = 0.15$ (left column), $v = 0.3$ (middle column) and $v = 0.5$ (right column). Top: cutaway plots of $r^2 \Delta \mathcal{E}/P$ where P is the power radiated by the quark. Middle: plots of $r^2 \Delta \mathcal{E}/P$ on the equatorial plane $\theta = \pi/2$ (i.e. $z = 0$). Bottom: solid blue curves are plots of $r^2 \Delta \mathcal{E}/P$ at $\theta = \pi/2$ and $\phi = \pi/2$. The dashed red curves in the bottom plots show $r^2 \mathcal{E}/P$ for the strongly coupled synchrotron radiation emitted by a quark in circular motion in vacuum [85], pulses of radiation that propagate outward to $r \to \infty$ at the speed of light without spreading.

middle row plot along one radial line. For reference, the dashed red curves in these bottom plots show $r^2 \mathcal{E}$ for the strongly coupled synchrotron radiation that a quark moving along the same circular trajectory would emit in vacuum [85]. In each of the bottom plots, we use the same P to normalize the dashed red curve as for the solid blue curve. All nine panels in Fig. 8.11 show the energy density at one instant of time, but the time-dependence is easily restored by replacing the azimuthal angle

ϕ by $\phi - \Omega t$, where $\Omega = v/R_0$ is the angular velocity. As a function of increasing time, the entire patterns in the upper and middle rows rotate with angular velocity Ω, as the spirals of radiation move outwards. As a function of increasing time, the patterns in the lower rows move outwards, repeating themselves after a time $2\pi/\Omega$.

As is evident from Fig. 8.11, as the quark accelerates along its circular trajectory, energy is radiated outwards in a spiral pattern which is attenuated as the radiation propagates outwards through the plasma to increasing r. However, the qualitative features of the spiral patterns differ greatly at the three different quark velocities shown. For $v = 0.15$, the spiral arms are very broad in r, as broad as their separation, and the spiral pattern propagates outwards at the speed of sound, while being attenuated with increasing r. Second order hydrodynamics for a conformal fluid with a gravity dual like $\mathcal{N} = 4$ SYM theory predicts a sound velocity $1/\sqrt{3} + 0.116\, q^2/(\pi T)^2 + \cdots$ [107] for sound waves with wave-vector q. The sound waves in the left column of Fig. 8.11 do not actually have only a single wave-vector but, roughly, they have $q \sim 1.3\,\pi T$ and are moving outward with a velocity ~ 0.74, quite close to the $\mathcal{O}(q^2)$ prediction for the sound velocity. The dashed red curve in the lower-left panel shows the energy density of the synchrotron radiation that this quark would have emitted if it were in vacuum, and we see that there is no sign of this in the results. So, at this v, corresponding to $\Xi = 1.0$, the rotating quark is emitting sound waves.

The results in the right column of Fig. 8.11, for $v = 0.5$, are strikingly different. The spiral arms are very narrow in r, much narrower than their separation, and they propagate outwards at the speed of light, as can be seen immediately in the bottom-right panel by comparing the results of the calculation, the solid blue curve, to the energy density of the synchrotron radiation that this quark would have emitted if it were in vacuum, shown by the dashed red curve. We see that at this v, corresponding to $\Xi = 17.1$, the rotating quark is emitting strongly coupled synchrotron radiation, as in vacuum [85], and we see that the radiation is being attenuated as it propagates outward in r, through the strongly coupled plasma. Remarkably, even as the outgoing pulses of energy are very significantly attenuated by the medium we see no sign of their broadening in either the θ or the ϕ or the r directions. Looking at the vertical sections in the upper-right panel, we see that if anything the spread of the beam of radiation in θ is becoming less as it propagates and gets attenuated. This conclusion is further strengthened by careful comparison of the upper-right panel of Fig. 8.11 to the analogous results for a quark in circular motion in vacuum [295]. It is certainly clear that the presence of the medium does *not* result in the spreading of energy away from the center of the beam at the equator out toward large polar angles. Just the opposite, in fact: at large polar angles the beam gets attenuated more rapidly than near $\theta = \pi/2$. Broadening in either the ϕ or the r directions would be manifest as widening of the pulses in the bottom-right panel,

and this is also certainly not seen. In fact, extending the plot in the bottom-right panel out to larger r, for several more turns of the spiral, shows continued rapid attenuation with no visible broadening [295].

We turn our attention now to the center column of Fig. 8.11. Here, with a rotation velocity of $v = 0.3$ corresponding to $\Xi = 4.6$, we clearly see both synchrotron radiation and sound waves. The synchrotron radiation is most easily identified with reference to the results for a quark with this rotation velocity in vacuum, shown in the dashed red curve in the bottom-center panel. In our results with $T \neq 0$, we see the emission of a pulse of synchrotron radiation whose amplitude is very rapidly attenuated, much more rapidly than in the right column. In part guided by our inspection of the results at large Ξ in the right column, we see that as the pulse of synchrotron radiation is attenuated, it too does not broaden. What we see here that is not so easily seen in the right column is that as the pulse of synchrotron radiation is attenuated it "sheds" a sound wave, leaving behind it a broad wave, reminiscent of the sound waves in the left column. Behind each pulse of synchrotron radiation we see the "compression half" of a sound wave, and behind that a deeper rarefaction, and then the next pulse of synchrotron radiation arrives. Once seen in the middle column, this phenomenon can perhaps also be discerned to a much lesser degree in the right column, with each pulse of synchrotron radiation trailed first by a region of slight compression and then by a region of some rarefaction. It is not really clear in the right column whether these can be called sound waves, both because of their smaller amplitude and because the next pulse of synchrotron radiation overwhelms them sooner than in the middle column. In the middle column, though, the interpretation is clear: the beam of synchrotron gluons is exciting sound waves in the plasma.

The results of Ref. [295], for example those in Fig. 8.11, demonstrate that at small Ξ the rotating quark emits only sound waves while at large Ξ it emits strongly coupled synchrotron radiation as in vacuum, with that beam of gluons subsequently being quenched by the plasma. The calculation has also been done at $v = 0.65$ [295], corresponding to $\Xi = 42.8$. In this case, the beam of gluons travels out to larger r as it is attenuated. Even so, as the beam is being almost completely attenuated by the plasma it continues to propagate at the speed of light and it does not broaden.

There are several (related) obstacles to obtaining definitive answers to the question of where the energy that is initially in the gluon beam goes as the gluon beam gets attenuated [295]. The first we have discussed above: we cannot watch the plasma behind one of the pulses of radiation very long before the next pulse comes along and obliterates whatever the previous pulse has left behind. A further obstacle arises because the analysis concerns a scenario in which the quark has been moving in a circle for an infinitely long time meaning that a steady-state in which the energy density at any position is a periodic function of time has been achieved.

We see in Fig. 8.11 that the energy density in the beam falls off faster than $1/r^2$ at large r. So, the natural expectation is that the beam heats the plasma up in the range of r over which it gets attenuated – perhaps it first makes sound waves, but ultimately these too will damp, leaving just a heated region of plasma. This expectation cannot be correct in a steady-state calculation, since a continual heating up of some region of space blatantly contradicts the steady-state assumption. So, what actually happens to the energy in this calculation? At sufficiently large r the energy density $\Delta \mathcal{E}$ is zero. This means that at sufficiently large r, there is an outward flux of energy whose magnitude, averaged over angles, is $P/(4\pi r^2)$ with P the energy lost by the rotating quark per unit time. This energy flux corresponds to a collective outward flow of the plasma with a velocity, averaged over angles, given by [295]

$$v_{\text{plasma}} = \frac{P}{4\pi r^2 (\mathcal{E} + p)} = \frac{\pi}{2N_c^2} \frac{P}{(\pi T)^2} \frac{1}{(r\,\pi T)^2}, \qquad (8.160)$$

where we have used the fact that the sum of the energy density and pressure of the plasma in equilibrium is $\mathcal{E} + p = \pi^2 N_c^2 T^4/2$. We see that in the large-N_c limit, the velocity v_{plasma} is infinitesimal. So, in the steady-state calculation whose results we have presented, the energy from the gluon beam ultimately finds its way into an infinite wavelength mode with infinitesimal amplitude [295]. A mode like this can be thought of as a sound wave with infinite wavelength and infinitesimal amplitude (i.e. infinitesimal longitudinal velocity). In a sense, this energy flux corresponding to an infinitesimal-velocity outward flow of the plasma is the closest that a steady-state calculation can come to describing the heating up of a region of the plasma.

8.6.3 Qualitative features, analytically

Much can be understood about the qualitative features of the results illustrated in Fig. 8.11 by studying the quasinormal modes of the AdS-BH spacetime that provide the dual gravitational description of the physics and that we introduced in Section 6.4. In the dual gravitational picture, the moving string excites a full spectrum of gravitational quasinormal modes, which propagate outwards and eventually get absorbed by the black hole. The propagation and absorption of these quasinormal modes manifests itself on the boundary as the propagation and attenuation of the spirals of energy density shown in Fig. 8.11. The dispersion relations $\omega(q)$ of the lowest quasinormal mode were obtained in Ref. [295] using methods developed previously [555].

   Figure 8.12 shows the dispersion relation for the lowest quasinormal mode (i.e. the one with the smallest imaginary part). As we saw in Section 6.4, for $q \ll \pi T$ this dispersion relation has the asymptotic form expected for the hydrodynamics of any conformal fluid [107]
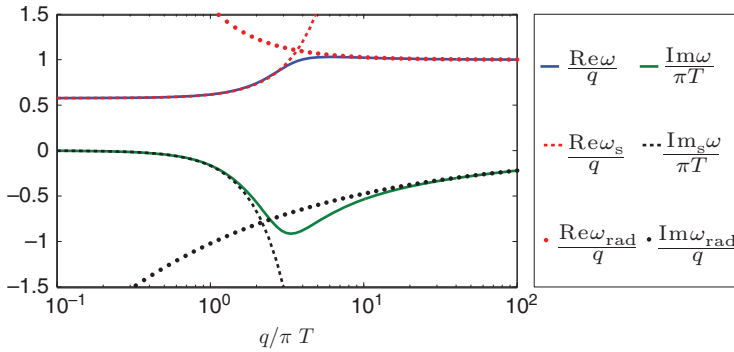
Figure 8.12 A plot of the real and imaginary parts of the dispersion relation of the lowest quasinormal mode taken from Ref. [295]. We plot $\mathrm{Re}\,\omega/q$ and $\mathrm{Im}\,\omega/(\pi T)$ since these ratios are both of order 1. For $q \ll \pi T$ the dispersion relation is that of sound waves whose dispersion relation is given up to order q^3 by Eq. (8.161), plotted as dashed lines in the figure. For $q \gg \pi T$ the dispersion relation is that of waves which propagate at the speed of light. The large-q asymptotic expression (8.163) that we have obtained by fitting the results in this figure is plotted as the dotted lines.

$$\omega_s(q) = c_s q - i\Gamma q^2 + \frac{\Gamma}{c_s}\left(c_s^2 \tau_\Pi - \frac{\Gamma}{2}\right)q^3 + \mathcal{O}(q^4)\,, \qquad (8.161)$$

where in $\mathcal{N} = 4$ SYM theory, with its classical gravity dual, all the constants are known analytically: the low-q speed of sound is $c_s = 1/\sqrt{3}$, the sound attenuation constant Γ is given by $\pi T\,\Gamma = 1/6$, and the relaxation time τ_Π is given by $\pi T\tau_\Pi = (2 - \log 2)/2$. These modes represent propagating sound waves which attenuate over a time scale

$$t_s^{\text{damping}} \sim \frac{1}{\Gamma q^2}\,. \qquad (8.162)$$

The dispersion relation (8.161) is plotted as the red and black dashed curves in Fig. 8.12; it describes the full dispersion relation very well for $q \lesssim 2\pi T$. This supports the observation that the waves in the left column of Fig. 8.11 are sound waves. Since these waves are not monochromatic (and since in the dual gravitational description they are not described solely by the lowest quasinormal mode) they cannot be compared quantitatively to (8.161), but their velocity is as (8.161) predicts for $q \sim 1.2\,\pi T$, which is comparable to the $q \sim 1.3\,\pi T$ obtained from their peak-to-peak wavelength. Using $q \sim 1.2\,\pi T$ in (8.162) predicts a sound attenuation timescale $(\Delta t)_{\text{sound}} \sim 4.5/(\pi T) \sim 30\,R_0$, which is comparable to but a little shorter than the exponential decay time for the amplitude of the waves in the left column of Fig. 8.11, which is closer to $40\,R_0$. So, the low-q regime of

the dispersion relation in Fig. 8.12 that describes sound waves does a reasonable job of capturing the qualitative features of the waves seen in the left column of Fig. 8.11.

The dispersion relations of the higher quasinormal modes (those with more negative imaginary parts) can also be determined [295]. At $q \ll \pi T$ they approach the asymptotic form $\omega = (\tilde{a} - i\tilde{b})\pi T$ where $\tilde{a}$ and $\tilde{b}$ are mode-dependent $\mathcal{O}(1)$ constants, with values that are larger and larger for higher and higher modes. (For the lowest quasinormal mode, $\tilde{a} = \tilde{b} = 0$.) At low q, disturbances of the plasma described by higher quasinormal modes attenuate on a time scale of order $1/(\tilde{b}\pi T)$ that is much shorter than that for the sound waves described by the lowest quasinormal mode, namely (8.162).

Let us turn now to $q \gg \pi T$. As we noted in Section 6.4, in this regime the dispersion relation for the lowest quasinormal mode takes the asymptotic form

$$\omega_{\text{rad}} = q + \pi T (a - ib) \left(\frac{\pi T}{q} \right)^{1/3} + \cdots , \tag{8.163}$$

as argued for on general grounds in Ref. [349], with $a \approx 0.58$ and $b \approx 1.022$ [295]. At $q \gg \pi T$ the dispersion relations of all quasinormal modes approach the asymptotic form (8.163), with a and b mode-dependent $\mathcal{O}(1)$ constants, again with values that are larger and larger for higher and higher modes. Therefore, generically the high q modes propagate at close to the speed of light and attenuate over a time scale

$$t_{\text{rad}}^{\text{damping}} \sim \frac{1}{\pi T b} \left(\frac{q}{\pi T} \right)^{1/3} , \tag{8.164}$$

where we shall use the value $b \approx 1.022$ from the lowest quasinormal mode in making estimates, keeping in mind that if the contribution of higher quasinormal modes were important this would increase the effective b somewhat. The fact that the pulses of energy in Fig. 8.11 are far from being monochromatic waves introduces a larger uncertainty than does not knowing how much the higher quasinormal modes contribute.

We have plotted the large-q asymptotic expression (8.163) for the dispersion relation for the lowest quasinormal mode as the dotted red and black curves in Fig. 8.12, and we see that it describes the full result very well for $q \gtrsim 20\pi T$, and has the right shape at a qualitative level down to about $q \sim 5\pi T$. This is consistent with our observation that the narrow pulses of synchrotron radiation in the middle column, where the pulses have a full width at half maximum (FWHM) $\sim 2.5\, R_0$ corresponding very roughly to $q \sim 6\pi T$, and the right column, where the pulses have a FWHM $\sim R_0$ corresponding very roughly to $q \sim 15\pi T$, propagate outwards at the speed of light. Converting the widths of these pulses into estimates of q is very rough because the pulses are neither sinusoidal nor Gaussian.

If we nevertheless try substituting $q \sim 15\pi T$ into (8.164) we find that it predicts $t_{\text{rad}}^{\text{damping}} \sim 16\, R_0$, which is roughly half the exponential decay time for the amplitude of the waves in the lower-right panel of Fig. 8.11. Again, quantitative comparison is not possible, but inferences drawn from the large-q dispersion relation for the lowest quasinormal mode (8.163) is at least in the right ballpark. The qualitative prediction from (8.164) is that narrower pulses, with higher q, can penetrate farther into the strongly coupled plasma, and this is also apparent in the numerical results.

It is interesting to note that the distance scale (8.164) over which the beam of gluons is quenched has the same parametric dependence as the maximal stopping distance (8.133) or (8.134). Both the present calculation and that in Section 8.4.2 describe the propagation of an energetic excitation injected into the plasma, but the means by which this injection is accomplished are completely different. It is therefore a pleasing sign of the robustness of the result that the same parametric dependence of the stopping distance is obtained.

The quasinormal mode analysis also has interesting qualitative implications for understanding the formation of quark–gluon plasma via the thermalization of some initially far-from-equilibrium state, as discussed in Chapter 7. If short wavelength excitations present in the initial conditions or created during the far-from-equilibrium evolution are sufficiently long lived, they can spend much of their lifetime propagating through nearly-equilibrated quark–gluon plasma, where their evolution can be understood via the quasinormal mode dispersion relations. Equation (8.164) indicates that the maximum thermalization time for modes of momentum $q \gg \pi T$ is $\sim q^{1/3}(\pi T)^{-4/3}$. This means that short wavelength modes thermalize more slowly than modes with momenta of order πT, a conclusion that has also been reached via a rather different analysis of the away-from-equilibrium correlation functions that govern Hawking radiation in a time-dependent spacetime [286].

We can also use the quasinormal mode dispersion relation to understand why the pulses do not broaden significantly in the radial direction as they propagate. The increase in the width of a pulse as it propagates for a time t is $\sim t\, \Delta q\, d^2\omega/dq^2$, where Δq is the width of the pulse in q-space. Taking $\Delta q \sim q$ and using the large-q dispersion relation (8.163), we find that after the radiation damping time given by (8.164) the pulse should have broadened by $\sim 4a/(9bq)$. If the pulse had a Gaussian profile, this would correspond to broadening by about 10% of the original FWHM of the pulse. So, the quasinormal mode dispersion relation predicts that by the time the pulses have been significantly attenuated, they should have broadened by an amount that is parametrically of order their initial width, but smaller by a significant numerical factor. It is therefore not surprising that we see no significant broadening in Fig. 8.11.

Having understood many of the most interesting features of Fig. 8.11 qualitatively, and even semi-quantitatively, by analyzing the quasinormal mode dispersion relations gives us confidence that no new qualitative phenomena emerge for narrower pulses (higher q; e.g. from a rotating quark with larger γ), since it is clear that the results at $v = 0.5$ and $v = 0.65$ are already exploring the high-q regime of the dispersion relation in Fig. 8.12, where the asymptotic expression (8.163) is a good guide. It is also important to stress that the quasinormal mode frequencies are determined entirely by the AdS-BH metric, meaning that they reflect properties of the strongly coupled plasma itself and have nothing to do with the details of how the beam of gluons shining through it was made by the rotating quark. Given that we have been able to use the quasinormal mode dispersion relations so successfully to understand the propagation, the rate of attenuation and the lack of broadening of a beam of gluons, we are confident that these phenomena are independent of how the beam of gluons is created.

Now that we understand the steady-state results in terms of quasinormal modes, we can use the fact that the phenomena we have found are independent of how the beam of gluons is created to answer the following question: suppose that we could engineer a single pulse of strongly coupled synchrotron radiation; what would happen to this pulse as it propagates through the strongly coupled plasma? The dual gravitational description of this radiation would be governed by the same quasinormal modes we have analyzed, just sourced by a different string worldsheet. As long as we look only at distances greater than of order $1/(\pi T)$ away from the source, the disturbance of the plasma must be described by a pulse of short wavelength radiation with the dispersion relation (8.163) that moves at the speed of light, that does not broaden, and that is attenuated on timescales (8.164) as well as long wavelength sound waves with the dispersion relation (8.161) that propagate outward at the speed of sound and that are attenuated on timescales (8.162). Since these sound waves move more slowly, the pulse of radiation leaves them behind – shedding them as we see in the middle column of Fig. 8.11. (The same would happen for shorter wavelength pulses as in the right column of the figure, but in such cases in our steady-state calculation the next pulse of synchrotron radiation arrives before we can see the sound waves being left behind. As we described in Section 8.6.2, it is difficult to use a steady-state calculation to draw conclusions about what the pulse of radiation leaves behind.) In the case of a single, isolated, short wavelength pulse, the short wavelength pulse itself will get far ahead of the sound waves it has left behind as it is attenuated only on the long time-scale (8.164). By the time the short wavelength pulse has damped away, the sound waves that it shed will be far behind and according to (8.162) all but those with the very smallest q will have dissipated away as heat. Only hydrodynamic modes with very small q (i.e. heat accompanied by almost no fluid motion) will remain. (These are represented in the

steady-state calculation by the outward-going energy flux with infinite wavelength and infinitesimal amplitude that we found at the end of Section 8.6.2.) We now see that the distinction between the middle and right columns of Fig. 8.11 is that in the former case the pulse of radiation is never well separated from the sound waves that it leaves behind, because the radiation does not have a large enough q for its damping time scale (8.164) to be very much longer than $1/(\pi T)$. So, by the time the radiation has been damped the sound waves are not far behind it and have themselves not yet thermalized.

8.6.4 *From quenching a beam of strongly coupled gluons to jet quenching*

There are many qualitative similarities between the quenching of the beam of strongly coupled synchrotron radiation in the strongly coupled $\mathcal{N} = 4$ SYM plasma that we have described in this section and jet quenching in heavy ion collisions, which we introduced in Section 2.3.

The highest energy jets that have been studied to date in heavy ion collisions at the LHC [2, 264, 266, 273, 268, 3] lose significant energy but emerge as jets that (within current experimental resolution) have not been deflected in angle [273] and whose moderate and high momentum fragments are distributed in angle and in momentum quite similarly to what is seen in ordinary jets in vacuum. The energy lost from the jets does not stay in or near the jet cone, and does not emerge in the form of moderate or high momentum fragments. Instead, the lost energy becomes an excess of soft particles (momenta $\lesssim$ 1 GeV [264]) at large angles ($> 45°$ [264]) relative to the jet direction.

At a qualitative level, the behavior of the beam of gluons that we have described in this section is similar. As it propagates through the strongly coupled plasma, losing significant energy, the beam of gluons moving at the speed of light does not spread in angle or get deflected in its direction. And, even as it is significantly attenuated, it does not spread in the direction along which it propagates which means that the way in which momentum is shared among the gluons in the beam is not much changed. The beam is quenched completely after traveling a distance proportional to $q^{1/3}/(\pi T)^{4/3}$, where q is the typical wave vector of the gluons in the beam. Finally, the lost energy ends up in soft, collective modes of the plasma that initially take the form of sound waves following behind the beam and that subsequently thermalize, heating the plasma.

As we saw in Section 8.6.3, the fact that we can describe all these phenomena in terms of quasinormal modes, independently of the details of how these quasinormal modes are excited, indicates that they will characterize the quenching of any excitation that is initially made of the high momentum modes which propagate through the strongly coupled plasma at the speed of light. To the degree that it has

been possible to investigate them to date, these qualitative features are also seen in the quenching of the energetic heavy (and light) quarks introduced into the strongly coupled plasma in Sections 8.1, 8.2 and 8.3 (and Section 8.4).

If in a heavy ion collision a jet loses energy by heating the plasma the lost energy would be manifest as an excess of soft particles moving in all directions. If the lost energy is in the form of sound waves following the jet, that would correspond to an excess of soft particles near the jet direction that may be more easily visible in the case of jets with lower energies or jets that did not travel far through the plasma (meaning that the sound waves they shed did not have time to thermalize) or both. There are preliminary indications of such jet broadening in the analysis of lower energy (20–40 GeV) jets produced in heavy ion collisions at both RHIC [660, 230, 21] and the LHC [629, 389], but at the time of writing the interpretation of these data is not yet settled.

Comparisons along these lines will never be more than qualitative, since the beam of strongly coupled radiation whose propagation through strongly coupled plasma we have described in this section is not a jet. However, the multiple qualitative resonances between jet quenching in heavy ion collisions and the quenching of a beam of strongly coupled radiation suggest that some of the phenomena observed in jet quenching are intrinsically strongly coupled. At the same time, the very fact that the hard fragments of the highest energy jets seen in heavy ion collisions do look so similar to those of jets produced in vacuum suggests that at least some of the phenomena observed in jet quenching must be described by perturbative QCD. One of the goals of research at the current frontier is to find the best ways to describe the whole story.

8.7 Velocity scaling of the screening length and quarkonium suppression

We saw in Section 2.4 that, because they are smaller than typical hadrons in QCD, heavy quarkonium mesons survive as bound states even at temperatures above the crossover from a hadron gas to quark–gluon plasma. However, if the temperature of the quark–gluon plasma is high enough, they eventually dissociate. An important physical mechanism underlying the dissociation is the weakening attraction between the heavy quark and antiquark in the bound state because the force between their color charges is screened by the medium. The dissociation of charmonium and bottomonium bound states has been proposed as a signal for the formation of a hot and deconfined quark-gluon plasma in heavy ion collisions [609], and as a means of gauging the temperatures reached during the collisions.

In the limit of large quark mass, the interaction between the quark and the antiquark in a bound state in the thermal medium can be extracted from the thermal

expectation value of the Wilson loop operator $\langle W^F(\mathcal{C}_{\text{static}})\rangle$, with $\mathcal{C}_{\text{static}}$ a rectangular loop with a short side of length L in a spatial direction (say x_1) and a long side of length $\mathcal{T}$ along the time direction. This expectation value takes the form

$$\langle W^F(\mathcal{C}_{\text{static}})\rangle = \exp\left[-i\,\mathcal{T}\,E(L)\right], \tag{8.165}$$

where $E(L)$ is the (renormalized) free energy of the quark–antiquark pair with the self-energy of each quark subtracted. $E(L)$ defines an effective potential between the quark–antiquark pair. The screening of the force between color charges due to the presence of the medium manifests itself in the flattening of $E(L)$ for L greater than some characteristic length scale L_s called the screening length. In QCD, the flattening of the potential occurs smoothly, as seen in the lattice calculations illustrated in Fig. 3.5 in Section 3.3, and one must make an operational definition of L_s. For example, in the parametrization of (2.45), L_s can be set equal to $1/\mu$. L_s decreases with increasing temperature and can be used to estimate the scale of the dissociation temperature T_{diss} as

$$L_s(T_{\text{diss}}) \sim d, \tag{8.166}$$

where d is the size of a particular mesonic bound state at zero temperature. The idea here is that once the temperature of the quark–gluon plasma is high enough that the potential between a quark and an antiquark separated by a distance corresponding to the size of a particular meson has been fully screened, that meson can no longer exist as a bound state in the plasma. This means that larger quarkonium states dissociate at lower temperatures, and means that the ground-state bottomonium meson survives to the highest temperatures of all. As we discussed at length in Section 2.4, there are many important confounding effects that must be taken into account in order to realize the goal of using data on charmonium and bottomonium production in heavy ion collisions to provide evidence for this sequential pattern of quarkonium dissociation as a function of increasing temperature. In this Section, we shall focus only on one of these physical effects, one on which calculations done via gauge/gravity duality have shed some light [674, 583, 281, 226, 61, 88, 362, 772, 279, 584, 89, 608, 646, 90, 336, 84, 585, 636, 347].

In heavy ion collisions, quarkonium mesons are produced moving with some velocity $\vec{v}$ with respect to the medium. It is thus important to understand the effects of nonzero quarkonium velocity on the screening length and consequent dissociation of bound states. To describe the interaction between a quark–antiquark pair that is moving relative to the medium, it is convenient to boost into a frame in which the quark–antiquark pair is at rest, but feels a hot wind of QGP blowing past it. The effective quark potential can again be extracted from (8.165) evaluated in the boosted frame with $\mathcal{T}$ now interpreted as the proper time of the dipole. While much progress has been made in using lattice QCD calculations to extract

the effective potential between a quark–antiquark pair at rest in the QGP, there are significant difficulties in using Euclidean lattice techniques to address the (dynamical as opposed to thermodynamic) problem of a quark–antiquark pair in a hot wind. In the strongly coupled plasma of $\mathcal{N} = 4$ SYM theory with large-N_c, however, the calculation can be done using gauge/gravity duality [583, 584, 281], and requires only a modest extension of the standard methods reviewed in Section 5.4. Here, we sketch the derivation from Ref. [584].

We start with a rectangular Wilson loop whose short transverse space-like side

$$\sigma = x_1 \in [-\frac{L}{2}, \frac{L}{2}] \tag{8.167}$$

defines the separation L between the quark–antiquark pair and whose long time-like sides extend along the $x_3 = v\,t$ direction, describing a pair moving with speed v in the x_3 direction. In this frame, the plasma is at rest and the spacetime metric in the gravitational description is the familiar AdS black hole (5.33). We then apply a Lorentz boost that rotates this Wilson loop into the rest frame (t', x_3') of the quark–antiquark pair:

$$dt = dt' \cosh \eta - dx_3' \sinh \eta, \tag{8.168}$$
$$dx_3 = -dt' \sinh \eta + dx_3' \cosh \eta, \tag{8.169}$$

where the rapidity η is given by $\tanh \eta = v$, meaning that $\cosh \eta = \gamma$. After the AdS black hole metric has been transformed according to this boost, it describes the moving hot wind of plasma felt by the quark–antiquark pair in its rest frame.

In order to extract $E(L)$ it suffices to work in the limit in which the time-like extent of the Wilson loop $\mathcal{T}$ is much greater than its transverse extent L, meaning that the corresponding string worldsheet "suspended" from this Wilson loop and "hanging down" into the bulk is invariant under translations along the long direction of the Wilson loop. Parametrizing the two-dimensional worldsheet with the coordinates σ and $\tau = t$, the dependence on τ is then trivial. The task is reduced to calculating the curve $r(\sigma)$ along which the worldsheet descends into the bulk from positions on the boundary brane which we take to be located at $r = r_0 \Lambda$, with Λ a dimensionless UV cut-off that we shall take to infinity at the end of the calculation. That is, the boundary conditions on $r(\sigma)$ are

$$r\left(\pm \frac{L}{2}\right) = r_0 \Lambda. \tag{8.170}$$

It is then helpful to introduce dimensionless variables

$$r = r_0 y, \qquad \tilde{\sigma} = \sigma \frac{r_0}{R^2}, \qquad l = \frac{L r_0}{R^2} = \pi L T, \tag{8.171}$$

where $T = \frac{r_0}{\pi R^2}$ is the temperature. Upon dropping the tilde, one is then seeking to determine the shape $y(\sigma)$ of the string worldsheet satisfying the boundary conditions $y\left(\pm\frac{l}{2}\right) = \Lambda$. From the boosted AdS black hole metric, one finds that the Nambu–Goto action, which must be extremized, takes the form

$$S(\mathcal{C}) = -\sqrt{\lambda}\, \mathcal{T} T \int_0^{l/2} d\sigma\, \mathcal{L}, \tag{8.172}$$

with a Lagrangian that reads ($y' = \partial_\sigma y$)

$$\mathcal{L} = \sqrt{\left(y^4 - \cosh^2 \eta\right)\left(1 + \frac{y'^2}{y^4 - 1}\right)}. \tag{8.173}$$

We must now determine $y(\sigma)$ by extremizing (8.173). This can be thought of as a classical mechanics problem, with σ the analog of time. Since $\mathcal{L}$ does not depend on σ explicitly, the corresponding Hamiltonian

$$\mathcal{H} \equiv \mathcal{L} - y'\frac{\partial \mathcal{L}}{\partial y'} = \frac{y^4 - \cosh^2 \eta}{\mathcal{L}} = q \tag{8.174}$$

is a constant of the motion, which we denote by q. In the calculation we are presenting in this section, we take $\Lambda \to \infty$ at fixed, finite, rapidity η. In this limit, the string worldsheet in the bulk is time-like, and $E(L)$ turns out to be real. (The string worldsheet bounded by the rectangular Wilson loop that we are considering becomes space-like if $\sqrt{\cosh \eta} > \Lambda$. In order to recover the light-like Wilson loop used in the calculation of the jet quenching parameter in Section 8.5, one must first take $\eta \to \infty$ and only then take $\Lambda \to \infty$.)

It follows from the Hamiltonian (8.174) that solutions $y(\sigma)$ with $\Lambda > \sqrt{\cosh \eta}$ satisfy the equation of motion

$$y' = \frac{1}{q}\sqrt{(y^4 - 1)(y^4 - y_c^4)} \tag{8.175}$$

with

$$y_c^4 \equiv \cosh^2 \eta + q^2. \tag{8.176}$$

Note that $y_c^4 > \cosh^2 \eta \geq 1$. The extremal string worldsheet begins at $\sigma = -\ell/2$ where $y = \Lambda$, and "descends" in y until it reaches a turning point, namely the largest value of y at which $y' = 0$. It then "ascends" from the turning point to its endpoint at $\sigma = +\ell/2$ where $y = \Lambda$. By symmetry, the turning point must occur at $\sigma = 0$. We see from (8.175) that in this case, the turning point occurs at $y = y_c$ meaning that the extremal surface stretches between y_c and Λ. The integration constant q can then be determined from the equation $\frac{l}{2} = \int_0^{\frac{l}{2}} d\sigma$ which, upon using (8.175), becomes

$$l = 2q \int_{y_c}^{\Lambda} dy \, \frac{1}{\sqrt{(y^4 - y_c^4)(y^4 - 1)}} \, . \tag{8.177}$$

The action for the extremal surface can be found by substituting (8.175) into (8.172) and (8.173), yielding

$$S(l) = -\sqrt{\lambda} \mathcal{T} T \int_{y_c}^{\Lambda} dy \, \frac{y^4 - \cosh^2 \eta}{\sqrt{(y^4 - 1)(y^4 - y_c^4)}} \, . \tag{8.178}$$

Equation (8.178) contains not only the potential between the quark–antiquark pair but also the static mass of the quark and antiquark considered separately in the moving medium. (Recall that we have boosted to the rest frame of the quark and antiquark, meaning that the quark–gluon plasma is moving.) Since we are only interested in the quark–antiquark potential, we need to subtract the action S_0 of two independent quarks from (8.178) in order to obtain the quark–antiquark potential in the dipole rest frame:

$$E(L)\mathcal{T} = -S(l) + S_0 \, . \tag{8.179}$$

The string configuration corresponding to a single quark at rest in a moving $\mathcal{N} = 4$ SYM plasma was obtained in Refs. [452, 394], as we have described in Section 8.1. From this configuration one finds that

$$S_0 = -\sqrt{\lambda} \, \mathcal{T} \, T \int_{1}^{\Lambda} dy \, . \tag{8.180}$$

To extract the quark–antiquark potential, we use (8.177) to solve for q in terms of l and then plug the corresponding $q(l)$ into (8.178) and (8.179) to obtain $E(L)$. Note that (8.177) is manifestly finite as $\Lambda \to \infty$ and the limit can be taken directly. (8.178) and (8.180) are divergent separately when taking $\Lambda \to \infty$, but the difference (8.179) is finite.

We now describe general features of (8.177) and (8.179). Denoting the right-hand side of (8.177) (with $\Lambda = \infty$) as function $l(q)$, one finds that for a given η, $l(q)$ has a maximum $l_{\max}(\eta)$ and Eq. (8.177) has no solution when $l > l_{\max}(\eta)$. Thus for $l > l_{\max}$, the only string worldsheet configuration is two disjoint strings and from (8.179), $E(L) = 0$, i.e. the quark and antiquark are completely screened to the order of the approximation we are considering. We can define the screening length as

$$L_s \equiv \frac{l_{\max}(\eta)}{\pi T} \, . \tag{8.181}$$

At $\eta = 0$, i.e. the dipole at rest with the medium, one finds that

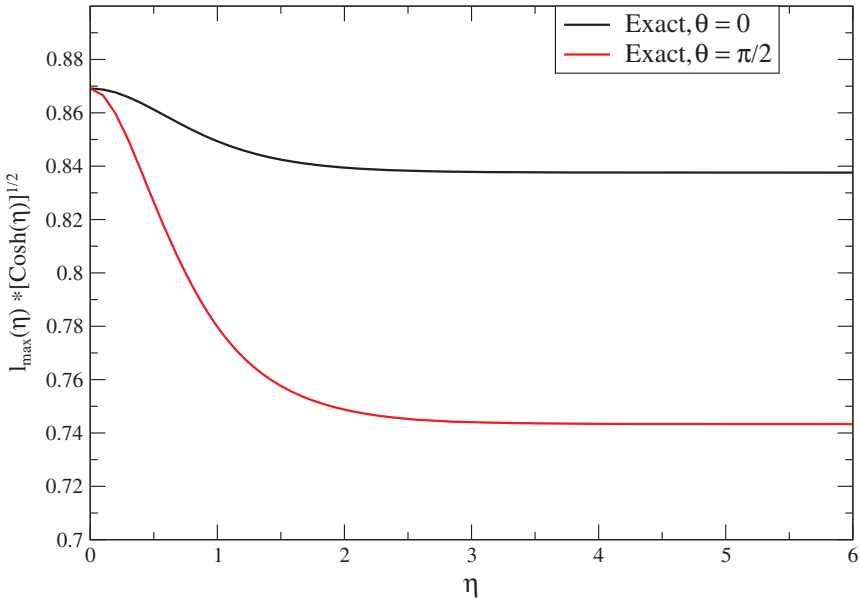$$L_s(0) \approx \frac{0.87}{\pi T} \approx \frac{0.28}{T} \, . \tag{8.182}$$

Figure 8.13 The screening length l_{max} times its leading large-η dependence $\sqrt{\cosh(\eta)}$. The two curves are for a dipole oriented perpendicular to the wind ($\theta = \pi/2$) and parallel to the wind ($\theta = 0$), respectively. Figure adapted from Ref. [584].

Similar criteria are used in the definition of screening length in QCD [522], although in QCD there is no sharply defined length scale at which screening sets in. Lattice calculations of the static potential between a heavy quark and antiquark in QCD indicate a screening length $L_s \sim 0.5/T$ in hot QCD with two flavors of light quarks [506] and $L_s \sim 0.7/T$ in hot QCD with no dynamical quarks [504]. The fact that there is a sharply defined L_s is an artifact of the limit in which we are working, in which $E(L) = 0$ for $L > L_s$.[6]

The screening length $L_s(\eta)$ can be obtained numerically, as illustrated in Fig. 8.13. One sees that the screening length decreases with increasing velocity to a good approximation according to the scaling [674, 583, 281]

$$L_s(v) \simeq \frac{L_s(0)}{\cosh^{1/2}\eta} = \frac{L_s(0)}{\sqrt{\gamma}}, \qquad (8.183)$$

with $\gamma = 1/\sqrt{1 - v^2}$. We have only discussed the case in which the direction of the hot wind is perpendicular to the dipole ($\theta = \pi/2$; the red curve in Fig. 8.13), but this discussion can be generalized to arbitrary angles θ. One finds [584] that

---

[6] We are considering the contribution to $E(L)$ that is proportional to $\sqrt{\lambda}$. For $l \gg l_{max}$, the leading contribution to $E(L)$ is proportional to λ^0 and is determined by the exchange of the lightest supergravity mode between the two disjoint strings [108].

the dependences of L_s and $E(L)$ on the angle between the dipole and the wind is very weak. For example, the black curve in Fig. 8.13 gives the η dependence of the screening length when the wind direction is parallel to the dipole. We see the difference from the perpendicular case is only about 12%.

The velocity dependence (8.183) suggests that L_s should be thought of as, to a good approximation, proportional to (energy density)$^{-1/4}$, since the energy density increases like γ^2 as the wind velocity is boosted. The velocity scaling of L_s has proved robust in the sense that it applies in various strongly coupled plasmas other than $\mathcal{N} = 4$ SYM [88, 226, 646, 585] and in the sense that it applies to baryons made of heavy quarks also [84].

If the velocity scaling of L_s (8.183) holds for QCD, it will have qualitative consequences for quarkonium suppression in heavy ion collisions [583, 584]. From (8.166), the dissociation temperature $T_{\text{diss}}(v)$, defined as the temperature above which J/ψ or Υ mesons with a given velocity do not exist, should scale with velocity as

$$T_{\text{diss}}(v) \sim T_{\text{diss}}(v = 0)(1 - v^2)^{1/4} \, , \tag{8.184}$$

since $T_{\text{diss}}(v)$ should be the temperature at which the screening length $L_s(v)$ is comparable to the size of the meson bound state. The scaling (8.184) indicates that slower mesons can exist up to higher temperatures than faster ones. As illustrated schematically in Fig. 8.14, this scaling indicates that J/ψ suppression (and Υ suppression) may increase markedly for J/ψs (Υs) with transverse momentum p_T above some threshold, on the assumption that the temperature in the plasma does not reach the dissociation temperature of J/ψ (Υ) mesons at zero velocity [521, 728]. The threshold p_T above which the production of quarkonium falls off due to their motion through the quark–gluon plasma depends sensitively on the difference between $T_{\text{diss}}(v = 0)$ and the temperature reached in the collision [413]. Modeling this effect requires embedding results for quarkonium production in hard scatterings in nuclear collisions into a hydrodynamic code that describes the motion of the quark–gluon fluid produced in the collision, in order to evaluate the velocity of the hot wind felt by each putative quarkonium meson. Such an analysis indicates that once p_T is above the threshold at which $T_{\text{diss}}(v)$ has dropped below the temperature reached in the collision, the decline in the J/ψ survival probability is significant, by more than a factor of four (two) in central (peripheral) collisions [412, 413]. We should caution that, as we discussed in Section 2.4, in modelling quarkonium production and suppression versus p_T in heavy ion collisions, various other effects like secondary production or formation of J/ψ mesons outside the hot medium at high p_T [519] remain to be quantified. The quantitative importance of these and other effects may vary significantly, depending on details of their model implementation. In contrast, Eq. (8.184) was obtained directly from
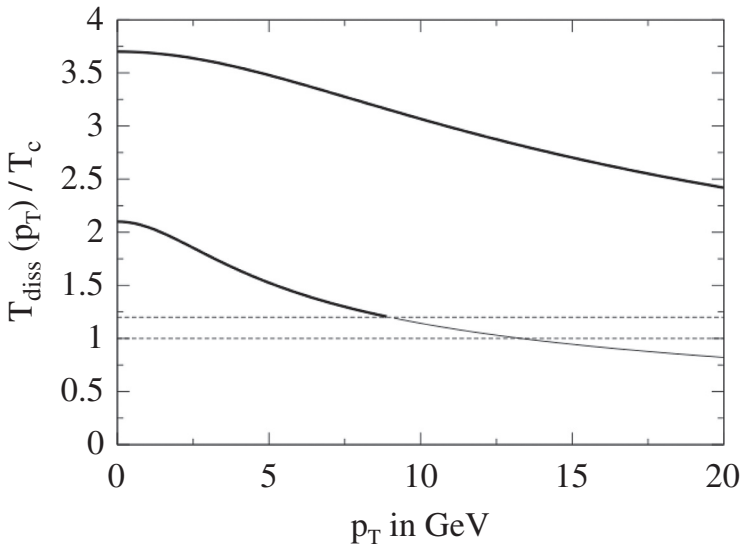
Figure 8.14 A $1/\sqrt{\gamma}$-velocity scaling of the screening length in QCD would imply a J/ψ dissociation temperature $T_{\mathrm{diss}}(p_T)$ that decreases significantly with p_T, while that for the heavier Υ is affected less at a given p_T. The curves are schematic, in that we have arbitrarily taken $T_{\mathrm{diss}}(0)$ for the J/ψ to be $2.1\,T_c$ and we have increased $T_{\mathrm{diss}}(0)$ for the Υ over that for the J/ψ by a factor corresponding to its smaller size in vacuum. At a qualitative level, we expect to see fewer J/ψ (Υ) mesons at p_Ts above that at which their dissociation temperature is comparable to the temperatures reached in heavy ion collisions at RHIC (at the LHC). Figure taken from Ref. [583].

a field-theoretical calculation and its implementation will not introduce additional model-dependent uncertainties.

The analysis of this section is built upon the calculation of the potential between a test quark and antiquark in the strongly coupled plasma of $\mathcal{N} = 4$ SYM theory, a theory which in and of itself has no mesons. Gaining insight into the physics of quarkonium mesons from calculations of the screening of the static quark–antiquark potential has a long history in QCD, as we have seen in Section 3.3. But, we have also seen in that section that these approaches are gradually being superseded as lattice QCD calculations of quarkonium spectral functions themselves are becoming available. In the present context also, we would like to move beyond drawing inferences about mesons from analyses of the potential $E(L)$ and the screening length L_s to analyses of mesons themselves. This is the subject of Chapter 9, in which we shall carefully describe how once we have added heavy quarks to $\mathcal{N} = 4$ SYM by adding a D7-brane in the gravity dual [513], as in Section 5.5, the fluctuations of the D7-brane then describe the quarkonium mesons of this theory. We shall review the construction first in vacuum and then in the

presence of the strongly coupled plasma at nonzero temperature. We shall find that the results of this section prove robust, in that the velocity scaling (8.184) has also been obtained [336] by direct analysis of the dispersion relations of mesons in the plasma [608, 336]. These mesons have a limiting velocity that is less than the speed of light and that decreases with increasing temperature [608], and whose temperature dependence is equivalent to (8.184) up to few percent corrections that have been computed [336] and that we shall show. This is a key part of the story, with the velocity-dependent dissociation temperature of this section becoming a temperature dependent limiting velocity for explicitly constructed quarkonium mesons in Chapter 9. However, this cannot be the whole story since the dispersion relations seem to allow for mesons with arbitrarily large momentum even though they limit their velocity. The final piece of the story is described in Section 9.4.2, where we review the calculation of the leading contribution to the widths of these mesons [347], which was neglected in the earlier calculations of their dispersion relations. Above some momentum, the width grows rapidly, increasing like $p_\perp^2$. And, the momentum above which this rapid growth of the meson width sets in is just the momentum at which the meson velocity first approaches its limiting value. The physical picture that emerges is that at the momentum at which the mesons reach a velocity such that the hot wind they are feeling has a temperature sufficient to dissociate them, according to the analysis of this section built upon the calculation of L_s, their widths in fact grow rapidly [347].